



Annual Report 2020

Laboratory of Radiochemistry

Cover

Radiochemistry in Switzerland in the spotlight:
As of December 10, 2020, the ETH Zurich appointed PSI's Prof. Dr. Patrick Steinegger as assistant professor of radiochemistry (tenure track). Thus, the ETH domain took first counter measures against the imminent loss of radiochemical expertise in Switzerland, emphasized in the "Weissbuch Radiochemie Schweiz" by the Swiss Academy of Sciences (SCNAT). Furthermore, the December issue of CHIMIA (Swiss Chemical Society) invited to present the diverse radiochemical activities throughout the country.

The photograph shows Patrick Steinegger with the December issue of CHIMIA as well as the SCNAT-report.

PAUL SCHERRER INSTITUT



Annual Report 2020

Laboratory of Radiochemistry

Editors

R. Eichler, A. Blattmann

Paul Scherrer Institut

Labor für Radiochemie

5232 Villigen PSI

Switzerland

Sekretariat +41 56 310 24 01

Fax +41 56 310 44 35

Reports are available from

Angela Blattmann

angela.blattmann@psi.ch

Paul Scherrer Institut

5232 Villigen PSI

Switzerland



See also our web-page

<https://www.psi.ch/lrc/>

TABLE OF CONTENTS

Editorial.....	1
Thermochromatography of Carrier-Free ^{197m}Hg on a Se Stationary Phase	3
P. Ionescu, R. Eichler, P. Steinegger, A. Türler	
Development of the Trace-Gas Reaction Analyzer for Chemistry (TRACY)	5
P. Ionescu, R. Eichler, T. K. Sato, P. Steinegger, G. Tiebel, A. Türler	
Performances of a diamond sensor in dependence of the applied electrical field and temperature	7
A. Smagghe, P. Steinegger	
Large area 4H-SiC-based detector for high temperature α -spectroscopy with superheavy elements.....	9
M. Jotterand, M. Carulla, R. Dressler, P. Steinegger	
DGFRS II simulation: The focal plane image for the ^{48}Ca on ^{242}Pu reaction.....	11
R. Eichler, P. Steinegger, D. Solovjov, N. Kovrizhnykh	
On the volatility of PaCl_5 and PaBr_5	13
H. W. Gäggeler, B. Eichler, R. Eichler, D. T. Jost	
New EU-Projects on Liquid Metal Chemistry	15
J. Neuhausen	
Separation of ^{179}Ta for the production of ^{180}Ta via neutron capture on radi-oactive ^{179}Ta	17
I. Kajan, R. Garg, C. Lederer-Woods, D. Schumann	
Towards an accurate determination of the ^{179}Ta half-life using γ -ray spectroscopy	19
M. Veicht, I. Kajan, D. Schumann	
^{53}Mn half-life determination	21
J. Ulrich, P. Cassette, R. Dressler, N. Kneip, K. Kossert, X. Mougeot, D. Schumann, P. Sprung, D. Studer, K. Wendt	
Half-life measurement of ^{154}Dy via the “direct method”	23
N. M. Chiera, Z. Talip, R. Dressler, P. Sprung, D. Schumann	
The influence of plating time, acidity and cathode material on the electrodeposition of Sm.....	25
N. M. Chiera, D. Schumann	
Preliminary characterization of holmium cathodes produced by molecular plating for the HOLMES experiment	27
G. de Bodin de Galembert, E. Maugeri	
Refuting a claim of the gravitational wave GW170817 affecting β -decay rates	29
P. A. Breur, J. C. P. Y. Nobelen, L. Baudis, A. Brown, A. P. Colijn, R. Dressler, R. F. Lang, A. Massafferri, C. Pumar, C. Reuter, D. Schumann, M. Schumann, S. Towers, R. Perci	

Determination of the excitation function for the production of ^{44}Ti in proton-irradiated vanadium samples.....	31
M. Veicht, I. Kajan, J.-C. David, S. Chen, E. Strub, I. Mihalcea, D. Schumann	
Separation of long-lived, non-carrier-added calcium, titanium, and aluminum isotopes from high - energy proton irradiated vanadium.....	33
J. Wilson, I. Mihalcea, M. Veicht, D. Cvjetinovic, D. Schumann	
Towards implementing ^{32}Si for environmental research (SINCHRON): Final purification and master solution preparation	35
I. Mihalcea, M. Veicht, A. Pautz, D. Cvjetinovic, D. Schumann	
Towards implementing ^{32}Si for environmental research (SINCHRON): Sample preparation and stabilization for scintillation measurements.....	37
I. Mihalcea, M. Veicht, A. Pautz, K. Kossert, O. Nähle, C. Bailat, Y. Nedjadi, D. Schumann	
Towards implementing ^{32}Si for environmental research (SINCHRON): Elimination of isobaric interferences in ICP-MS: ^{32}Si and ^{32}S	40
M. Veicht, P. Sprung, I. Mihalcea, A. Pautz, D. Schumann	
Towards implementing ^{32}Si for environmental research (SINCHRON): AMS measurements of ^{32}Si	42
M. Schlomberg, C. Vockenhuber, H.-A. Synal, D. Schumann, I. Mihalcea, M. Veicht, A. Wallner	
Report on the production of a ^{205}Tl target for a neutron capture experiment at the n_TOF facility (CERN).....	43
A. Casanovas, E. A. Maugeri, A. Tarifeño-Saldivia, F. Calivño, S. Heinitz, D. Schumann, R. Dressler, P. Sprung, C. Guerrero	
Sulphur-Bearing Macrocyclic Chelators for ^{64}Cu Radiopharmaceuticals: Ra-diolabeling and In Vitro Stability Evaluation.....	45
M. Tosato, C. Favaretto, Z. Talip, N. P. van der Meulen	
Determination of the gamma-emission probabilities of ^{169}Er	46
Z. Talip, F. Juget, J. Ulrich, Y. Nedjadi, T. Buchillier, M. T. Durán, F. Bochud, C. Bailat, N. P. van der Meulen	
Development of direct Ga-68 production by cyclotron irradiation of Zn-68 solid targets: preliminary results.....	48
P. V. Grundler, A. Varbella, N. P. van der Meulen	
Production and radiochemical purification of ^{155}Tb for SPECT imaging purposes.....	50
C. Favaretto, Z. Talip, F. Borgna, P. Grundler, R. Schibli, C. Müller, N. P. van der Meulen	
Determination of the gamma and X-ray emission probabilities of ^{161}Tb	51
F. Juget, Z. Talip, T. Buchillier, M. T. Durán, Y. Nedjadi, F. Bochud, J. R. Zeevaart, P. Grundler, N. P. van der Meulen, C. Bailat	
Efficient production of high specific activity ^{167}Tm at PSI and CERN-MEDICIS	52
Z. Talip, R. Heinke, E. Chevally, K. Chrysalidis, T. E. Cocolios, C. Duchemin, V. Fedosseev, L. Lambert, B. Marsh, T. Stora, M. Tosato, S. Wilkins, N. P. van der Meulen, H. Zhang	

List of publications.....	53
Internal Reports.....	58
Contributions to conferences, workshops and seminars.....	59
Poster presentations	61
Members of scientific committees, external activities.....	62
Public relations and outreach activities	62
Lectures and courses.....	63
Semester work.....	63
Doctoral thesis.....	64
Awards	65
Organigram.....	66
Author index.....	67
Affiliation index	69

EDITORIAL

Dear reader,

This special year will certainly stay in our memories. The down side is clearly the worldwide tragedy due to the pandemic situation. Our sincere thoughts are with those who suffered most. However, we were able to work on our research projects, despite the virus kept us out of the laboratories for a substantial amount of time. Thus, the up side is clearly that we demonstrated our responsibility and our ability to adapt our daily procedures to the rapidly changing needs. Here, I would like to thank the members of the LRC for their patience and flexibility.

Let me start with something that made this year a particularly successful one for Swiss radiochemistry. Right before Christmas, we received news from the ETH council that Patrick Steinegger was accepted as tenure track assistant professor of radiochemistry at ETH Zürich. Let us congratulate him sincerely to this success. We wish him a prosperous and successful career in academia. The connection of our Laboratory to the Universities is extremely important to fulfill our politically important tasks as knowledge keepers in nuclear chemistry and radiochemistry. Thus, we will be able to secure academic supervision of master and doctoral students in the future. Another success for the Swiss radiochemistry was the finalization of the Whitebook Radiochemistry illustrating the societal need for a future Radiochemistry Switzerland. Furthermore, in a special issue of CHIMIA we were able to present our research field in nice review articles. My thanks go to all those, who participated actively and made these things happen.

After the long shut down, the restart of our SINQ-NIS installations went exceptionally well. We now have access again to fission products from a ^{235}U fission source via the renewed SINQ Gas-jet facility. This year we plan to characterize the product spectrum available from this source to include them into the radionuclide portfolio for our research.

Our participation at international conferences was scarce due to travel restrictions. However, we tried

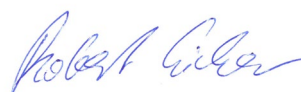
to participate as actively as possible in on-line events. Furthermore, three PhD students successfully finished their work under the challenging circumstances of COVID. Dr. Jiri Ulrich received the Young Scientist Prize of the Swiss Neutron Science Society 2020 for his outstanding performance. Our sincere congratulations to this success!

Our traditional joint social activities this year had to be organized partially as remote happenings too:

- Fortunately, we could complete our traditional laboratory summer excursion, which was well organized by Patrick Steinegger. We traveled by train through the impressive entrance of the Val-de-Travers to visit the Historical Asphalt Mines in Site de la Presta, Travers. These, once famous mines produced asphalt for all kinds of sealing and medical purposes for almost three centuries. In the very beginning of extensive automobilism Swiss asphalt covered streets and places in almost all big cities all over the world - Times Square and Piccadilly Circus to name a few - really impressive! After a tasty lunch with the site-specific tradition of ham cooked under asphalt coverage and some Absinth tasting we had a really enjoyable hiking trip in best weather through the Gorges de l' Areuse to Boudry, following the river Areuse, which cut impressive structures into the Jura mountains – beautiful.

- Our remote Christmas party via ZOOM was very well organized by Paul Ionsecu and Mario Veicht. Thank you guys so much for your efforts. It was a fun party with a double Santa experience by Ivan Kajan (Santa Claus) and Ivan Danilov (Father Frost). The Secret Santa presents were as usual well selected. We even had guests from our Alumni Kathi (Argonne, USA) and Benni (Safetec GmbH, D), very nice!

As you will recognize, LRC is vital despite COVID. So enjoy reading our scientific report 2020!



Thermochromatography of Carrier-Free ^{197m}Hg on a Se Stationary Phase

P. Ionescu (Univ. Bern & PSI), R. Eichler (PSI), P. Steinegger (ETHZ & PSI), A. Türlér (Univ. Bern)

Introduction

Using gas adsorption thermochromatography (TC) the interaction of different chemical compounds on specific surfaces can be studied. Coupled with radioactive tracers, this technique is able to determine surface interactions to the single-atom level with applications in fundamental research such as transactinide chemistry [1,2].

Preparations for costly, difficult to perform transactinide experiments are generally done off-line with their lighter homologs in the periodic table. The herein presented TC experiments of carrier-free ^{197m}Hg radioisotopes on Se surfaces seek to better understand the single-atom chemical interaction of the heavier homolog of element copernicium (Cn, $Z = 112$) with the structurally complex element Se [3]. The latter is known to have multiple allotropes, with three main allotropes encountered at STP, i.e., trigonal 'gray' (thermodynamically most favorable), crystalline 'red', and amorphous 'black-red' Se [4].

Experimental section

For the reproducible manufacture of homogeneous Se surfaces a method of physical vapor deposition (PVD) followed by conversion of the deposited red amorphous Se to the trigonal state was developed. Clean quartz slides were coated with a thin amorphous Se layer (ca. 100 – 500 nm thickness). These slides were then exposed to a 255 nm UV-C lamp, which enhanced the conversion to gray Se through photocatalysis (see Fig. 1).

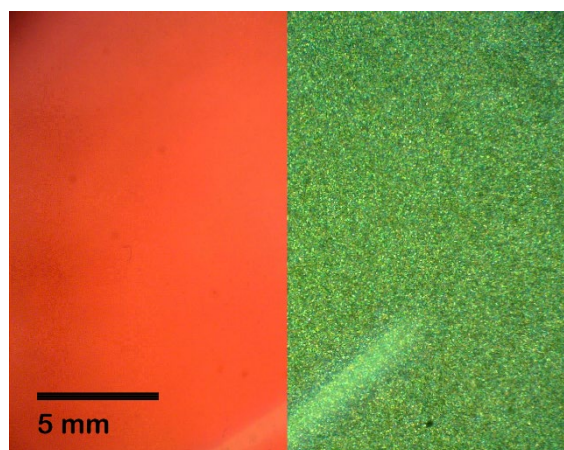


FIGURE 1: Microscopy picture of a Se slide after PVD (left) and after UV-C exposure for 48 hours (right).

Se slides were placed in a rectangular chromatography channel, exposing the ^{197m}Hg tracer to amorphous or gray Se on one side, and inert Teflon on the other (see Fig. 2).

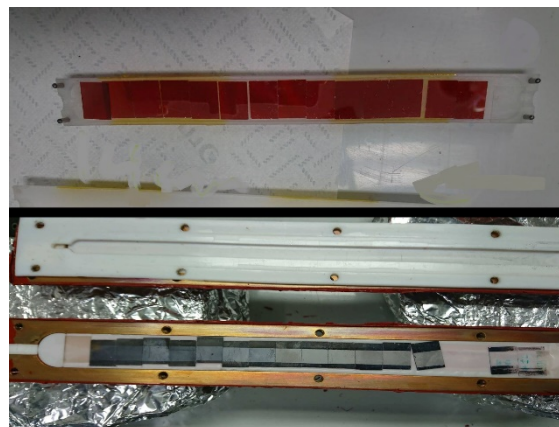


FIGURE 2: The opened chromatography channel showing the exposed cross section with Se plates. Isothermal Teflon column with amorphous Se thin films (top) and copper TC channel with trigonal Se thin films (bottom).

Following a first, comparative isothermal chromatography experiment, TC experiments were performed to evaluate the interaction between carrier-free ^{197m}Hg ($t_{1/2} = 23.8$ h), produced at the HIPA facility at PSI (see nuclear reaction 1), and the amorphous and trigonal allotropes of Se. The resulting deposition patterns of the Hg tracer were then interpreted using Monte-Carlo (MC) simulations to determine the adsorption enthalpy [5] as well as the surface composition of the chromatographic channels.



A stream of 50 ml/min He traversed a Ta getter operating at 950°C to remove residual O_2 impurities, which were observed to influence the system otherwise. The ^{197m}Hg was thermally released from a gold foil at 1000°C. Tl granules were placed on both sides of the gold foil as an additional getter and to ensure the elemental state of Hg. Any ^{197m}Hg not deposited in the chromatographic channel was captured on an activated charcoal trap (see Fig. 3).

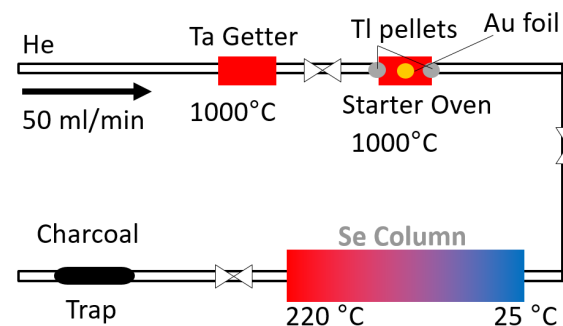


FIGURE 3: Typical setup for inverse thermochromatography (see text for details).

Results

The isothermal chromatography experiments confirmed previously established enthalpies of adsorption of $-\Delta H_{ads}^{t-Se}(Hg) < 45$ kJ/mol as well as $-\Delta H_{ads}^{a-Se}(Hg) > 85$ kJ/mol (see Fig. 4) [3]. Using MC simulations, the identity of the Se allotrope on the Se-covered channel surface as well as the degree of conversion from amorphous to the gray crystalline phase was evaluated, thus confirming a 99% efficient conversion (see Fig. 4).

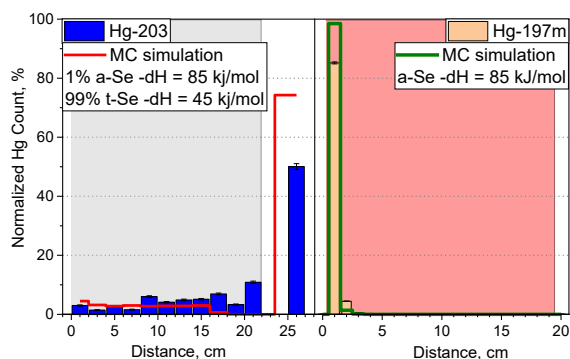


FIGURE 4: Deposition pattern (bar graphs) of isothermal chromatography experiments with Hg radioisotopes on gray Se (left) and amorphous Se (right). MC simulations (lines) show the expected deposition. Shaded areas indicate the location of gray/red Se. Graph resolutions are 2 cm (left) and 1 cm (right).

Inverse TC experiments were performed over a positive temperature gradient from room temperature up to the melting point of Se at 221°C. These experiments were designed to pinpoint a temperature range within which gaseous Hg begins reacting with the inert gray Se (see Fig. 5), i.e., the activation energy is high enough.

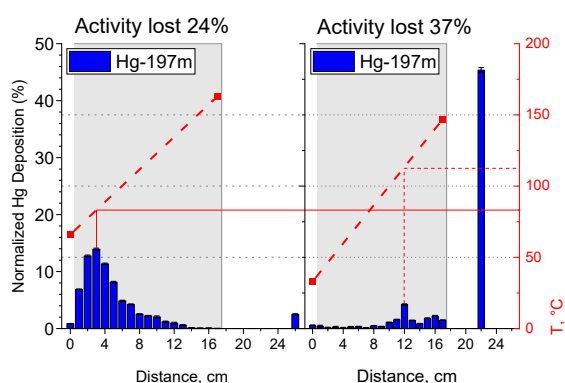
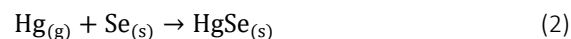


FIGURE 5: Inverse TC deposition patterns in successive experiments with different positive temperature gradients (dashed red lines, right hand scale) with deposition peak maxima at approx. 80°C (left side, solid red line) and 110°C (right side, dotted red line). Shaded areas indicates the gray Se column position; bar graph resolution: 1 cm.

It was notable, that a large amount of ^{197m}Hg activity (over half) was typically lost during these experiments. After repeated attempts, it became apparent that the loss stemmed from an O_2 contamination in the He carrier gas. The installation of a getter and the simplification of the experimental setup by minimizing potential leak sites resulted in a much improved yield. These effects were not observed in the isothermal experiments, likely due to the fact that Hg does not readily form HgO at STP. In a heated column however, an appreciable amount of the activity was found on inert Teflon surfaces (see Fig. 2) near the heating elements at the entrance of the channel. This implies that the mercury tracer likely formed non-volatile HgO , which deposited immediately. An important outcome of the herein presented experiments is the discovery of the temperature range at which mercury starts reacting with Se. This was found to lie between 80 – 110°C. While on its own it is not conclusive, current developments in the MC simulation will allow the determination of kinetic data such as the activation energy E_a of the reaction:



Conclusion

It is worthy of note that, as isothermal experiments have shown, reaction (2) is spontaneous at room temperature for amorphous Se, while it requires additional heat for the trigonal allotrope. The adsorption enthalpies for mercury on amorphous and trigonal Se have been used to determine the degree of conversion between the two allotropes using isothermal chromatography. Meanwhile, inverse TC experiments will allow the determination of an activation energy range for the reaction of Hg with Se. Furthermore, it is apparent that working with single atom quantities, it is of utmost importance to minimize residual impurities in the system, as even minor interferences can have significant impact on the results. This has triggered the development of the TRACY experiment [6].

References

- [1] R. Eichler *et al.*, *Nature*, **47** (2008), pp. 3262 - 3266
- [2] R. Eichler *et al.*, *Radiochim. Acta*, **98** (2010), pp. 133-139
- [3] N. M. Chiera, 'Towards the Selenides of the Superheavy Elements Copernicium and Flerovium', PhD Thesis, University of Bern, 2016
- [4] D. M. Chizikov, V. P. Shchastliviy, *Selenium and Selenides*, Collet's Publishers Ltd.: London, 1968
- [5] R. Eichler, B. Eichler, 'Thermochemical Data from Gas-Phase Adsorption and Methods of their Estimation' in: M. Schädel, D. Shaughnessy (eds.), *The Chemistry of Superheavy Elements*, 2nd ed., Springer-Verlag: Berlin Heidelberg, 2014
- [6] P. Ionescu *et al.*, *LRC Annual Report 2020* (2021), pp. 5-6

Development of the Trace-Gas Reaction Analyzer for Chemistry (TRACY)

P. Ionescu (Univ. Bern & PSI), R. Eichler (PSI), T. K. Sato (JAEA), P. Steinegger, G. Tiebel (ETHZ & PSI), A. Türler (Univ. Bern)

Introduction

Advances in the research of transactinide element chemistry have allowed us to interpret the properties of Superheavy elements (SHEs, $Z \geq 104$) by comparing them to their lighter homologs as is customary. Relativistic effects on elements increase with $\approx Z^2$ [1,2]. Hence, SHE experiments shed light on the chemical behavior of such heavy elements where relativistic effects exhibited are considerably stronger.

Gas adsorption chromatography (GC) is one of the leading research methods and was used in the benchmark chemical characterization of Cn ($Z = 112$) [3] and Fl ($Z = 114$) [4]. However, SHE experiments suffer from extremely low production rates in the order of atoms per day or week(s). Consequently, it is imperative to guarantee a high transport and detection efficiency. In most recent experimental campaigns, observations showed that the number of detected SHEs was about 50% lower than expected, in parallel to fluctuations in the detection rates of co-produced homologs. This calls for an improvement of the experimental techniques and deepening our understanding of involved factors.

Cn Experiments at FLNR in 2018

The most recent SHE experimental campaign at the Flerov Laboratory of Nuclear Reactions (FLNR), Russian Federation, resulted in the detection of 5 Cn events over the course of 5 weeks. Given the cross section data for the reaction $^{242}\text{Pu}(^{48}\text{Ca}, 3n)^{287}\text{Fl}$ and the associated transport efficiencies, this corresponded to about half of the events expected. Additionally, the detection yield of co-produced radioisotopes of At and Hg was found to fluctuate with a factor of up to 6 (see Fig. 1).

In GC with a carrier gas mixture of Ar and He (30/70%), these fluctuations were found to correlate with the presence of residual gas impurities (see Fig. 1). Basic kinetic molecular theory states that, an At atom (202 pm radius [5]) will collide at 25°C and a pressure of 1.2 bar, with a 1 ppm impurity just under 4000 times per second. This gives the nuclear reaction products countless opportunities to react with smallest quantities of impurities in the carrier gas during an average transport time from the production site to the detector of roughly 4 s. The conclusion is that the significant loss of yield in GC is detrimental to the study of SHEs and must be investigated.

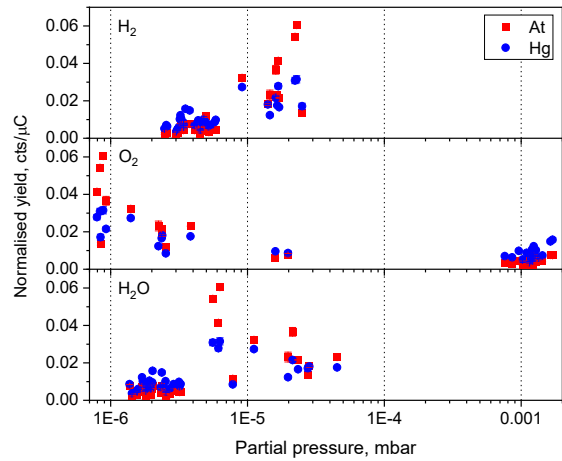


FIGURE 1: Normalized yield of ^{211}At and $^{184-188}\text{Hg}$ radioisotopes in relation to impurities H_2 (top), O_2 (middle), and H_2O (bottom) in the carrier gas held at 1.3 bar.

Development of TRACY

As demonstrated above, there is a great need for understanding of the relationship between gas contaminants and the chromatographic yield. The observed correlations of the latter with impurities of hydrogen, oxygen and water (see Fig. 1) were not entirely reliable as ^{211}At , with a half-life of more than 7 h, provided only very delayed indications of changes in the chemical conditions.

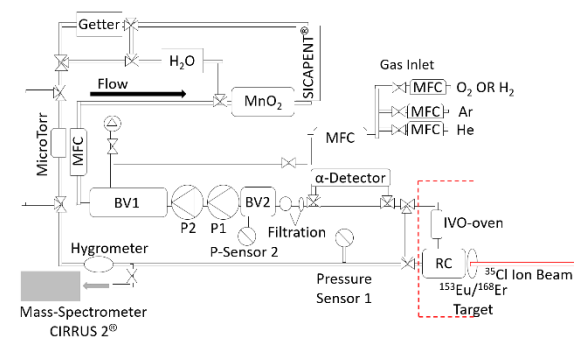
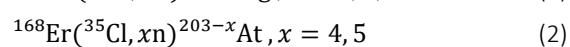
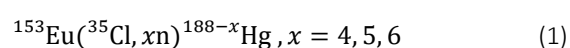


FIGURE 2: GC loop of TRACY, a design closely related to the COLD setup; it allows for controlled mixing in of trace and macro amounts of O_2 , H_2 , and H_2O . Abbreviated components are the buffer volumes (BV), the mass flow controllers (MFC), the loop pumps (P), the recoil Chamber (RC), and the in-situ volatilization oven (IVO).

Furthermore, due to the nature of the Cryo On-Line Detector (COLD) setup, the Ta oven, acting as O_2 getter, releases H_2 into the system via reduction of H_2O . It was therefore unclear whether the absence of O_2

or the presence of H₂ was responsible for yield fluctuations if not both. Hence, a dedicated experiment was designed to investigate these three impurities with high precision using the Trace-Gas Reaction Analyzer for Chemistry, TRACY.

In the framework of the Swiss-Japanese Young Researcher's Exchange Program, we have prepared a dedicated setup (see Fig. 2). First experiments are envisaged to be carried out at Tandem accelerator facility of the Japanese Atomic Energy Agency (JAEA), Japan. Using a ³⁵Cl ion beam in combination with a mixed ^{nat}Eu/^{nat}Er-target, the following nuclear fusion-evaporation reactions will be addressed (only the most interesting reaction channels are mentioned):



Based on the calculated cross sections for the nuclear reactions (1) and (2) (see Fig. 3) [6], short-lived radioisotopes of Hg and At are accessible at sufficiently high production rates. Thus, using a gas loop system and variable, but well-defined, carrier gas compositions, the setup allows for monitoring in real-time changes in the transport yield of the short-lived radiotracers. Whereas the rough gas composition is established over separate gas inlets (see Fig. 2), the fine-tuning of residual impurities can be achieved using a MnO₂-filled oven (O₂ generation), a Sicapent cartridge (H₂O removal), a thermoelectric dewpoint controller (H₂O content), and a Ta-based getter oven (O₂ removal or H₂ addition).

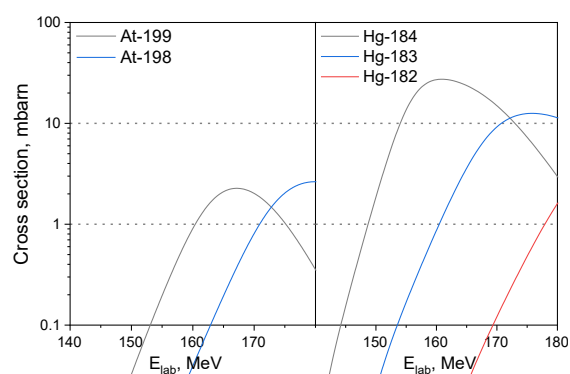


FIGURE 3: Calculated cross sections for the targeted nuclear-fusion evaporation reactions using a ³⁵Cl ion beam and a mixed target of natural Eu and Er up to the maximum possible beam energy of 180 MeV [6].

All reaction products disintegrate by α -decay, and therefore can be detected and differentiated based on their energy. For that purpose, a short version of the COLD array is employed (2x 8 detector pairs). Upon finalizing TRACY, the setup will be thoroughly tested before being shipped to Japan for the planned six-day long beam time in June 2021.

Conclusions

Due to improvements in sensitivity regarding the measurement possibilities of the gas composition in recent SHE experiments, it has become apparent how important a tightly controlled gas composition is. Residual impurities in the carrier gas were found to at least in part be responsible for the lower-than-expected yields in recent GC experiments with SHEs. A new experiment 'TRACY' has been developed for the dedicated investigation of such residual gas effects. This experiment is expected to be deployed for the first time in 2021 in collaboration with the Advanced Science Research Center of JAEA in Japan.

References

- [1] A. Türler et al., *J. Alloys Compd.*, **271-273** (1998), pp. 287-291
- [2] P. Pyykkö, *Chem. Rev.*, **88** (1988), pp. 563-594
- [3] R. Eichler et al., *Nature*, **447** (2007), pp. 72-75
- [4] R. Eichler et al., *Radiochim. Acta*, **98** (2010), pp. 133-139
- [5] John R. Rumble (ed.), *CRC Handbook of Chemistry and Physics*, 100th ed., CRC Press/Taylor & Francis: Boca Raton, FL, 2019
- [6] A. V. Karpov et al., *Nucl. Instrum. Methods Phys. Res., Sect. A*, **859** (2017), pp. 112-124 (nrv.jinr.ru)

Performances of a diamond sensor in dependence of the applied electrical field and temperature

A. Smaghe (PSI), P. Steinegger (ETHZ & PSI)

Introduction

Most superheavy elements (SHEs, $Z \geq 104$) undergo α -decay when disintegrating. A state-of-the-art approach for chemically characterizing SHEs is gas-adsorption thermochromatography. Due to the short-lived character of SHEs, an *in-situ* detection of their respective decay is inevitable. Thus, the chromatographic channels consist of Si-based semiconductor solid state detectors in a sandwich geometry with the active areas facing inwards. In this setup, the front faces of the detectors act as the stationary surface. This experimental approach is fast, highly efficient and allows for continuous measurements. However, the commonly used Si-based detector technology limits the starting point of the negative temperature gradient to around 50°C. Consequently, in order to study the properties of relatively less volatile chemical species, a new detector material has to be found for future investigations of SHEs, relying on high-temperature α -spectroscopy.

Therefore, diamond has been investigated: With its wide bandgap of 5.46 eV (i.e., almost five times larger than the one of Si with 1.11 eV), diamond should enable stationary surface temperatures of up to 1000°C, while, at the same time, feature a stable detector performance. However, the needed single crystal, electronic grade chemical vapor deposition diamond material is very expensive (approx. EUR 8000/cm²) and it is available at rather small sizes only (4.5 × 4.5 × 0.5 mm³). Additionally, previous experiments have indicated an upper temperature limit for a stable detector operation of about 200°C [1,2]. Despite looking into alternative materials, such as 4H-SiC, we are presenting here further α -spectroscopic measurements exploring the high temperature limit of yet another diamond sample.

Experimental details

The sensor used in the herein presented experiments was prepared beforehand according to the procedure outlined in [1]. The diamond sensor was placed in a three-layered, ceramic printed circuit board (PCB) with the front electrode being partly exposed through a small hole in the outermost PCB-layer. This ensured the α -particles from the standard ²⁴¹Am reference source ($E\alpha = 5.486$ MeV, $A \approx 15$ kBq) to reach the detector with no energy loss. The detector assembly was then enclosed in an electrically grounded copper heating block, whose temperature could be controlled by two heating cartridges. A type K thermocouple (TC), inserted in an

opening close to the sensor, was used to measure the actual sensor temperature. This assembly was finally placed in a vacuum housing ($< 1 \cdot 10^{-4}$ mbar) with an electrical feed-through for the signal read-out and bias application. As for the measurement electronics, a combination of a CIVIDEC Cx spectroscopic amplifier in combination with a Tukan8k ADC/MCA unit was employed. The detector biasing occurred with a Keithley 2470 Source Meter. Further details concerning the experimental setup can be found in [2].

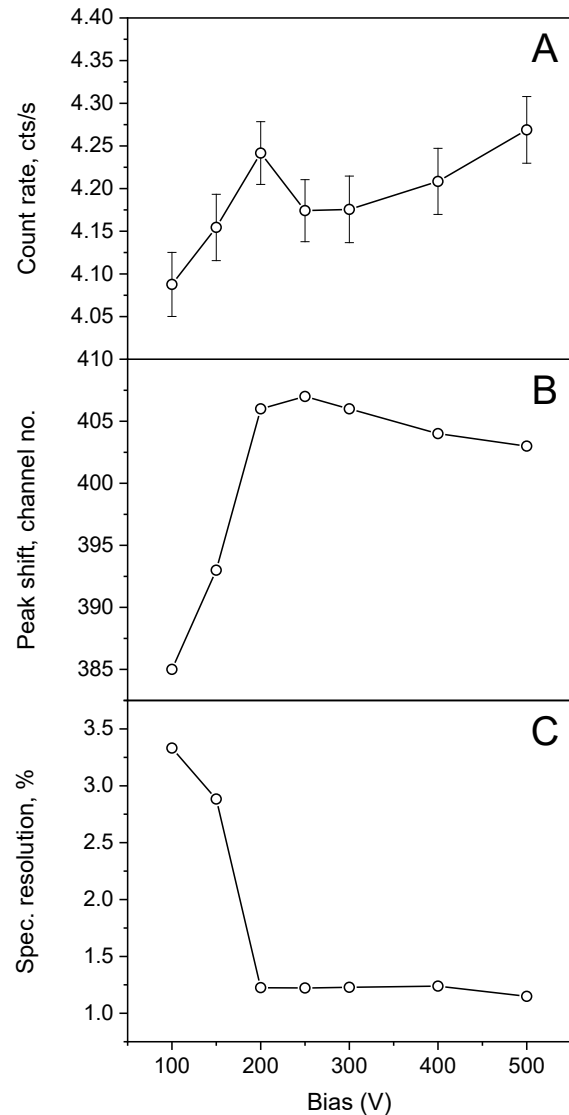


FIGURE 1: The count rate (A), the peak shift (B), and the FWHM α -spectroscopic resolution at $E\alpha = 5.486$ MeV (C) as functions of the applied detector bias at RT; the associated errors of the measures presented in B and C are too small to be shown.

Results and discussion

In a first step, the diamond sensor was operated at room temperature (RT) but varying detector bias potentials (see Fig. 1). As expected, the count rate stayed largely constant within the given uncertainties, while a saturating peak shift (i.e., a measure of the charge carrier collection efficiency) as well as an improving spectroscopic resolution was observed beyond a detector bias potential of +150 V. Whereas the α -spectroscopic resolution remained constant for detector biases ≥ 200 V, a slight peak shift towards lower channel numbers surfaced at ≥ 400 V. It is worth mentioning here, that the general behavior is fully reproducible when going from the highest potential values back to the lower ones.

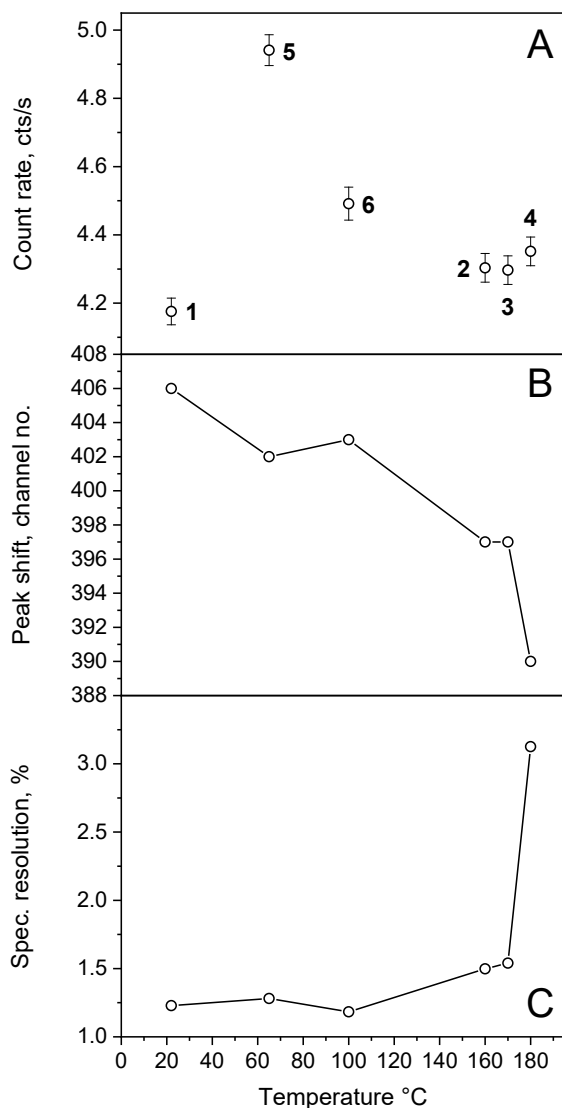


FIGURE 2: The count rate (A; the numbers indicate the measurement sequence), the peak shift (B), and the FWHM α -spectroscopic resolution at $E\alpha = 5.486$ MeV (C) as functions of the applied detector temperature (detector bias potential of +300 V); the associated errors of the measurements presented in B and C are too small to be shown.

Further measurements explored the performance at a detector bias potential of +300 V, under the influence of changing sensor temperatures (see Fig. 2). For the investigated temperature range, the spectroscopic resolution remains constant until drastically deteriorating at $>170^\circ\text{C}$. In parallel, increasing sensor temperatures led to a peak shift to lower channel numbers, thus following an inverse trend as observed in [1]. This may be attributed to an increased probability for charge carrier recombination at higher sensor temperatures. Meanwhile, the count rate showed a rather surprising increase after returning from 180°C (at this temperature the sensor ceases operation) into an assumingly adequate temperature range in terms of a stable detector operation (mind the measurement sequence in Fig. 2A). Both, the decreasing charge carrier collection efficiency as well as the anomalies in the behavior regarding the count rate with increasing sensor temperature have yet to be explained or reproduced, respectively.

Sensor temperature

In order to verify the accuracy of the values measured by the 1 mm type K TC, pushed inside the PCB structure as presented in [2], comparative measurements were carried out (see Fig. 3). A second 0.5 mm thick type K TC, mounted in the position of the diamond sensor, agreed very well with the main TC, thus bolstering the reliability of the temperature measurements in [2].

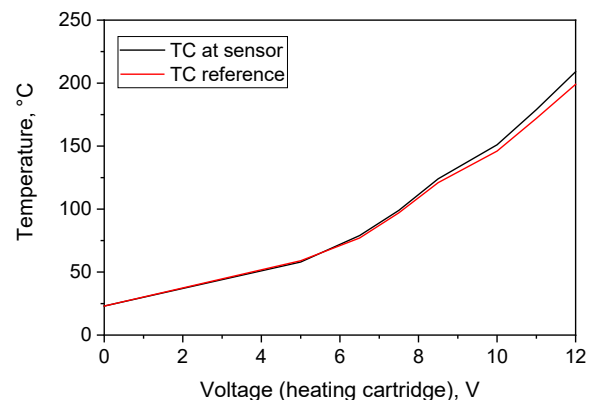


FIGURE 3: Comparative measurement between the sensor temperature (black; TC at the side, not in direct contact with diamond) and a reference TC mounted in the position of the sensor itself (red).

References

- [1] P. Steinegger et al., *Nucl. Instrum. Methods Phys. Res., Sect. A*, **850** (2017), pp. 61-67
- [2] B. Kraus et al., *Nucl. Instrum. Methods Phys. Res., Sect. A*, **989** (2021), pp. 164947

Large area 4H-SiC-based detector for high temperature α -spectroscopy with superheavy elements

M. Jotterand (EPFL/ETHZ & PSI), M. Carulla (LMN/PSI), R. Dressler, P. Steinegger (ETHZ & PSI)

Introduction

High-temperature α -spectroscopy is of high interest for the chemical characterization of relatively less volatile transactinide elements [1,2]. Thereto, the laboratory of radiochemistry participates in the framework of a PSI-Cross proposal on the use of silicon carbide with the Laboratory for Micro and Nanotechnology and other laboratories at PSI. Herein, we report on the fabrication, preparation and characterization of a large area 4H-SiC-based detector and its α -spectroscopic performance.

Sensor fabrication

The sensor design (layout as a PIN diode) is schematically shown in Fig. 1. It is produced by epitaxial growth of a nitrogen-doped n-layer followed by an aluminium-doped p-layer on a n-type substrate (the respective doping densities are given in Fig. 1). Following reactive ion beam etching of the top layer (p-type), using a specific mask-layout to allow for a variety of different chip sizes on the initial 4-inch wafer, the sample was metallized with 20 nm Ti, 40 nm Al, as well as 60 nm Ni (back side: only 100 nm Ni). In a final step, the wafer was annealed at 950°C for one minute (rapid thermal annealing) before being cut into the different chip sizes, including samples of $10 \times 10 \text{ mm}^2$. One such sample was then used for the experiments addressing the performance of such a large area sensor for α -spectroscopic purposes.

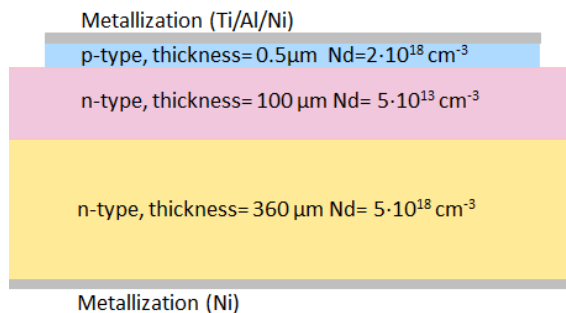


FIGURE 1: Scheme of extrinsic 4H-SiC sensor setup (see text for detailed description of fabrication).

Simulations

The depletion thicknesses for different reverse bias voltages were simulated using the Sentaurus Structure Editor for the definition of the sensor structure and the Sentaurus Device Simulation Tool to simulate the electric field inside the sensor (both Synopsys' TCAD; see Fig. 2). In these simulations the front

face of the outermost p-layer is positioned at $0 \mu\text{m}$, with the pn-junction at $0.5 \mu\text{m}$.

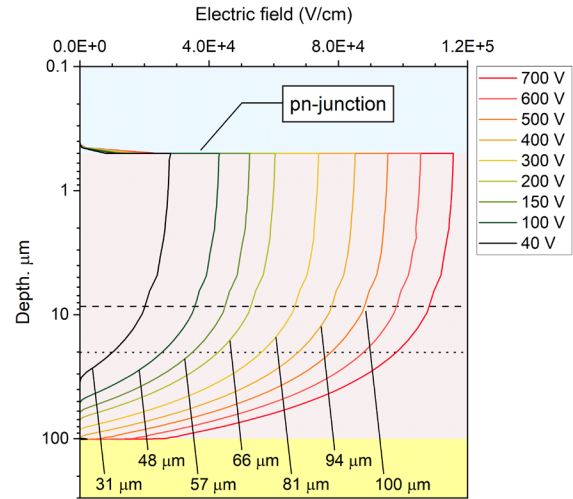


FIGURE 2: Simulations of the thickness of the depletion region (i.e., the internal, electric fields) for the 4H-SiC sensor as a function of the applied reverse bias (p-type layer at ground potential, back side at indicated positive potential); the colored areas in the back indicate the different doping regions (cf. Fig. 1), the numbers state the actual depletion thickness for the given sensor potentials (maximum: $100 \mu\text{m}$), while the dashed and dotted lines mark the penetration depths of α -particles from ^{148}Gd ($3.18 \text{ MeV} \cong 8.5 \mu\text{m}$) and ^{244}Cm ($5.80 \text{ MeV} \cong 20.1 \mu\text{m}$), respectively.

Detector and experimental setup

The sensor was mounted on a ceramic leadless chip carrier (CLCC) using the electrically conductive epoxy EPO-TEK H20S from EPOXY Tech., Inc. (curing at 150°C for 1 hour). The front electrode was connected via aluminum wire-bonding before the entire detector structure was mounted on a PCB and SMA-plug (see Fig. 3, left side). The α -particles were collimated using a second CLCC with a small hole (2 mm in diameter; see Fig. 3, right side). The detector was mounted in a vacuum chamber with minimum pressures of $< 10^{-3} \text{ mbar}$ and biased using a Keithley 2470 Source Meter. The signal readout was established using either a CIVIDEC Cx spectroscopic amplifier or dedicated (pre)amplifier electronics for Si-based detectors (PSI in-house development; maximum voltage: 100 V). Finally, the spectra of a $^{148}\text{Gd}/^{244}\text{Cm}$ mixed-nuclide α -source (at approx. 10 mm distance from the detector front face) were recorded using a Tukan8k ADC/MCA unit.

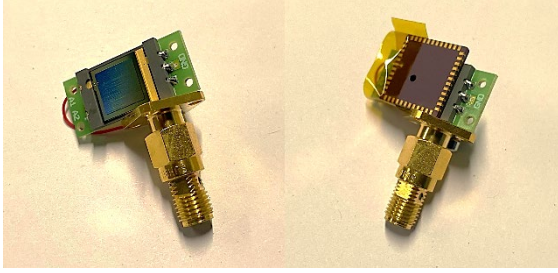


FIGURE 3: Detector assembly without (left side) and with 2 mm collimator (right side); see text for details.

Results and discussion

Trying to check the performance of the large area 4H-SiC-sensor at standard operating condition (i.e., *in vacuo*, complete darkness and at 40 V), led to the observation of a shoulder at lower energies of the main α -lines of ^{148}Gd and ^{244}Cm (see Fig. 4). This observation can be traced back to the not fully depleted intrinsic sensor region (purple in Fig. 2). Furthermore, the measurement electronics optimized for the low capacity of diamond detectors, features a second shoulder on the low-energy side of the main α -line. The quite different behaviour of the two employed readout electronics suggests an electronic mismatch. Fitting the shoulder and the main α -line at both energies separately with Gaussian-like fit functions leads to sufficient spectroscopic resolutions of less than 80 keV (i.e., using the readout electronics optimized for Si and a detector bias of 40 V) for the envisaged experiments.

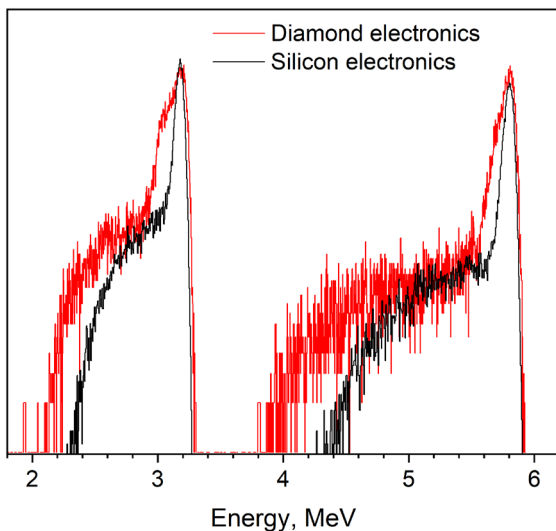


FIGURE 4: Qualitative comparison between two measurements at +40 V using dedicated diamond electronics (CIVIDEC Cx, red) and the PSI (pre)amplifier (optimized for Si-based detectors, black); due to different measurement times and amplifier gains, the normalized spectra are shown at arbitrary units.

The common shoulder-feature in case of both measurement electronics was furthermore explored as a function of the applied detector bias. As the electronics optimized for Si-based detectors is designed

for a maximum voltage of +100 V, the CIVIDEC Cx spectroscopic amplifier was used for this part of the study. While the resolution (FWHM) as well as the charge collection (i.e., the peak shift towards higher channel numbers) expectedly increase with the detector potential, the broader shoulder disappears between +300 V and +400 V (see Fig. 5). Meanwhile, the second, exclusively observed shoulder in case of the diamond electronics, remains unchanged.

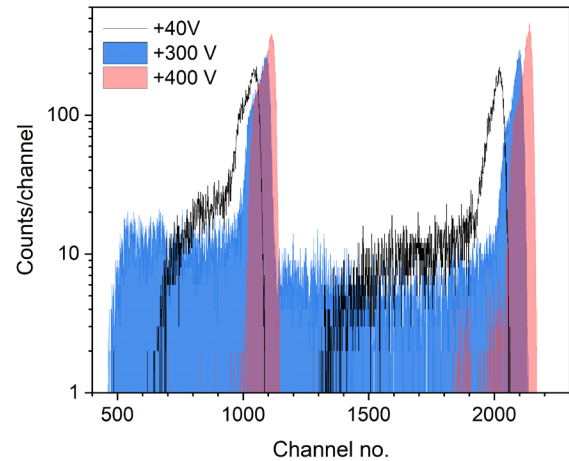


FIGURE 5: Three spectra recorded with the 4H-SiC-based detector in combination with the CIVIDEC Cx spectroscopic amplifier at +40 V (black line graph), +300 V (blue bar graph) and +400 V (red bar graph); whereas the broad shoulder disappears between +300 V and +400 V, the second one closer to the main α -lines of ^{148}Gd and ^{244}Cm remains unchanged.

Further experiments will target the application of readout electronics optimized for Si-based detectors, allowing a biasing beyond +100 V and thus, allowing for a fully depleted 4H-SiC sensor.

Conclusion

A large-area 4H-SiC detector was successfully fabricated and subsequently tested in terms of its α -spectroscopic performance in vacuum and at room temperature. Two types of readout electronics were tested. Whereas the first type was optimized for Si-based detectors, the second type was specifically designed in order to match the lower capacitance of diamond sensors of comparable size. The results obtained with the first type were markedly better, thus suggesting a problem regarding impedance matching in combination with a not fully depleted 4H-SiC sensor.

References

- [1] P. Steinegger et al., *Nucl. Instrum. Methods Phys. Res., Sect. A*, **850** (2017), pp. 61-67
- [2] B. Kraus et al., *Nucl. Instrum. Methods Phys. Res., Sect. A*, **989** (2021), pp. 164947

DGFRS II simulation: The focal plane image for the ^{48}Ca on ^{242}Pu reaction

R. Eichler (PSI), P. Steinegger (ETHZ & PSI), D. Solovjov, N. Kovrizhnykh (FLNR)

Introduction

The use of recoil separators is an important way to clean up the product spectrum of a heavy-ion-induced nuclear fusion reaction. Due to the different instrumentation and background requirements, experiments designed for the determination of physical (decay) properties have different separation requirements compared to chemical investigations. The use of physical pre-separation for the chemical investigations of transactinides was pioneered at the Lawrence Berkeley National Laboratory (LBNL), California, USA [1,2]. The generally short half-lives of transactinides demand for a fast transfer of the products of the nuclear fusion reaction to the chemistry devices. The required time scales vary from several milliseconds up to seconds. Hence, the size of the focal plane (FP) image of a physical pre-separator plays a major role in the design of attached chemical apparatuses. Here, we present the results of simulations of ion trajectories through the Dubna Gas-filled Recoil Separator II (DGFRS II), a machine recently commissioned at the Superheavy Elements Factory (SHE Factory) of the Flerov Laboratory of Nuclear Reactions, Dubna, Russian Federation [3].

Simulation

Based on the ion trajectory code, developed at LBNL for describing the Berkeley Gas-filled Separator (BGS) [4], an updated version of the ion transport in hydrogen-filled separators was implemented using the magnetic field maps of DGFRS II. The initial ion distribution and trajectories of the nuclear reaction products were generated using SRIM2013 [5]. Thereto, in a specific target of a certain selected thickness, the ions were simulated to be produced according to a Gaussian-shaped excitation function with a 3.5 MeV FWHM considering the energy loss of the heavy-ion beam passing through the target material. The produced ions recoil, with the momentum of the ion beam particles, through the remaining target material [4]. The energy and angular distribution of 10'000 recoiling ions is calculated as input for the DGFRS II ion transport code (DSIM). Subsequently, the statistical charge exchange of the ion with the hydrogen filling gas [6] is superimposed on the transport of the ions in the magnetic fields of the DGFRS II. This leads to trajectories of the ions through the separator that are traced forward towards its focal plane. Thus, information about the place and energy of the recoiling ions in the focal

plane as well as the transmission yield of the separator, as function of the magnetic settings and the magnetic rigidity of the products, are assessable. This data can then be used for the optimization of the design of future chemistry experiments behind the DGFRS II and III at the SHE Factory. In the following we will show two selected cases of simulations: $^{206}\text{Pb}(^{48}\text{Ca}, 2n)^{252}\text{No}$ ($E^* = 22$ MeV) [7] as the benchmark case and $^{242}\text{Pu}(^{48}\text{Ca}, 3n)^{287}\text{Fl}$ ($E^* = 40$ MeV) [8] for the prediction of the envisaged transactinide experiment with Fl/Cn.

Results: $^{206}\text{Pb}(^{48}\text{Ca}, 2n)^{252}\text{No}$ (benchmark)

Figure 1 shows the focal plane distributions obtained for the nuclear reaction with a 0.43 mg/cm² thick ^{206}Pb target, irradiated at an energy of the incident ^{48}Ca ion beam of 240 MeV. Before reaching the target, the ion beam passed through a Ti window and target backing with a total thickness of 0.90 mg/cm². The Bp of the ^{252}No in 1.29 mbar H₂ was calculated as 2.1605 Tm. The magnet current settings of the DGFRS II $Q_v D Q_h Q_v D$ -configuration were 252 A, 513 A, -58 A, 215 A, and 285 A.

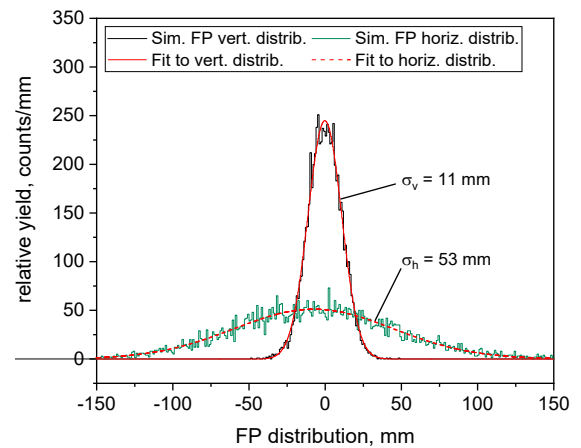


FIGURE 1: Horizontal (green) and vertical (black) distributions of 10'000 ^{252}No ions passing DGFRS II. The corresponding Gaussian fits are indicated (red lines).

The simulations reproduce the experimentally obtained distributions fairly well. The $\sigma_h = 64$ mm and $\sigma_v = 15$ mm, as measured for ^{252}No at the given experimental conditions [9], is in reasonable agreement with the results from the simulations, i.e., $\sigma_h = 53$ mm and $\sigma_v = 11$ mm.

Results: $^{242}\text{Pu}(^{48}\text{Ca}, 3n)^{287}\text{Fl}$ (prediction)

Simulations were carried out for the nuclear reaction of ^{48}Ca with a $^{242}\text{PuO}_2$ target, having a thickness of

0.6 mg/cm² (all other target parameters are identical to the benchmark case above). The H₂ pressure inside the separator was set to 1.16 mbar. A screening for the optimum magnet settings to obtain the smallest focal plane images was performed using first a parameter sweep over quadrupole lens currents Q2 & Q3 (see Fig. 2). Secondly, with the optimum settings of Q2 & Q3, the Q1 setting was optimized (not shown).

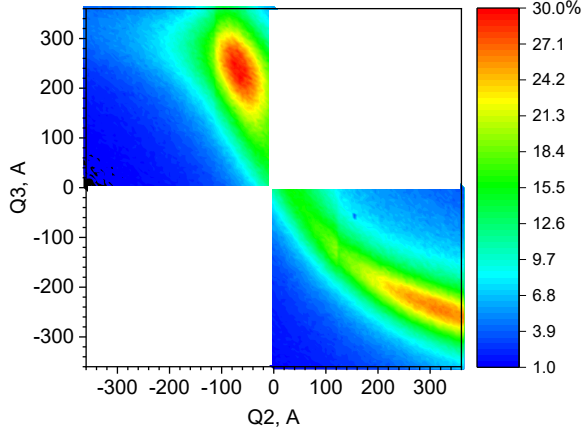


FIGURE 2: Transmission efficiency into a 10 × 6 cm², oval-shaped recoil chamber as a function of quadrupole lens currents Q2 and Q3 (Q1 = 300 A).

Thus, “optimum” magnet current configurations of the DGFRS Q_vDQ_hQ_vD (I) and Q_vDQ_vQ_hD (II) were determined (see Tab. 1). These two configurations were then used to calculate associated input efficiencies for three different geometries of recoil transfer chambers (RTC) attached in the focal plane of DGFRS II (see Tab. 2).

TABLE 1: The currents for the quadrupole lenses in configurations I and II. A negative current corresponds to a horizontally focusing quadrupole. The dipole settings were kept at D1 = 568 A and D2 = 315 A

CONFIG.	Q1	Q2	Q3
I	300 A	-58 A	230 A
II	300 A	315 A	-240 A

The simulated shapes of the focal plane images for configurations I and II of DGFRS II are shown in Figure 3. The ultimate goal of these simulations is the yield optimization for short-lived nuclear reaction products being flushed out of the RTCs connected to the focal plane of the separator. The final RTC design will certainly be a compromise between its inner volume and the area it covers of the focal plane image.

TABLE 2: The maximum input efficiencies of three different RTC geometries mounted in the focal plane of DGFRS II operated in magnet configurations I and II (see Tab. 1).

CONFIG.	GEO. I 20x20 cm square	GEO. II 6 cm round	GEO. III 10x6 cm oval
I	48%	20%	30%
II	36%	20%	25%

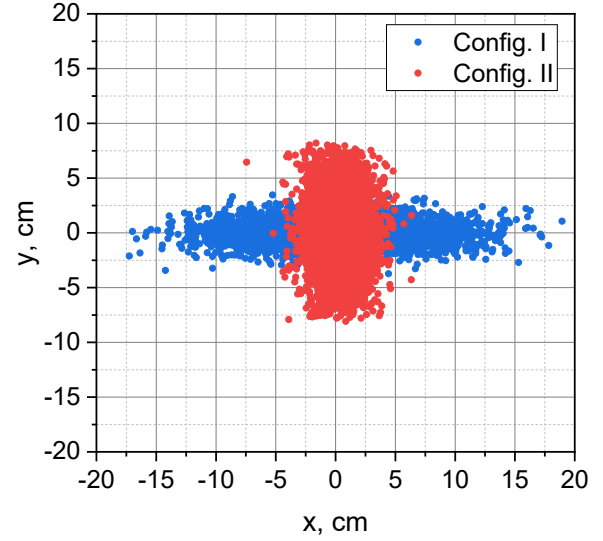


FIGURE 3: The focal plane image of ²⁸⁷Fl after separation in DGFRS II in magnet configuration I (blue) and II (red); for configurational details see Tab. 1.

With a transmission yield of 30% one would expect for the given conditions – assuming ion beam intensities of about 5 pA – four to five ²⁸⁷Fl ions entering the RTC per day. The optimization of the geometry of such a RTC for rapid flush-out times is ongoing.

References

- [1] J. P. Omtvedt et al. *Eur. Phys. J. D*, **45** (2007), pp. 91-97
- [2] Ch. E. Duellmann *Eur. Phys. J. D*, **45**, (2007), pp. 75-80
- [3] A. G. Popeko, *Nucl. Instrum. Methods Phys. Res., Sect. B*, **376** (2016), pp. 144–149
- [4] K. E. Gregorich, *Nucl. Instrum. Methods Phys. Res., Sect. A*, **711** (2013), pp. 47-59
- [5] J. F. Ziegler et al., *Nucl. Instrum. Methods Phys. Res., Sect. B*, **268** (2010), pp. 1818-1823
- [6] Yu. Ts. Oganessian et al., *Phys. Rev. C*, **64** (2001), pp. 064309
- [7] Yu. Ts. Oganessian et al., *Phys. Rev. C*, **64** (2001), pp. 054606
- [8] Yu. Ts. Oganessian, *J. Phys. G: Nucl. Part. Phys.*, **34** (2007), pp. R165–R242
- [9] V. Utyonkov, *private communication*, 2020

On the volatility of PaCl_5 and PaBr_5

H. W. Gäggeler (PSI & Univ. Bern), B. Eichler, R. Eichler, D. T. Jost (PSI)

Introduction

Protactinium is one of the rarest naturally occurring elements. It was discovered 1918 simultaneously by O. Hahn and L. Meitner [1] and by F. Soddy and J. A. Cranston [2]. Early interest in this element came from nuclear energy R & D in connection with the development of a ^{232}Th -based fast reactor, which produces large amounts of ^{233}Pa (see, e.g., [3]). Until G. T. Seaborg's suggestion of a new group of elements, the actinides, Pa was believed to be a *d*-element of group V of the periodic table, the reason being its chemical similarity to Nb and Ta.

In our study, we determined the volatility of PaCl_5 and PaBr_5 in preparation of later experiments with Db, the latest member of group V. In addition, we also investigated different compounds of Pa, presumably the oxyhalides, which, however, have not yet been analyzed and will therefore not be discussed in this contribution.

Experimental

For production of Pa we used the $\text{Th}(p, xn)$ -reaction. In proton-induced nuclear fusion evaporation reactions, the effective target thicknesses are very small, due to the low recoil energies of the formed nuclear reaction products. On the other hand, the energy loss of protons in matter is very small, which allows for using multiple targets. For the herein presented experiments, we used $50 \mu\text{g}\cdot\text{cm}^{-2}$ thick ^{232}Th metal targets on $20 \mu\text{m}$ thick Al foils that were welded on $100 \mu\text{m}$ thick Al plates. These targets were prepared by the target laboratory of GSI, Darmstadt, Germany.

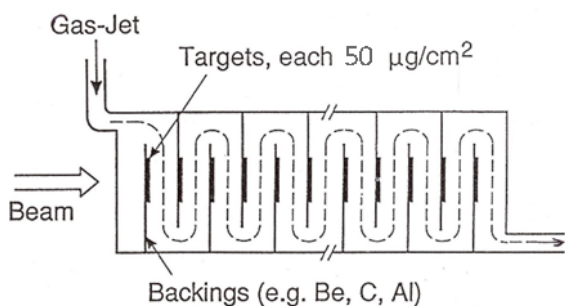


FIGURE 1: Target chamber with 15 ^{232}Th targets.

A 58 MeV proton beam was delivered by the PSI-PHILIPS cyclotron with a proton beam intensity of about $2 \mu\text{A}$. At this proton beam energy, mainly ^{226}Pa and ^{227}Pa are formed in the $(p, 7n)$ - and $(p, 6n)$ -reactions, respectively. A stack of 15 targets was mounted in an irradiation chamber with a dis-

tance of 5 mm between each target (Fig. 1). Consecutive targets had opposed holes, thereby forcing the aerosol containing carrier gas to flow along each target in order to collect recoiling products that escaped individual ^{232}Th -layers with an average recoil range of 0.7 mm. The total energy loss of the proton beam within the target stack was 5 MeV.

The gas jet transportation system was operated with $1 \text{ L}\cdot\text{min}^{-1}$ He carrier gas loaded with either MoO_3 particles (for the study of the chlorides) and KCl (for the study of the bromides). The OLGA II system [4, 5] was used for the measurement of retention times in a quartz column kept at different isothermal temperatures. At the entrance to the column, kept at 900°C , the reactive gases Cl_2 , saturated with CCl_4 (chloride study), and HBr, saturated with BBr_3 (bromide study), were added to the He carrier gas. For the measurements only ^{226}Pa ($t_{1/2} = 1.8 \text{ min}$) was analyzed due to its short half-life, that enabled to achieve saturation activity within about 10 min.

Results and discussion

Fig. 2 and 3 depict the measured yield curves behind OLGA II for the chloride and the bromide system. Due to the strong halogenating strength of both reactive gases and their ability to efficiently, chemically deplete traces of oxygen in the gas, we assume the pure halides were formed and therefore assign the compounds to PaCl_5 and PaBr_5 , respectively.

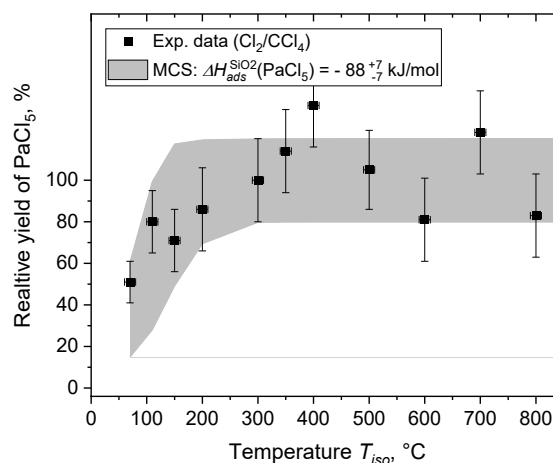


FIGURE 2: Relative yield of ^{226}Pa behind the isothermal quartz column with Cl_2/CCl_4 as reactive gas as a function of column temperature.

In both figures, Monte Carlo simulations (MCS; shaded areas) are shown which describe the experimental results best and allow for a determination of adsorption enthalpies [6] of the chemical species on

the quartz surfaces. There is an empirical correlation of the microscopic adsorption behavior of single atomic chlorides with their macroscopic volatility, expressed as their sublimation enthalpy (see for review [7]). Assuming a similar correlation valid for bromides, PaCl_5 is deduced to be more volatile than PaBr_5 , which is in agreement with similar studies of group V halides [5], where the bromides show lower volatilities.

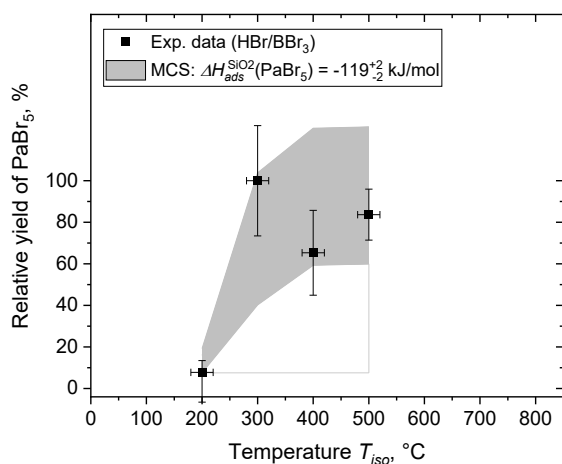


FIGURE 3: Relative yield of ^{226}Pa behind the isothermal quartz column with HBr/BBr_3 as reactive gas as function of the column temperature.

The other way around, the experimental adsorption enthalpies (ΔH_{ads}) can be compared with predicted values based on thermochemical estimates of sublimation enthalpies (ΔH_{subl}) for PaCl_5 and PaBr_5 available in literature [8] using the equation

$$\Delta H_{ads} = (0.600 \pm 0.025) \cdot \Delta H_{subl} + (21.5 \pm 5.2)$$

from [7]. The resulting values are $-\Delta H_{ads} = 99.4 \pm 9.9$ kJ/mol and $-\Delta H_{ads} = 141.4 \pm 8.5$ kJ/mol for the pentachloride and pentabromide, respectively. The deduced adsorption enthalpies shown in Figures 2 and 3 are in fair agreement with these predictions. Thus, the expected trend of an increased adsorption interaction strength towards silica surfaces moving from chlorides to bromides is well reproduced once more. This too, hints also to a correct identification of the chemical state of protactinium in these studies.

References

- [1] O. Hahn, L. Meitner, *Phys. Z.*, **19** (1918), pp. 208-218
- [2] F. Soddy, J. A. Cranston, *Proc. Roy. Soc.*, **94** (1918), pp. 384-404
- [3] H.-J. Born (ed.), *Tagungsbericht der 3. Internationalen Protactinium Konferenz*, 15.-18. April 1969, Schloss Elmau, Germany, 1971 (German Report BMBW-FBK-71-17)
- [4] H. W. Gäggeler et al., *Nucl. Instrum. Methods Phys. Res., Sect. A*, **309** (1991), pp. 201-208

- [5] H. W. Gäggeler, A. Türlér, 'Gas-Phase Chemistry of Superheavy Elements' in: M. Schädel, D. Shaughnessy (eds.), *The Chemistry of Superheavy Elements*, 2nd ed., Springer-Verlag: Berlin Heidelberg, 2014
- [6] I. Zvara, *Radiochim. Acta*, **38** (1985) pp. 95-101
- [7] A. Türlér, V. Pershina, *Chem. Rev.*, **113** (2013), pp. 1237-1312
- [8] D. D. Wagman et al., *J. Phys. Chem. Ref. Data*, **11** (1982), p. 252

New EU-Projects on Liquid Metal Chemistry

J. Neuhausen (PSI)

Introduction

Heavy liquid metals such as lead and lead bismuth eutectic (LBE) are considered as spallation target material for next-generation neutron sources and as coolant of fast neutron spectrum nuclear reactors that are developed to facilitate more efficient use of nuclear fuel as well as transmutation of long-lived nuclear waste. During the operation of such facilities, the heavy liquid metal will be activated by nuclear reactions. Additionally, fission product radionuclides may be introduced into the liquid metal from leaking fuel pins or by fission of the target nuclei in spallation. The chemical behaviour of these radioactive contaminants in the liquid metal - especially their immediate volatilization or volatilization of formed secondary compounds - may affect the safety of such facilities. Throughout the last two decades PSI's Laboratory of Radiochemistry conducted extensive research towards a better understanding of the chemical behaviour of potentially hazardous radionuclides in LBE. This research was triggered by PSI taking a leading role in the development and realization of the prototype liquid metal spallation target MEGAPIE which was operated in the spallation neutron source SINQ in 2006 [1]. After the successful operation of MEGAPIE, LRC continued to contribute to EC-EURATOM funded projects related to heavy liquid metal based nuclear facilities such as EUROTRANS, GETMAT, SEARCH and MYRTE. A summary of this research was published in a recent review [2]. While some of the most urgent questions with respect to the chemical behaviour of radionuclides in lead and LBE have been answered in these projects, many phenomena still need to be understood in more detail, and a number of new questions were raised by results obtained within MYRTE and the preceding projects. This stimulated the two new EURATOM Horizon2020 projects PATRICIA (Partitioning And Transmuter Research Initiative in a Collaborative Innovation Action) and PASCAL (Proof of Augmented Safety Conditions in Advanced Liquid-metal-cooled systems) that have been started end of 2020. These projects are aimed to answer remaining open questions resulting from previous research, but also to address problems that have never been tackled before. Both projects see an increased number of international partners working on topics related to the coolant chemistry within the realm of heavy liquid metal reactors, reflecting an increased interest in the subject.

The present report outlines the research planned to be performed in the two new projects, focussing on the contributions of LRC.



PATRICIA

Among the most important issues that need to be understood in more detail to ensure the safe operation of LBE based nuclear facilities is the low temperature (< 500 °C) evaporation behaviour of the polonium isotopes generated from bismuth during operation of the facilities. Results of previous projects show that oxide layers on the LBE as well as moisture present in the gas phase can lead to formation of highly volatile polonium compounds leading to enhanced volatilization of polonium [3-5]. In PATRICIA, LRC will perform polonium evaporation experiments using LBE samples from the MEGAPIE experiment. These samples are unique in that they contain all the impurities that are generated or incorporated in the LBE by nuclear reactions and corrosion processes in a high power spallation target. The goal of this study is to find out whether the impurities generated during operation of the spallation target influence the evaporation behaviour of polonium. Furthermore, LRC will assess the evaporation of rhodium from LBE using radiotracers present in the MEGAPIE_LBE samples. Additionally, data obtained from transpiration experiments in the MYRTE project will be evaluated to extract data on thallium evaporation from LBE. Finally, LRC will attempt to synthesize LBE samples doped with the elements rhenium, rhodium and osmium, with the purpose of studying their evaporation from the liquid metal. Radionuclides of these elements are formed in non-negligible amounts in LBE-based reactors and spallation targets, and it is suspected that they could evaporate from the liquid metal in form of volatile oxides. In collaboration with LRC, the Joint Research Centre of the European Commission (JRC) in Karlsruhe will study the retention of tellurium, a major fission product and homologue of the hazardous polonium, in LBE using Knudsen Effusion Mass spectrometry (KEMS). Additionally, JRC will attempt to characterise tellurium hydroxides and oxy-hydroxides by matrix isolation combined with Raman and UV-Vis spectroscopy. Besides characterising these volatile tellurium species as such, these studies are also aimed at identifying the volatile polonium compounds observed in earlier studies.

In parallel, University of Gent will perform quantum chemistry calculations to determine the stability of candidates for the volatile polonium containing molecules. These molecules are most likely polyatomic polonium hydroxides and oxyhydroxides. Since the ab-initio methodology that was successfully developed and applied to diatomic polonium-containing molecules in the MYRTE project [6] is computationally too expensive to be applied to such complex molecules, University of Gent has proposed to develop a machine-learning algorithm trained to predict high quality thermodynamic data from computationally less expensive calculations based on Density Functional Theory.

At SCK•CEN, a coupled simulation platform will be developed, combining Gibbs Energy minimization (GEM) and Computational Fluid Dynamics (CFD) software packages. This tool is intended to provide a quantitative understanding of chemical and transport phenomena in lead and LBE cooled systems. Such information is invaluable for the safe operation of the MYRRHA reactor developed at SCK•CEN [7]. In parallel, SCK•CEN will continue to investigate the release kinetics of polonium from LBE in the presence of water vapour using transpiration-type evaporation experiments.



PASCAL

In previous projects, in each series of experiments the evaporation of one specific radionuclide or element from LBE was studied. In the PASCAL project, evaporation experiments will be performed on more complex systems containing two different radionuclides dissolved in LBE. In particular, LRC will study the influence of the interaction of caesium and iodine dissolved in LBE on their evaporation. This study was triggered by results of thermodynamic assessments indicating that evaporation of these two fission products could be enhanced by the formation of a caesium iodide phase that separates from the liquid metal. LRC will also study the evaporation and deposition of the important fission product and polonium homologue tellurium from LBE using the transpiration method and thermochromatography. This study is complementary to the KEMS studies performed at JRC in the PATRICIA project and aims at the characterisation of particularly volatile species that might form in moist atmospheres in analogy to the behaviour of polonium. In parallel, SCK•CEN intends to characterise the fission product molecules evaporated from the LBE using molecular beam mass spectrometry. Within PASCAL, it is planned to

investigate iodine, tellurium, and caesium gas molecules released from the heavy liquid metals lead and LBE, with the aim to identify the different molecules forming under variation of the gas phase composition.

Other subtasks of PATRICIA and PASCAL will extend the scope of the chemical studies related to the behaviour of lead and LBE and the impurities contained therein. One prominent topic, which is going to be investigated in a collaboration of TU Delft, Chalmers University in Gothenburg and JRC in Karlsruhe, is studying the interaction of nuclear fuel with the liquid metal in order to understand to what extent and by which mechanisms radioactive material can be transferred from the fuel to the coolant. Furthermore, the first systematic study on the formation of lead and LBE aerosols and their transport in a gas stream will be performed in a collaboration of groups at SCK•CEN and KTH Stockholm.

References

- [1] W. Wagner et al., *J. Nucl. Mater.* **377** (2008), pp. 12-16
- [2] J. Neuhausen, *CHIMIA* **74(12)**, (2020), pp. 976-983
- [3] M. Rizzi et al., *J. Nucl. Mater.* **450** (2014), 304-313
- [4] B. Gonzalez Prieto, PhD Thesis. KU Leuven 2015
- [5] E. A. Maugeri et al., *J. Nucl. Mater.* **450** (2014), 292-298
- [6] M. A. J. Mertens et al., *J. Phys. Chem. Letters* **10** (2019), 2879-2884
- [7] MYRRHA website: <https://myrrha.be/>

Separation of ^{179}Ta for the production of ^{180}Ta via neutron capture on radioactive ^{179}Ta

I. Kajan (PSI), R. Garg, C. Lederer-Woods (Univ. of Edinburgh), D. Schumann (PSI)

Introduction

$^{180\text{m}}\text{Ta}$ is the rarest isotope in nature with an unusually low abundance considering the yields of various processes in its mass region [1]. Its astrophysical origin is still an open question. It is thought to be produced during the slow neutron capture process in the Asymptotic Giant Branch stars through two mechanisms: via the β -decay of $^{180\text{m}}\text{Hf}$ (formed via n-capture on ^{179}Hf) [2], and via the n-capture on ^{179}Ta (formed via the β -decay of thermally excited ^{179}Hf) [3]. The former route has been studied previously and it was shown that this mechanism alone is not sufficient to explain the observed abundance of $^{180\text{m}}\text{Ta}$ [4]. In the present project, we aim to investigate the latter of mechanism, and this requires the cross-section measurement of the n-capture reaction on the ^{179}Ta isotope which is unstable with a half-life of 1.82(3) years. The presented work describes the efforts towards the separation of ^{179}Ta originating from the proton irradiated hafnium metal, in order to supply pure tantalum fraction for the neutron cross section experiments.

Separations and outcome

The ^{179}Ta sample was produced via $^{180}\text{Hf}(p,2n)^{179}\text{Ta}$ reaction by impinging 27 MeV protons on a high purity hafnium disk of 1 mm thickness and 15 mm diameter. The proton irradiation was carried out for ~ 7 hours with an average beam current of 32 μA at MC40 cyclotron, University of Birmingham. Unavoidably, also other isotopes were produced during the proton bombardment, inducing a significant dose rate from the sample. Therefore, after transfer of the sample to PSI, γ -ray spectroscopic measurements were performed in order to characterize γ and X-ray emissions from the sample. The obtained spectra with radionuclides attributed to the emissions are shown in Figures 1 and 2. The main dose rate contributor was identified to be ^{175}Hf produced by $^{nat}\text{Hf}(p,xn)^{175}\text{Ta}$ reaction and subsequent decay of ^{175}Ta . Other significant radioactive impurities were ^{172}Hf in secular equilibrium with its radioactive daughter ^{172}Lu . As shown later, these radioactive isotopes of hafnium produced during the irradiations were conveniently used for the decontamination factor determination during the radiochemical separations.

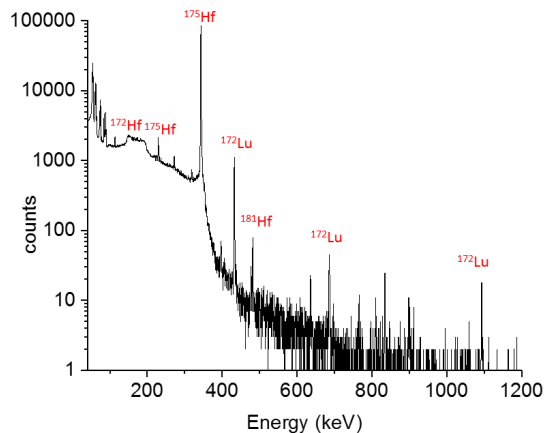


FIGURE 1: Spectrum of the proton irradiated hafnium sample.

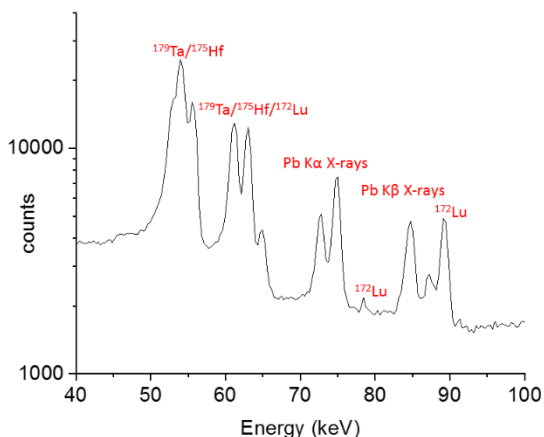


FIGURE 2: Spectrum of hafnium sample scaled for lower energies.

Separations on TBP resin

The partial dissolution of the sample was performed in concentrated hydrofluoric acid. Followed by the dilution with deionized water from MilliQ system yielding into $1 \text{ M}\cdot\text{L}^{-1}$ concentration and applied to the chromatographic column (internal diameter 5mm, height 150 mm) filled with TBP resin (Triskem). During this separation step the majority of hafnium matrix passes through the column while ^{179}Ta was extracted by the resin. Elution of ^{179}Ta from the resin was thereafter performed by 0.1 M HCl. After the ^{179}Ta fraction was collected, the decontamination factor from hafnium was determined to be in the order of $3\cdot 10^2$. The decontamination factor (Df) is defined in Eq. 1.

$$Df = \frac{C_{Hf}^0}{C_{Hf}^s} \approx \frac{A_{175Hf}^0}{A_{175Hf}^s} \quad \text{Eq. 1.}$$

Where C^0 and C^s represent relative hafnium concentrations, while A^0 and A^s represent the radioactivity of ^{175}Hf demonstrated by its 343.4 keV γ -ray emission from the sample before and after the separation. As radioactivity of the sample represented by ^{175}Hf is proportional to the total concentration of hafnium in the sample the decontamination factor could be determined from γ -ray spectroscopic measurements.

Separation on TEVA resin

The second separation step was based on the method developed by Snow et.al [5] The eluate from TBP resin was evaporated to dryness and re-dissolved in 6 M HCl/0.02 M HF mixture. The sample was thereafter applied to a chromatographic column filled with 2 grams of TEVA resin (Triskem). After the loading, the column was continuously washed with the same acid composition till no ^{175}Hf signal was found in eluate. The elution of ^{179}Ta from the column was performed with 6 M HNO_3 /0.02 M HF mixture. After the γ -spectroscopic analysis only weak signal of ^{175}Hf was found in the eluate containing ^{179}Ta , yielding to the minimum separation factor in the order of 10^4 . Representative γ -ray spectra used for the decontamination factor determination are presented in Figure 3. Note that the spectrum before the separation was measured at 80 mm distance from detector, whether the separated sample was placed on the detector endcap yielding the scaling factor of ca. 280.

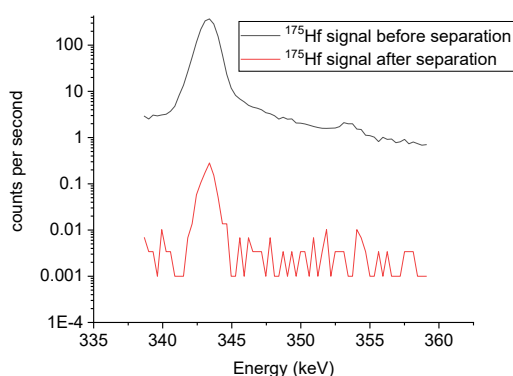


FIGURE 3: Measured count rate of the 343.4 keV γ - line originating from the decay of ^{175}Hf before and after the separation on TEVA resin.

The separation procedure on TEVA resin was repeated once more without the use of additional radiotracers in order to remove last traces of hafnium from the sample. The eluate was free from the ^{175}Hf

signal in the spectra collected over 24h measurement time. The overall chemical yield of ^{179}Ta was determined to be $(80 \pm 10)\%$. Overall, 2.323(35) MBq of ^{179}Ta could be produced by this method.

References

- [1] Zs. Németh et al., *Astroph. J.*, **392** (1992), pp. 277-283
- [2] H. Beer and R. Ward, *Nature* **291** (1981), pp. 308-310
- [3] K. Yokoy and K. Takahashi, *Nature*, **305** (1983), pp. 198-200
- [4] S. Kellog and E. B. Norman, *Phys. Rev. C*, **46** (1992), pp. 1115
- [5] M. S. Snow et al., *J. Chromatogr. A*, **1484** (2017), pp. 1-6

Towards an accurate determination of the ^{179}Ta half-life using γ -ray spectroscopy

M. Veicht (EPFL & PSI), I. Kajan, D. Schumann (PSI)

Introduction

Half-life measurements of radionuclides performed by γ -ray spectroscopy present a convenient tool for the nuclear data determination. Very good energy resolution of gamma spectroscopic systems greatly diminishes the demand for a radiochemical purity of the measured sample. Drawbacks, however, related to these measurements, are the relatively low efficiency of the germanium detectors, the need for suitable γ - or X-ray emissions of the examined radionuclides including well-known branching ratios and transition probabilities, and instability of the HPGe systems. Yet, γ -ray spectroscopy is a convenient tool used to refine or confirm the previously measured half-lives for γ -ray emitting nuclides, by directly following the decrease of the respective nuclide's activity. It is noteworthy to mention that the half-life values of surprisingly many relatively short-lived ($T_{1/2} < 10$ a) radionuclides were measured only once, or the measured values are very scattered. Consequently, many half-life values call for new measurements.

^{179}Ta is a good example of such a case. Its currently recommended value ($T_{1/2} = 1.82(3)$ a) is based on a weighted average of two measurements, 664.9(14) d and 588(10) d, which are somewhat biased [1]. Thus, an accurately determined half-life of ^{179}Ta is a prerequisite for its use, as being considered of relevance to s-process analyses by means of stellar energies $^{179}\text{Ta} (n,\gamma) ^{180m}\text{Ta}$ cross sections. So far, the ^{180m}Ta abundances claimed by the various models are limited by uncertainties in the underlying nuclear physics data [2]. Since ^{179}Ta decays via electron capture into stable ^{179}Hf , the decay of ^{179}Ta is accompanied by several X-ray and Auger-electron emissions. The most prominent X-ray emissions in the decay of ^{179}Ta are 54.6 keV ($I=13.6\%$) and 55.79 keV ($I=23.7\%$), providing suitable energies for the HPGe system to follow the decrease of the radioactivity over time.

In this report, we present the efforts towards determining the ^{179}Ta half-life utilizing γ -spectroscopy, applying a reference source method.

Experimental

Sample preparation

The sample containing ^{179}Ta originated from the separations of proton irradiated hafnium matrix as described in [3].

A point like source was prepared by evaporation of 100 μL ^{179}Ta solution, with high specific activity of approx. 10 kBq \times mL $^{-1}$ on a circular polyethylene foil with a diameter of 2.5 cm (specified density = 21.3 ± 1.8 mg \times cm $^{-2}$). Afterwards, 50 μL of ^{44}Ti ($T_{1/2} = 59.1(3)$ a) solution, containing around 2 kBq of activity, was evaporated on the same spot. After that, the source was sealed with scotch tape and attached onto a circular sample holder assuring the stable geometrical position against the detector over the campaign period. The sample holder was thereafter glued onto the distancer, providing a distance of 80 mm from the detector endcap.

Gamma measurements

For the half-life determination, the method measuring the ratios of activities of the investigated nuclide (^{179}Ta) against the reference nuclide with a well-known half-life (^{44}Ti) for each measured spectrum has been utilized as proposed by Parker [4]. This method greatly decreases errors originating from dead time corrections or long-term instabilities of the detector system compared to the direct activity measurements. The measurements were performed on an n-type Broad Energy Germanium detector (Mirion Technologies, Inc., U.S.A) with a carbon endcap providing good sensitivity for the low energy emissions. During the campaign, the ratios between the 54.6 keV and 55.79 keV X-rays originating from the decay of ^{179}Ta against the 67.9 keV and 78.3 keV γ -ray emissions from ^{44}Ti decay have been followed. As the energy of the $K\alpha_1$ and $K\alpha_2$ lines are very close, their energies can be resolved only as a doublet, as shown in Fig 1. The net count rates from the ^{179}Ta doublet area were summed up for the evaluations.

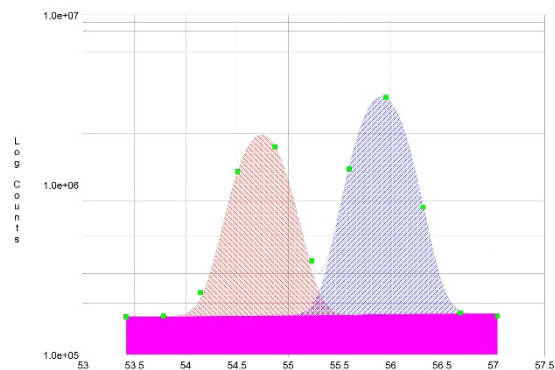


FIGURE 1: Representative peak shape of the 54.6 keV and 55.79 keV lines originating from the decay of ^{179}Ta .

Half-life determination

The ratio of the counts (or counts per live time) in the ^{179}Ta and ^{44}Ti peaks, corrected for decay during the measurement, yield an exponential curve defined by Eq. 1:

$$\frac{N_{\text{Ta}}(t)}{N_{\text{Ti}}(t)} \cdot \frac{F_{\text{cTa}}}{F_{\text{cTi}}} = \frac{A_{\text{Ta}}(t_0)}{A_{\text{Ti}}(t_0)} \cdot \frac{\varepsilon_{\text{Ta}}(t)}{\varepsilon_{\text{Ti}}(t)} \cdot e^{-(\lambda_{\text{Ta}} - \lambda_{\text{Ti}})t} \approx C e^{-(\lambda_{\text{Ta}} - \lambda_{\text{Ti}})t} \quad (\text{Eq. 1})$$

in which $N(t)$ refers to the net peak area (per live time) at time t . F is the decay correction factor [5]. $A(t_0)$ is the activity at the start of the campaign. $\varepsilon(t)$ represents the full-energy peak detection efficiency, which is interpreted broadly to include a non-exhaustive list of variables, such as variations in the counting geometry, source integrity, peak fitting, dead time, and pulse pileup. The assumption of the method is that the product of the factors in front of the exponential is quasi constant, equal to the factor C . Least-squares fit of an exponential function to the experimental data yields the amplitude C and the slope $(\lambda_{\text{Ta}} - \lambda_{\text{Ti}})$ from which the half-life of ^{179}Ta can be conveniently determined.

Results and Discussion

The presented results are only preliminary and are based on 72 data points collected during the measurement campaign, currently ongoing for 120 days. The measured net count rate ratio of the ^{179}Ta (54.6 +55.79) keV peaks and the ^{44}Ti (67.9+78.3) keV peaks as a function of time is shown in Figure 2. The line is fitted with an exponential function from the right side of Eq. 1. The corresponding normalized residuals of the measured $^{179}\text{Ta}/^{44}\text{Ti}$ count ratios are presented in Figure 3.

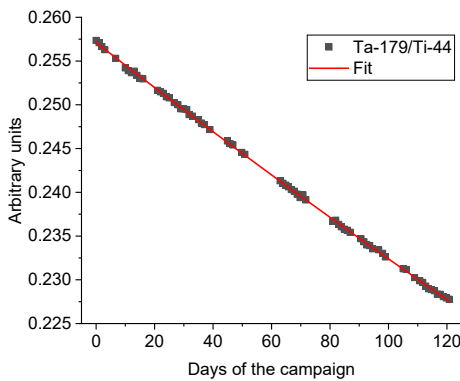


FIGURE 2: Measured net count ratios ($^{179}\text{Ta}/^{44}\text{Ti}$) with a fitted exponential function as a function of time.

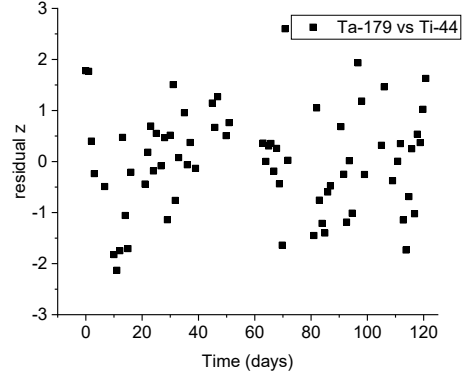


FIGURE 3: Residuals of the fit.

Based on carefully executed spectrometric measurements, applying the reference-source method with ^{44}Ti , the half-life of ^{179}Ta was preliminarily determined to be 664.9(35) d. This preliminary result is compatible with the currently recommended value of 664.7(109) d but with a significantly lower uncertainty (Table 1). The measurement campaign is planned to continue for approximately one more half-life period.

TABLE 1: Overview of the half-lives, including our preliminary value, based on the measurements from the current campaign.

YEAR	1950, 1963	1974-1	1974-2	THIS WORK
$T_{1/2}$ (D)	~ 600*	664.9	588	664.9
$\Delta T_{1/2}$ (D)	-	14	10	3.5
Uncertainty (%)	-	2.11	1.70	0.53

*likewise reported without an uncertainty.

Acknowledgement

This project is funded by the Swiss National Science Foundation (SNSF) as part of SINERGIA No.177229. Moreover, funding from Swissnuclear (LRC_20_02) is greatly appreciated.

References

- [1] C. M. Baglin, *Nucl. Data Sheets*, **110** (2009), pp. 265-506
- [2] F. Käppeler et al., *AIP Conf. Proc.*, **529** (2000), pp. 307-314
- [3] I. Kajan et al., *LRC Annual Report 2020* (2021)
- [4] J. L. Parker, *Nucl. Instrum. Methods Phys. Res., Sect. A*, **286** (1990), pp. 502-506
- [5] S. Pommé, *Metrologia*, **52** (2015), p. 51

⁵³Mn half-life determination

J. Ulrich (PSI), P. Cassette (LNE/LNHB), R. Dressler (PSI), N. Kneip (JGU Mainz), K. Kossert (PTB), X. Mougeot (LNE/LNHB), D. Schumann (PSI), P. Sprung (AHL/PSI), D. Studer, K. Wendt (JGU Mainz)

Introduction

⁵³Mn is a short-lived cosmogenic radionuclide mainly produced in alpha-rich freezeout of explosive burning in both thermonuclear and core-collapse supernovae explosions [1, 2]. Analyses of meteoritic samples proved the presence of ⁵³Mn in the protosolar nebula. This enables the usage of ⁵³Mn/⁵³Cr as sensitive chronometer for dating of events in the early Solar System [3]. ⁵³Mn from more recent stellar events is observed in form of « cosmic fallout » on the Earth [4]. Such accreted interstellar dust can help to identify and date supernovae occurred in our astronomical neighborhood within the last 30 Ma. Small amounts of ⁵³Mn are also produced by bombardment with high-energy cosmic rays in surface-near rocks on the Earth. The utilization of terrestrial spallogenic ⁵³Mn for exposure dating has been successfully shown in [5]. Thanks to the development of accelerator mass spectrometry (AMS), there is a growing interest in the use of ⁵³Mn in the earth sciences, both for terrestrial and extra-terrestrial samples. The current usability of ⁵³Mn as radio-chronometer is, however, limited due to the large uncertainties of associated nuclear data.

Half-Life Determination

Precise and accurate value of the half-life is a mandatory prerequisite for successful application of ⁵³Mn in geological dating both on the Earth and in space. Last half-life measurements of ⁵³Mn were published in the early 1970s. But the 10% relative uncertainty of the currently adopted value of 3.7(4) Ma years [6] is unsuitable for precise dating and must be reduced below 3% to obtain reasonable results. Re-measuring the half-life with modern methods could not only reduce the uncertainty to the requested level, but even explain some discrepancies discussed in the literature, e.g. when comparing data of the ⁵³Mn/⁵³Cr chronometer with other chronometers in meteorites formed in early Solar System [7].

Half-lives larger than few hundred years cannot be measured directly by simple observation of the decay. Instead, the following basic relation must be utilized:

$$t_{1/2} = \ln(2) \cdot \frac{N}{A} \quad (1)$$

where N and A denote the ⁵³Mn concentration and specific activity of the sample, respectively and $t_{1/2}$ the half-life. The determination of the ⁵³Mn content was performed by multi-collector (MC)-ICP-MS.

As ⁵³Mn decays by electron capture (EC) directly into the ground state of its daughter ⁵³Cr; the decay is not accompanied by the emission of gamma-rays. Only low-energy relaxation radiation (electrons and X-rays) is emitted during the re-arrangement of the electronic shells after the decay to the daughter nuclide. Liquid scintillation (LS) counting is the method of choice for activity determination of low and medium Z pure EC-decay radionuclides like ⁵³Mn due to relatively high detection efficiency compared with other methods. The sample used for LS measurements has to be of high radiochemical purity because of the limited spectroscopic capabilities of LS counting. ⁵³Mn material available at PSI was extracted from highly-activated accelerator waste [8]. Whereas other radiochemical impurities could be removed from the ⁵³Mn fraction by chemical methods, it still contained considerable activities of ⁵⁴Mn since isotopes of the same element behave principally identically during chemical treatment. Thus, mass separation by laser resonance-ionization mass-spectroscopy was performed using the RISIKO separator at University Mainz. A novel three-step ionization scheme was developed at Univ. Mainz, enabling separation and implantation of manganese with an overall efficiency of up to 30% [9]. Even at a high implantation current of 100 nA, necessary to process the required amounts of ⁵³Mn, efficiencies between 10% and 20% could be maintained. A total of 1.2 kBq (or 2×10^{17} atoms) ⁵³Mn was mass separated and implanted into three 6 μ m thick Al foils (an example is shown in Fig. 1) during a three week campaign. This amount is conveniently measurable by LS counting, even when split into several individual samples.

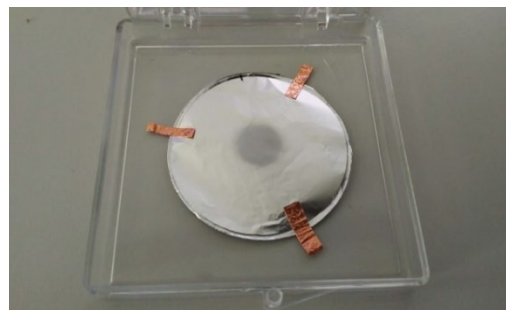


FIGURE 1: One of the three 6 μ m Al foils with implanted ⁵³Mn. The implantation area is visible as a darker spot of about 12 mm diameter in the middle of the foil.

Central parts of the foils with diameter of 13 mm, slightly larger than the visible spots with implanted

^{53}Mn , were punched out and completely dissolved in 1 mL warm, concentrated HCl (TraceSelect Ultra). The solution was evaporated to dryness and the residue re-dissolved in 0.7 mL 0.1 M HCl, prepared from HCl of TraceSelect Ultra grade and MilliQ water. Major part of this stock solution was shipped to the PTB in a crimped glass vial. Preliminary studies were performed at PSI to test the compatibility as well as the long-term stability of model solutions of similar chemical composition as the ^{53}Mn stock solution with the commonly used Ultima Gold scintillator

^{53}Mn concentration in Sample

A small aliquot of the stock solution was kept for analysis by ICP-MS at the Hotlaboratory facility of PSI. There, all mass spectrometric measurements were conducted using a Nu Instruments Plasma 3 MC-ICP-MS at a resolving power above 8000. The ion beams of masses 52 up to 59, covering besides ^{53}Mn the main isotopes of the elements chromium to cobalt, were collected simultaneously in separate Faraday cups. The Faraday cup signals were corrected for instrumental background separately by subtracting the signal obtained prior to each measurement using the same pure 0.28 M HNO_3 solution as it was used in the preparation of all standards and sample analytes. Instrumental mass discrimination was characterized and corrected for using the exponential law [10]. The necessary corrections for the samples were done either normalizing internally to the natural isotopic ratio of $^{57}\text{Fe}/^{58}\text{Fe}$ or externally, measured mixed natural Fe-Cr standard solutions at equivalent signal intensities and normalizing the results afterwards to the natural abundance (see [11]) of $^{57}\text{Fe}/^{56}\text{Fe} = 0.023094$ or $^{53}\text{Cr}/^{52}\text{Cr} = 0.11339$.

The Mn-55 concentration was determined by the gravimetric standard addition method using Fe as an additional internal standard [12]. In addition, the reverse isotope dilution technique [13] was employed to reduce the uncertainties of the measured isotopic ratios. The absolute number of ^{53}Mn atoms in the stock solution was obtained from the measured isotopic ratio $^{53}\text{Mn}/^{55}\text{Mn}$ of a Mn-standard-free analyte and the previously measured total ^{55}Mn concentration. This procedure yields a value of $1.6075(51) \times 10^{17}$ atoms ^{53}Mn per g stock solution.

Specific activity of ^{53}Mn sample

Activity measurements were carried using the TDCR (triple-to-double-coincidence ratio) method [14] in two custom-built counters at PTB and three TDCR counters developed at LNHB. The LS samples were measured first at PTB in Braunschweig, afterwards at LNHB in Saclay and eventually again at PTB for consistency check reasons. All measurement results agree well and the LS samples were found to be stable at least over several months. The analysis of the

experimental data were carried out with state-of-the-art methods using a stochastic model for the atomic rearrangement and taking into account all required corrections [15]. Supplementary measurements were carried out using commercial counters. The obtained LS spectra confirm the absence of any radioactive impurity. The activity determination requires some nuclear decay data as input for the efficiency computation. In particular, the fractional electron-capture probabilities of the 2nd forbidden non-unique transition are needed. Improved theoretical calculations, which take all required corrections and the atomic and nuclear structure into account, are still ongoing [16]. Hence, the activity determination and the related uncertainty estimation are not yet completed. As a preliminary result, the activity concentration of the ^{53}Mn stock solution was determined to be 1.0367(79) kBq/g.

Half-Life of ^{53}Mn

Using both values, a preliminary value of ^{53}Mn half-life of 3.406(28) Ma is obtained according to Eq. (1). This value is compatible with previous measurements, but its combined standard uncertainty is now almost an order of magnitude lower than in previous measurements. Therefore, this value qualifies ^{53}Mn as precise dating tool for the desired applications in geosciences.

References

- [1] K. Maeda, *et al.*: *Astrophys. J.* **712** (2010) 624
- [2] F.-K. Thielemann, *et al.*: *Astrophys. J.* **460** (1996) 408
- [3] G.W. Lugmair and A. Shukolyukov: *Geochim. Cosmochim. Acta* **16** (1998) 2863
- [4] D. Koll, *et al.*: *Phys. Rev. Lett.* **123** (2019) 7
- [5] J. Schaeffer, *et al.*: *Earth Planet. Sci. Lett.* **251** (2006) 334
- [6] M. Honda and M. Imamura: *Phys. Rev. C* **4** (1971) 1182
- [7] L. E. Nyquist, *et al.*: *Geochim. Cosmochim. Acta* **73** (2009) 5115
- [8] D. Schumann, *et al.*: *J. Phys. G* **35** (2008) 014046
- [9] N. Kneip: Master Thesis JGU Mainz (2018)
- [10] A.-L. Hauswaldt, *et al.*: *Accredit. Qual. Assur.* **17** (2011) 129
- [11] J. Vogl and W. Pritzkow: *MAPAN – J. Metrol. Soc. India* **25** (2010) 135
- [12] W. A. Russell, *et al.*: *Geochim. Cosmochim. Acta* **42** (1978) 1075
- [13] J. Meija, *et al.*: *Pure Appl. Chem.* **88** (2016) 293
- [14] R. Broda, *et al.*: *Metrologia* **44** (2007) S36
- [15] K. Kossert and A. Grau Carles: *Appl. Radiat. Isot.* **68** (2010) 1482
- [16] X. Mougeot: *Appl. Radiat. Isot.* **154** (2019) 108884

Half-life measurement of ^{154}Dy via the “direct method”

N. M. Chiera, Z. Talip, R. Dressler (PSI), P. Sprung (AHL/PSI), D. Schumann (PSI)

Introduction

Based on the stellar nucleosynthesis theory, all the elements heavier than boron composing the Universe have been produced through nuclear reactions taking place in stars, during supernova explosive events, and *via* cosmic ray spallation [1]. Collision between neutron stars was appointed as a source of neutron-rich matter as well [2]. Nowadays, one of the main challenges in nuclear astrophysics is to understand and to reconstruct the sequence of reactions that lead to the known abundances of stable isotopes in the Solar System. Benchmark radionuclides for astrophysics studies are for example the radiolanthanides ^{146}Sm , $^{148,150}\text{Gd}$ and ^{154}Dy [3]. From the analysis of the abundances of these radionuclides and their daughters, for example in meteorites, it is possible to investigate the circumstances that led to the formation of the Sun and of the first solar system solids. Among these radionuclides, ^{154}Dy is of especial interest since through its pure α -decay chain (i.e., the decay sequence $^{154}\text{Dy} \rightarrow ^{150}\text{Gd} \rightarrow ^{146}\text{Sm} \rightarrow ^{142}\text{Nd}$), it influences the isotopic composition of stable Nd in the Solar System, and it directly contributes to the $^{146}\text{Sm}/^{142}\text{Nd}$ isochron method used as a Solar System clock [4]. It is apparent that for these studies an accurate knowledge on the nuclear properties of the above-mentioned radionuclides is essential. However, the currently accepted half-life data of ^{154}Dy ($t_{1/2} = 3.0 \pm 1.5$ My) has 50 % uncertainty [5]. The latter derives from the revision made in ref [6] of the works of MacFarlane (1.5 ± 0.9 My) [7] and Gono (4 My) [8]. In addition, two other half-life values for ^{154}Dy with high uncertainties are available in literature, i.e., 2.9 ± 1.5 My [9] and 10 ± 4 My [10].

Methods

For the determination of $t_{1/2} \gg 100$ years, the so-called “direct method” is applied. This consists on the determination of the number of atoms of interest per gram of solution (N) using ICP-MS or MC-ICP-MS, followed by the measurement of its specific activity (A):

$$t_{1/2} = \frac{N \cdot \ln 2}{A} \quad (1)$$

In this report, a preliminary result on the ^{154}Dy half-life is presented.

A pure Dy fraction containing the α -emitter ^{154}Dy ($E_{\alpha} = 2.87$ MeV ($I_{\alpha} = 100\%$)) was separated from irradiated Ta samples, as described in [11]. The concen-

tration of ^{154}Dy in the retrieved fraction was determined as 1.497 nmoles per gram of solution (solvent: 1 M HNO_3), with an uncertainty of 3.7% (1 SD %) using SF-ICP-MS (Thermo Fisher Scientific Element 2 and MC ICP MS (Nu Instruments Plasma 3). SF-ICP-MS analysis used an external standard calibration scheme in which several dilutions of a Dy standard solution at concentrations bracketing one of the sample solution were repeatedly analyzed (before, in-between, and after the replicate analysis of the sample solution). The concentration of ^{154}Dy was calculated from the amount of ^{161}Dy in the sample and from the $^{154}\text{Dy}/^{161}\text{Dy}$ isotope ratio in solution, which was determined by MC-ICP-MS. ^{161}Dy was chosen due to the absence of isobaric interferences for mass 161. ^{nat}Er was added to the sample solution for MC-ICP-MS analysis allowing for an empirical, semi-external Er-based mass discrimination correction. For the determination of the activity of ^{154}Dy , an aliquot of the Dy fraction (2.774098 g of solution, corresponding to 4.153 nmoles of ^{154}Dy) was taken for the preparation of a thin radioactive source with the molecular plating technique. The electro-deposition yield was calculated by following the activity of the ^{159}Dy tracer using γ -ray spectrometry ($t_{1/2} = 144.4$ d, $E_{\gamma} = 58$ keV (2.3 %)) contained in the Dy sample. Efficiency calibration was performed with a ^{133}Ba ($t_{1/2} = 10.54$ y, $E_{\gamma} = 80.99$ keV (32.9 %)) source allowed for quantifying the total activity of the ^{159}Dy tracer in the Dy solution being 286 Bq. The molecular plating parameters described in [12] were applied. However, at those conditions no electro-deposition of ^{159}Dy was observed. Instead, the formation of a brown, hydrophilic compound was obtained. The compound was soluble in acidic water media, with the tendency to form a colloidal suspension in organic solvents like iPrOH. The formation of a Dy polymeric compound with electrolyzed iPrOH and with residues of the chelating agent HIBA used in the last step of separation from the Ta matrix is postulated. Characterization of the observed compound is still pending. Hence, a different procedure for the preparation of the electrodeposition solution was followed. The aliquot was dried at 70°C under a N_2 flow, dissolved in 6 M HNO_3 to promote the formation of nitrate species, and evaporated to dryness. Any organic species were digested by addition of modified aqua regia (1.5 mL H_2O_2 + 4.5 mL conc. HCl + 1.5 mL conc. HNO_3). The solution was then evaporated to dryness (80°C in N_2 flow), and re-dissolved in a mixture of 2 mL conc. HNO_3 , 6 mL conc. HCl , and 2 mL conc. HF for the destruction of any silica compound that might derive from the radiolysis

of the ion exchange resins used in the separation of the Dy fraction from the Ta matrix. The solution was then evaporated to dryness (80°C in N₂ flow), dissolved in 1 M HNO₃, and re-evaporated to dryness (70°C in N₂ flow). Finally, the electroplating solution was obtained by adding to the dried solid a 50:50 MeOH:iPrOH mixture, for a total volume of 10 mL. The electrodeposition of ¹⁵⁴Dy on a graphite foil (15 μm) was achieved in 8 hours, by applying a constant voltage of 550 V. The distance between the two electrodes was 10 mm. The measured activity of the ¹⁵⁹Dy deposited on the graphite foil was 1.12 Bq. It follows that the amount of ¹⁵⁴Dy electroplated was 9.751×10^{12} atoms. The activity of the ¹⁵⁴Dy plated on the graphite foil was quantified by α-spectrometry. The efficiency of the α-spectrometer was derived by measuring the count rate of a certified ²⁴¹Am source with activity $A = 442 \pm 8$ Bq @11.12.20. From the α-spectrum shown in Fig. 1, it was possible to calculate the ¹⁵⁴Dy activity of 0.18 Bq. A slight contamination of ¹⁴⁸Gd ($E_{\alpha} = 3.18$ MeV ($\alpha = 100\%$)), contained in the separated Dy fraction, was visible as well. The contribution of the count rate of ¹⁴⁸Gd to the ¹⁵⁴Dy peak was estimated to be <5%.

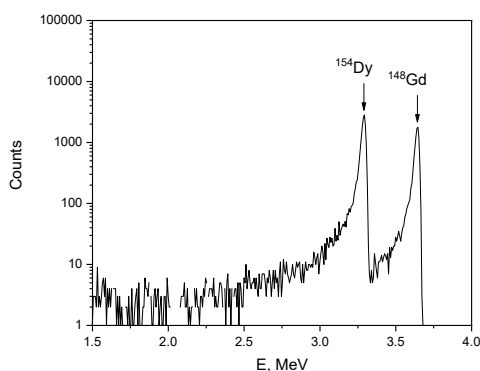


FIGURE 1: α-spectra of the electrodeposited ¹⁵⁴Dy on a graphite foil. The α-peak of ¹⁴⁸Gd, contained in traces in the Dy separated fraction, is visible as well.

Results and Discussion

Applying Equation 1, a preliminary half-life value of 1.18 My for ¹⁵⁴Dy was determined, with an estimated total uncertainty below 10%. The $t_{1/2}$ value derived in this work is in agreement with the calculated $t_{1/2} = 1.2$ My [13]. Using $t_{1/2} = 1.18 \pm 0.12$ My obtained in this work, the production cross-sections of ¹⁵⁴Dy in proton-irradiated Ta targets, reported in [14], were recalculated. As shown in Fig. 2, a significant increase in accuracy of the experimental excitation function for ¹⁵⁴Dy was achieved, in agreement with theoretical values obtained with INCL++ [15] and ABLA 07 codes [16]. For the sake of completeness, the comparison with the experimental cross-

section results calculated using $t_{1/2} = 3.0 \pm 1.5$ My are depicted as well. An independent α-activity measurement will be conducted at TU Dresden in order to corroborate the $t_{1/2}$ deduced in this work.

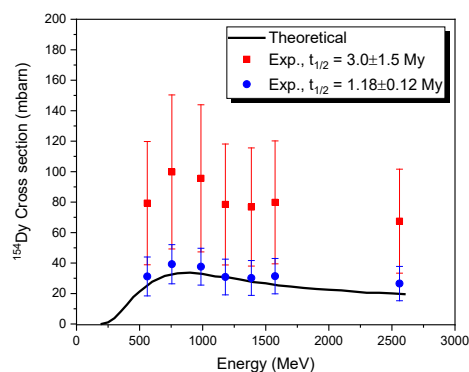


FIGURE 2: Excitation functions for the production of ¹⁵⁴Dy in proton irradiated Ta targets.

Acknowledgement

This project is funded by the Swiss National Science Foundation (SNF grant no 200021-159738).

References

- [1] A. K. Olive et al., *Phys. Rep.*, **333** (2000), pp. 389-407
- [2] D. Eichler et al., *Nature*, **340** (1989), pp. 126-128
- [3] G. Shaviv (Ed.), *The synthesis of the elements: the astrophysical quest for nucleosynthesis and what it can tell us about the universe*, Springer Science & Business Media, 2012
- [4] N. M. Kinoshita et al., *Science*, **335** (2012), pp. 1614-1617
- [5] C.W. Reich, *Nucl. Data Sheets*, **110** (2009), pp. 2257-2532
- [6] N.E. Holden, Brookhaven National Lab. Report BNL-NCS-36960 (1985), pp. 1-19
- [7] R. D. MacFarlane, *J. Inorg. Nucl. Chem.*, **19** (1961), pp. 9-12
- [8] Y. Gono et al., *J. Phys. Soc. Japan*, **30** (1971), pp. 1241-1242
- [9] I. Mahunka, *Bull. Acad. Sci. USSR, Phys. Ser.* **29** (1965) pp. 1126
- [10] N.A. Golovkov, *Bull. Acad. Sci. USSR, Phys. Ser.*, **31** (1968), pp.
- [11] N.M. Chiera et al., *Plos One*, **15** (2020), pp. 0235711.
- [12] N.M. Chiera et al., *LRC Annual report 2019* (2020), pp. 34-35
- [13] B. Buck et al., *J. Phys.*, **G17** (1991), pp. 1223
- [14] Z. Talip et al., *Anal. Chem.*, **89** (2017), pp. 13541-13549
- [15] (a) D.M. Unruh et al., *Geophys. Res.*, **89** (1984), pp. B459-B477; (b) H. Fujimaki et al., *Geophys. Res.*, **89** (1984), pp. B662-B672
- [16] V.M. Salters, *Anal. Chem.*, **66** (1994), pp. 4186-4189

The influence of plating time, acidity and cathode material on the electrodeposition of Sm

N. M. Chiera, D. Schumann (PSI)

Introduction

In the framework of the ERAWAST (Exotic Radionuclides from Accelerator Waste for Science and Technology) project, diverse parameters influencing the electrodeposition of Dy, Sm, and Gd are studied. The goal is the preparation of α -sources of ^{146}Sm , $^{148,150}\text{Gd}$, and ^{154}Dy for activity measurements related to the half-life determination of the above-mentioned radionuclides. Optimized conditions for the preparation of thin layers of Dy *via* the molecular plating technique were reported in [1]. Here, the same parameters were explored for the electrodeposition of nanomoles of Sm.

Experimental

A description of the electrodeposition cell can be found in [2]. The experimental procedure followed the one described in [1]. Electrodeposition test solutions were prepared by transferring an aliquot of a 0.0033 M $\text{Sm}(\text{NO}_3)_3$ stock solution to a HDPE 20 ml vial, and diluting it in 5 mL 1 M HNO_3 . ^{145}Sm ($t_{1/2} = 340$ d, $E_\gamma = 61.25$ keV ($I_\gamma = 12.15\%$)) tracer was added in order to quantify the deposition yield *via* γ -spectrometry. Successively, the solution was evaporated to dryness (70°C under N_2 flow) and re-dissolved in 10 ml *i*PrOH (WVR AnalR NOR-MAPURE® grade, >99.7%). Then, the solution was transferred to the electrodeposition cell (diameter of deposition area: 20 mm) and plated at 550 V with an anode-cathode distance of 10 mm on an Al deposition foil (thickness thk : 15 μm). A flat spiral Pt anode was utilized. The cathode was maintained at 15°C during the entire plating by a Peltier cooler.

Results and Discussion

As shown in Fig. 1, for a constant initial amount of Sm (75 $\mu\text{L} = 250$ nmols), deposition yields $\geq 90\%$ were reached by applying continuous plating times above 300 minutes. For comparative purposes, the deposition yield of Dy under the same electroplating conditions is depicted as well. It can be observed that for the lighter lanthanide, a longer time is needed in order to obtain the same electrodeposition yield as Dy. This effect can be explained as the result of a higher mobility of the Dy complexes in comparison to the Sm ones. It is known that the nitrate salts present in the studied electroplating solutions (i.e., $\text{Dy}(\text{NO}_3)_3 \cdot 6\text{H}_2\text{O}$ and $\text{Sm}(\text{NO}_3)_3 \cdot 6\text{H}_2\text{O}$), are strong electrolytes. Moreover, they are present in the millimolar concentration range. Thus, it is reasonable to

consider them being completely dissociated in the plating solution.

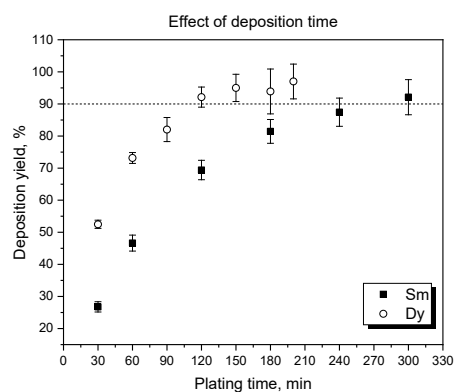


FIGURE 1: Effect of the plating time on the deposition yield of 250 nmols of Sm (squares) and Dy (circles) on an Al foil. No HNO_3 was added to the plating solution. Voltage applied = 550 V.

In [3] it was shown that during the molecular plating process part of the solvent undergoes electrolytic decomposition. This leads to the possible formation of alkoxide complexes (e.g., isopropoxides) with the Dy^{3+} and the Sm^{3+} ions. Electrochemical synthesis of metal alkoxides in alcohols like isopropanol was already reported in [4-6]. Formation of inorganic-organic complexes taking place during electrodeposition was first observed in [7] during the molecular plating of barium chloride and copper sulphate in organic media. Under the applied conditions, both materials formed colloidal suspensions. In the same work, the electrodeposition of thorium and uranium nitrate from isopropanol solutions gave deposition films of different chemical nature, in dependence of the voltage applied. By examining the cathode deposition curve as a function of voltage, it was concluded that below 50 V a steady migration of the charged molecules (proportional to the applied voltage) occurs. In the 50-150 V region, a deposition plateau, corresponding to the formation of inorganic-organic complexes, takes place. Finally, at voltages up to 600 V, the charging and the steady migration of the newly formed complex molecules to the cathode ensues, with an efficiency dependent on the applied voltage.

Hence, it can be assumed that at the electroplating conditions applied in the present work, a molecular rather than an ion migration is observed. During a static plating process where no stirring occurs, the flux J of electroactive species reaching the cathode

depends on both the ionic concentration gradient and the applied electric field. J is defined as the number of moles of species per unit of surface of the electrode and per unit of time. For a one-dimensional flux, $J(x)$ can be expressed by the Nernst-Planck equation [8]:

$$J(x) = -D \left(\frac{\partial c}{\partial x} + \frac{zF}{RT} c \frac{\partial \phi}{\partial x} \right) \quad (1)$$

with D = diffusion coefficient, c = concentration, and z = charge number of the species. F , R , ϕ , and T are the Faraday constant, the universal gas constant, the Galvani potential at the cathode-solution interface, and the applied temperature, respectively. The first term in Equation 1 is the flux due to diffusion, whereas the second term refers to the flux due to migration. Since the molecular plating conditions are unchanged during the electrodeposition of Sm and Dy, and assuming that both cations are in the oxidation state +3, then the only parameter influencing the flux of Sm and Dy species towards the cathode is D . The diffusion coefficient for a solute A at very low concentrations in a solvent B can be estimated with the Wilke-Chang method [9]:

$$D = \frac{7.4 \cdot 10^{-8} (\chi_B M_B)^{0.5} T}{\mu_B V_A^{0.6}} \quad (2)$$

with M_b being the molecular weight of solvent, μ_b its viscosity, and χ_b its association factor (for iPrOH, $\chi = 1.3$ [10]). V_a indicates the molar volume of solute A at its normal boiling point.

Characterization of alkoxide species of Sm and Dy showed that, given the same complexant and molecular structure, the Sm-ligand bonds are longer than the Dy-ligand ones [11], indicating hence a bulkier structure of the Sm compounds. Thus, it can be postulated that the more voluminous Sm-complexes have a lower diffusion coefficient than the Dy ones, which is translated into a decreased value of J , and thus, into a lower electrodeposition yield given the same plating time.

In future experiments, the deposition of Dy, Sm, and Gd as a function of the applied voltage will be explored. As observed in the electrodeposition of Dy [1], also the plating efficiency of Sm was drastically decreased with increasing the acidity of the initial solution, due to a competitive reduction of H^+ at the cathode (Fig. 2). In fact, the flow of H^+ ions competes with the diffusion and the migration of the Sm and Dy charged species towards the negative pole. The higher the mobility of the species, the higher is its flow towards the cathode. Hence, the reduction of H^+ at the cathode is favored in both the Sm and the Dy plating solutions, decreasing therefore their

plating efficiency. Finally, due to the greater diffusion of the Dy species than the Sm ones, the deposition yield of Dy is higher in comparison to the one of the lighter lanthanide at the very same plating conditions.

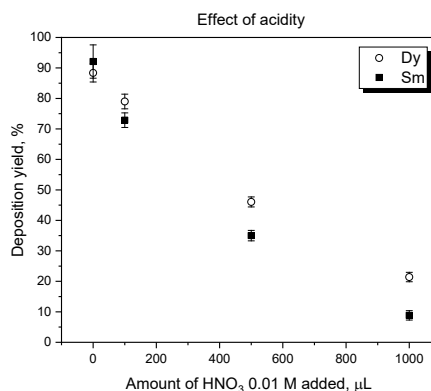


FIGURE 2: Effect of acidity (i.e., amount of 0.01 M HNO_3 added to the plating solution) in the deposition yield of 250 nmols of Sm (squares) Dy (circles) on an Al foil. Plating time = 140 min (for Dy) and 300 min (for Sm). Voltage applied was 550 V.

As done in [1], four different types of deposition foils were tested, namely glassy C (thk: 15 μm), Ta (thk: 50 μm), Cu (thk: 15 μm), and Ag (thk: 15 μm). During these experiments, no HNO_3 was added in order to prevent dissolution/etching of the Cu and Ag foils. Again, the type of cathode material did not affect the deposition yield at the applied conditions. In a future work, the same parameters will be tested for the electrodeposition of nanomoles of Gd.

Acknowledgement

This project is funded by the Swiss National Science Foundation (SNF grant no 200021-159738).

References

- [1] N.M. Chiera et al., *LRC Annual Report 2019* (2020), pp. 34-35
- [2] E.A. Maugeri et al., *J. Instrum.*, **12** (2017), pp. P0216
- [3] A. Vascon et al., *Nucl. Instrum. Methods Phys. Res., Sect. A*, **696** (2012), pp. 180-191
- [4] E.P. Kovsman et al., *J. Sol-Gel Sci. Technol.*, **2** (1994), pp. 61-66
- [5] V.A. Schreider et al., *Inorg. Chim. Acta*, **53** (1981), pp. L73-L76
- [6] A.N. Vereshchagin, *Russ. Chem. Bull.*, **64** (2015), pp. 464-465
- [7] W. Parker, *Nucl. Instrum. Methods.*, **26** (1964), pp. 55-60
- [8] P. Atkins, J. De Paula (eds.), *Atkins' Physical Chemistry*, 7th ed., Oxford University Press, Oxford, 2002
- [9] C.R. Wilke, P. Chang, *AIChE J.*, **1** (1955), pp. 264-270
- [10] B.E. Jacobson, *Acta Chem. Scand.*, **9** (1955), pp. 0997-1006
- [11] T.J. Boyle, L.A. Ottley, *Chem. Rev.*, **108** (2008), pp. 1896-1917

Preliminary characterization of holmium cathodes produced by molecular plating for the HOLMES experiment

G. de Bodin de Galembert (PSI & EPFL), E. Maugeri (PSI)

Introduction

First proposed in 1982 by A. De Rújula and M. Lusignoli as a tool for measuring the mass of the neutrino [1], the calorimetric measurement of the spectrum of the Electron Capture (EC) decay of ^{163}Ho gained new interest in the last decades, driven by advances in the field of the Low Temperature Detectors. The HOLMES experiment [2] is one of three international projects aiming to assess the feasibility of this measurement and its potential to reach sub-eV sensitivities. For this purpose, it is foreseen to use 1000 Transition Edge Sensors implanted with 300 Bq of ^{163}Ho thanks to a custom-made ion implanter.

This ion implanter operates with a Penning sputter ion source for which special targets containing the holmium must be made. The production process currently under consideration for these targets is based on several successive steps of which the total efficiency is highly uncertain [3]. In this work we investigate the potential use of Molecular Plating (MP) as an alternative route to produce the sputtering target required by the HOLMES project.

Sample Production

A molecular plating setup with a palladium anode was used to plate circular cathodes of different material. In particular, 0.01 mm thick copper foil was used as backing to produce two cathodes, which were plated for 60 minutes (experiments MP1 and MP2) and one plated for 40 minutes (experiment MP3). A 0.025 mm thick gold backing was used to produce a single cathode plated for 40 minutes (experiment MP4).

The plating solutions of the different experiments consisted of 10 mL of isopropanol to which 5 μL of a $^{166\text{m}}\text{Ho}$ standard solution, 0.991 mg/mL $^{\text{nat}}\text{Ho}$ in 0.01 M HNO_3 (Sigma Aldrich), were added. In experiment MP2, 5 μL of a 109.5 Bq/ μL solution of $^{166\text{m}}\text{Ho}$ in 0.01 M HNO_3 were added to the plating solution as tracer. For the experiments MP1, MP3 and MP4, 5 μL of a five-fold dilution of this solution with a corresponding specific activity of 21.9 Bq/ μL , was used as tracer.

Results

Yield

The yield of the deposition was evaluated by measuring the gamma-ray spectrum of the plating solutions before and after the plating. The use of the

same detector and keeping the measurement geometry unchanged for all the measurements, allowed to calculate the yield without requiring an efficiency calibration of the detectors, as follows:

$$y = \frac{cps_{\text{before}} - cps_{\text{after}}}{cps_{\text{before}}}$$

The values obtained from these experiments, compiled in the Table 1, show that the molecular plating consistently reaches yields close to 100%, which makes this method an attractive feature for the HOLMES project.

EXPERIMENT	PLATING TIME [min]	CATHODE MATERIAL	YIELD [%]
MP1	60	Cu	99.58
MP2	60	Cu	99.94
MP3	40	Cu	99.40
MP4	40	Au	99.91

TABLE 1: Deposition yield at the end of the Molecular Plating experiments

Homogeneity

The homogeneity of the deposition of the cathodes of experiments MP1, MP2 and MP4 was evaluated by radiographic imaging. Three images were taken for each cathode with 8, 16 and 64 exposure hours, respectively. These images were saved as 16-bit gray-value TIFF files. The maximum gray-value (i.e. intensity) of each image was extracted and a linear correlation between the maximal value and the exposure time was observed as shown in Fig. 1. Based on this correlation, an ideal exposure time can be determined to maximize the intensity and to achieve the best possible statistics, while avoiding the saturation of the imaging.

For instance, the saturation of the imaging of MP1 and MP4 cathodes (≈ 110 Bq) would be achieved after 595 exposition hours while for cathode of MP2, which activity is much higher (≈ 550 Bq), saturation is achieved after 59.5 h (Fig. 1). This helped to identify the best available images, offering the highest statistics, to be used for the homogeneity evaluation.

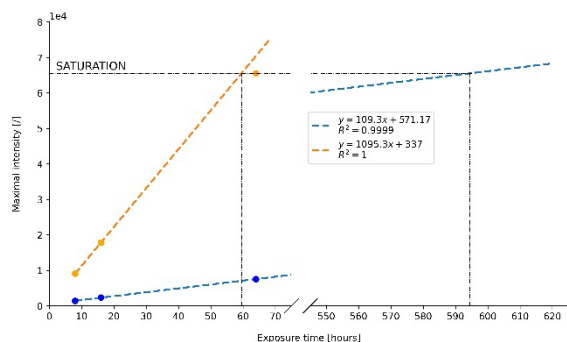


FIGURE 1: Linear correlation between the maximal intensity of the radiographic image and the exposure time for the experiments MP1 (blue) and MP2 (orange) with the indication of the saturation limit.

In particular, for MP1 and MP4, best images were the ones obtained with a 64 h exposure, while the 16 h image was chosen for experiment MP2, Fig. 2.

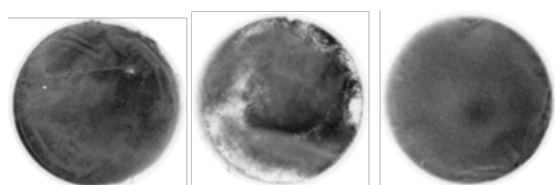


FIGURE 2: Radiographic images of the cathodes of MP1 (64 h), MP2 (16 h) and MP4 (64 h).

The visual inspection of MP1 and MP4 images indicates relatively homogeneous deposition resembling previously reported results obtained by Vascon for molecular plating of other lanthanides [4]. The deposition of the MP2 cathode is less homogeneous than MP1 and MP4 one, probably due to a bad contact between the cathode of the molecular plating cell and the backing. A stirring mechanism will be implemented for the future experiments to obtain a better homogeneity, as suggested in [5].

Microstructure

The microstructure of the deposited layer of the MP4 cathode was investigated via Scanning Electron Microscopy. The obtained image, Fig. 3, shows a clear island-like structure of the deposited layer. No grains can be seen within these islands, which have an average size of about $10\ \mu\text{m}$, suggesting that the deposited layer has an amorphous structure. In addition, cracks, flaking and detachment of the deposition is observed. Besides these phenomena, small surface outgrowths are also visible over the whole cathode. The structure of the deposited layer below these outgrowths, was investigated using a Focused Ion Beam. The result indicate, Fig. 4, that the outgrowths are filled. Thus they are not resulting from the formation of gas bubbles under the deposited

layer (e.g. hydrogen production or solvent evaporation) but were rather created on top of surface defects of the backing.

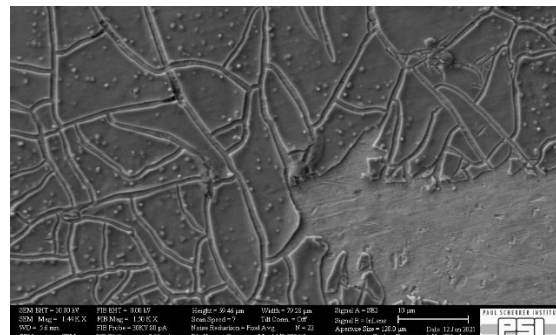


FIGURE 3: Image SEM imaging (x1440 magnification).

Flaking-inducing cracks and morphology-following surface outgrowths were also observed by Vascon [4]. From this study, two important parameters were identified influencing both crack and outgrowth formation: the volatility of the organic solvent and the surface roughness of the backings.

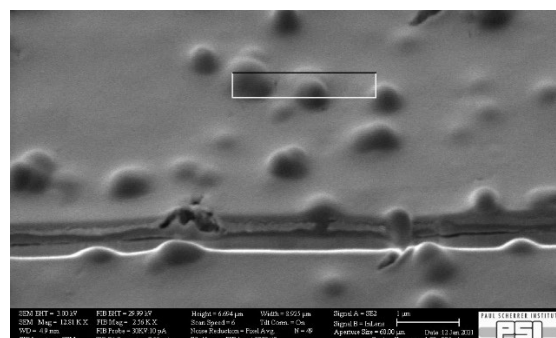


FIGURE 4: FIB cut through outgrowths (x12810 magnification).

While the outgrowths may not be a major problem in the context of HOLMES, the cracking, flaking and detachment are much more critical as loss of material and of radioactive contamination may occur. This requires investigations of the influence less volatile organic solvents as well as the use of deposition substrates with lower surface roughness, aiming at reduction of the cracking and subsequent flaking of the deposit.

References

- [1] A. De Rújula and M. Lusignoli, *Phys. Lett. B*, **118** (1982), pp. 429
- [2] B. Alpert et al., *Eur. Phys. J. C* **75**, (2015), pp. 112
- [3] M. De Gerone et al., *Nucl. Instr. Meth. Phys. Res. A*, **936** (2019), pp. 220
- [4] A. Vascon, *Molecular plating of thin lanthanide layers with improved material properties for nuclear applications*. (2013)
- [5] Z. Talip et al., LRC Annual Report 2016, (2017), pp. 47

Refuting a claim of the gravitational wave GW170817 affecting β -decay rates

P. A. Breur, J. C. P. Y. Nobelen (Nikhef), L. Baudis, A. Brown (UZH), A. P. Colijn (Nikhef, Utrecht), R. Dressler (PSI), R. F. Lang (Purdue U), A. Massafferri (CBPF), C. Pumar (CBPF), C. Reuter (Purdue U), D. Schumann (PSI), M. Schumann (U Freiburg), S. Towers (Purdue U), R. Perci (CBPF)

Introduction

Radioactivity is understood to be well described by a Poisson process. However, there are reports [1] of measurements of nuclear decays that appear to exhibit unexpected (annual) variations, time-dependent rates or even correlations with astronomical events. Generally, the isotopes for which these effects are reported have long half-lives, which are plagued by large measurement uncertainties.

To scrutinize those claims a dedicated experiment was set-up for the stable long-term measurement of gamma emissions resulting from β -decays [2]. Its high-quality data was used to refute claims of correlations between solar flares and β -decay rates [3] as well as of a claim that the gravitational wave GW170817 from binary neutron star inspiral would affect β -decay rates [4]. The latter work is summarized here.

The Experiment

The experiment measures gamma radiation from several radioactive sources. It delivers high-quality data and was optimized for the identification of potential systematic effects which might be the origin of some of the claims. Radioactive isotopes are monitored redundantly by thirty-two 76 mm \times 76 mm NaI(Tl) detectors in four separate temperature-controlled setups (see Figure 1). These are installed in four laboratories (UZH/CH, Nikhef/NL, Purdue/USA, COHEP/Brazil) across three continents. In each setup, the monitoring of environmental and operational conditions facilitates correlation studies. The sources (and the background radiation) are monitored by a dead time-free data acquisition system which individually digitizes the photomultiplier (PMT) waveforms of all events. This allows for a study of time-dependent effects spanning microseconds to years, using both time-binned and unbinned analyses.

Several environmental parameters are being constantly measured in order to identify possible correlations. These are temperature, pressure, magnetic field, relative humidity, PMT high voltage and the radon activity. The temperature inside each setup is controlled with heaters to minimize any impact and each setup can be purged with N₂ to remove radon. A combination of data from the different setups around the world further reduces systematic effects.

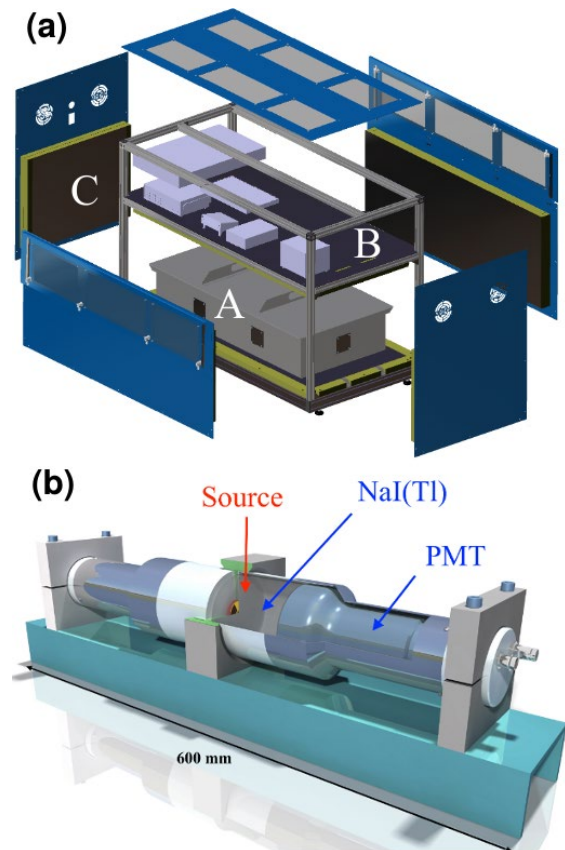


FIGURE 1: (a) Explosion view of one of the four setups. The temperature-controlled box (A) encloses four identical NaI(Tl) detector pairs (b) read out a photomultiplier (PMT) which view one source in a $\sim 4\pi$ geometry.

The Sources

Each setup accommodates four PMT-pairs (Figure 1b) which are individually shielded by Pb-layers. Three detector pairs monitor the de-excitation photons following β -decays from sources of ~ 1 kBq activity; the third pair measures background. The used sources are ^{44}Ti , ^{54}Mn , ^{60}Co , and ^{137}Cs and each source is monitored in three of the setups. (^{133}Ba is available but currently not installed.)

An isotope that has received much attention is ^{44}Ti with a half-life of 59.1(3) y. There are both claims [5] and counter-claims [6] of an annual modulation of its decay rate. As ^{44}Ti is commercially not available, the source was manufactured at the Laboratory of Radiochemistry at PSI.

No correlation with GW170817

GW170817, detected on August 17, 2017, was the first gravitational wave signal from a binary neutron star inspiral [7]. X-ray, radio and optical counterparts were also observed for this event. An additional claim was made of observing a correlation of the decay rates of two β -decaying isotopes (^{32}Si , ^{36}Cl) in a 5 h interval following the inspiral [8]. This correlation was explained by a hypothesized increase in neutrino flux at Earth created during the inspiral.

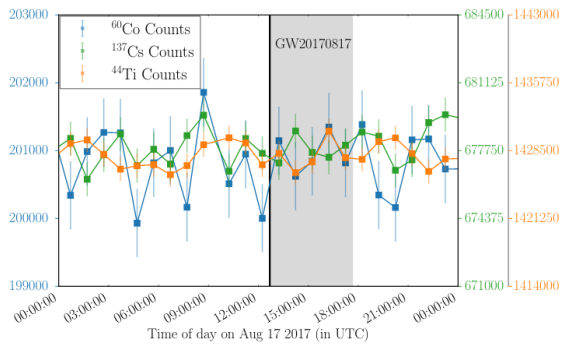


FIGURE 2: The number of counts per hour from the ^{60}Co , ^{137}Cs , and ^{44}Ti sources around the gravitational wave GW170817 do not reveal any correlation with the event. The gray shaded area corresponds to a 5 h interval.

At the time of GW170817, only the setup at Nikhef/Amsterdam was running and thus only this data was used to scrutinize the claim of [8]. The number of counts in the full absorption peak of the three sources (Figure 2) were determined via full spectral fits. Thanks to the design of the experiment, systematic influences due to experimental conditions remain below $2 \cdot 10^{-5}$ and are thus irrelevant. The statistical Pearson Correlation test was used to test for a hypothetical correlation between the independent β -decay rates of ^{44}Ti , ^{60}Co and ^{137}Cs during and following GW170817. In absence of a physical explanation for the correlation claimed in [8], arbitrary time intervals were considered in the test and the “Look-Elsewhere-Effect” [9] was taken into account to calculate the global significance of a correlation. As a result, no statistically significant correlation between the individual β -decay rates in the period following GW170817 could be identified [4]. The radioactive rates are well described by a Poissonian process.

References

- [1] For references of claims/counter-claims see [2]
- [2] J. R. Angevaare et al., *J. Instrum.*, **13** (2018) pp. P07011
- [3] J. R. Angevaare et al., *Astropart. Phys.*, **110** (2019), pp. 62

- [4] P.A. Breur et al., *Astropart. Phys.*, **119** (2020), pp. 102431
- [5] D. O’Keefe et al., *Astrophys. Space Sci.*, **344** (2013), pp. 297-303
- [6] E.B. Norman et al., *Astropart. Phys.*, **31** (2009) pp. 135-137
- [7] B.P. Abbott et al., *Phys. Rev. Lett.*, **119** (2017) pp. 161101
- [8] E. Fischbach et al., *Astropart. Phys.*, **103** (2018) pp. 1-6
- [9] L. Lyons, *Ann. Appl. Stat.*, **2** (2008), pp. 887-915

Determination of the excitation function for the production of ^{44}Ti in proton-irradiated vanadium samples

M. Veicht (EPFL & PSI), I. Kajan (PSI), J.-C. David (CEA, France), S. Chen (SFU, Canada), E. Strub (Univ. of Cologne), I. Mihalcea, D. Schumann (PSI)

Introduction

The artificial production of the long-lived cosmogenic radioisotope ^{44}Ti was first reported in 1953 [1], whereby scandium oxide was irradiated with 30–45 MeV protons at the Harvard 95-inch synchrocyclotron utilizing the $^{45}\text{Sc}(p,2n)^{44}\text{Ti}$ reaction. Since then, studies have focused on accurately determining the nowadays-recommended half-life value of 59.1(3) a [2]. Simultaneously, the interest and demand in ^{44}Ti gradually increased over recent years due to the versatility of the radionuclide's field of applications. For instance, lately, the radionuclide is employed in astrophysics [3], e.g., to probe nucleosynthesis environments and, thus, help trace back isotopic abundances at the time of the Supernova explosion. The use for radiopharmaceutical applications is also in the spotlight of research, where the interest for ^{44}Ti arises as a possible generator system for the daughter nuclide $^{44\text{g}}\text{Sc}$ ($T_{1/2} = 3.97(4)$ h), which serves as a promising nuclide for positron emission tomography (PET) [4]. The utilization of such a radionuclide generator ($^{44}\text{Ti}/^{44\text{g}}\text{Sc}$) could conveniently provide $^{44\text{g}}\text{Sc}$. Several strategies were already investigated to design such a generator, back in the 1960s to 1970s. In contrast, recent publications report eventually on final designs, allowing maximal elution of $^{44\text{g}}\text{Sc}$ with a minimal breakthrough of parent ^{44}Ti [5]. Consequently, its potential off-site availability challenges published direct production routes, e.g., enriched calcium carbonate targets via $^{44}\text{Ca}(p,n)^{44\text{g}}\text{Sc}$ [6], which also allows to provide carrier-free $^{44\text{g}}\text{Sc}$.

Here, we report the determination of the excitation function utilizing the nuclear reaction $^{\text{nat}}\text{V}(p,X)^{44}\text{Ti}$ to provide a comprehensive and consistent data set for proton energies ranging from 111 MeV to 1350 MeV. Consequently, the experimentally obtained results are also compared with model calculations.

Experimental

Sample Description

In this work, seven purified natural vanadium discs (mass ≈ 132 mg, diameter ≈ 1.50 cm, chemical purity of vanadium: 99.8%, Manufacturer: Goodfellow Cambridge Limited, UK) were investigated. These were irradiated with protons of different energies at two irradiation facilities in Europe: Laboratoire National Saturne (LNS) in Saclay (France) and Svedberg Laboratory (TSL) in Uppsala (Sweden). The irradiations took place between October 1995 and March

1996 and covered proton energies ranging from 111 MeV up to 954 MeV [7].

Sample Preparation

To accurately determine the ^{44}Ti activity in each vanadium disc sample, in-house prepared calibration sources utilizing the same geometry as the measured samples were prepared.

At first, the initial specific ^{44}Ti -activity of an in-house ^{44}Ti -solution (carrier-free in 1 M HCl) was measured as a point-like sample (PLS). The PLS was prepared by gravimetrically traced droplet deposition (≈ 20 $\mu\text{L}/\text{droplet}$) using a pycnometer and immediate evaporation of the solution on a circular polyethylene foil with a diameter of 2.5 cm (specified density = 21.3 ± 1.8 $\text{mg} \times \text{cm}^{-2}$). The activity concentration of the PLS was determined on the efficiency calibrated position of a High-Purity Germanium (HPGe) detector, utilizing the $^{44\text{g}}\text{Sc}$ daughter of ^{44}Ti in secular equilibrium, with an efficiency of $\epsilon = 6.88\text{E-}4$ for the 1157 keV-line ($I_{\gamma} = 99.9(4)\%$). Here, $^{44\text{g}}\text{Sc}$ was used to derive the ^{44}Ti activity. Advantages of this approach are twofold; the emission branching ratio for ^{44}Sc is precisely known and use of the high energy region avoids unnecessary complications caused by complex background and steep changes in the efficiency curve. Since the PLS was gravimetrically prepared, the stock solution's activity was determined to be 1.140(13) Bq/mg. Consequently, from the calibrated stock solution, two reference sources with volumes of 2 mL and 5 mL, respectively, were also gravimetrically prepared in the same high-density polyethylene (HD-PE) LSC-vials. For each sample, 1 mL of the ^{44}Ti stock solution was used, and either 8M HNO_3 (for 2 mL Reference) or 8M HCl (for 5 mL Reference) was added to reach the final volume. These solutions were then used for the relative efficiency calibrations of both Low Energy Germanium (LEGe) and HPGe detectors used for determination of ^{44}Ti activity.

Production Cross-Sections

Once the activity A is determined, the cross-section σ_{PSI} can be calculated, according to a simplified equation (Eq. 1):

$$\sigma_{\text{PSI}} = \frac{A_{\text{Sample}} e^{\lambda t_w}}{N_T \Phi_E (1 - e^{-\lambda P t_{\text{irr}}})} \quad \text{Eq. 1}$$

where λ is the decay constant of the radionuclide, t_w is the time between irradiation (end of beam) and

counting, N_T refers to the number of target atoms, Φ_E represents the proton flux density, and t_{irr} is the irradiation time. Further, the previously determined cross-section values, need to be re-calculated, with the nowadays accepted half-life of ^{44}Ti (Eq. 2):

$$\frac{T_{1/2}^*}{T_{1/2}} \cdot \sigma = \sigma^* \quad \text{Eq. 2}$$

where $T_{1/2}^*$ is the current accepted half-life (59.1 a) and $T_{1/2}$ the old half-life (47.0 a, and 47.9 a, respectively), σ represents the former value for the production cross-section and σ^* represents the adjusted value for the comparison.

Results and Discussion

Figure 1 shows that the cross-sections in the range greater than 70 MeV are consistently high, and even constant in the range from 100 MeV to 150 MeV. Yet, the new data set allows to have a reliable reference for the comparison with the model calculations, indicating an overestimation.

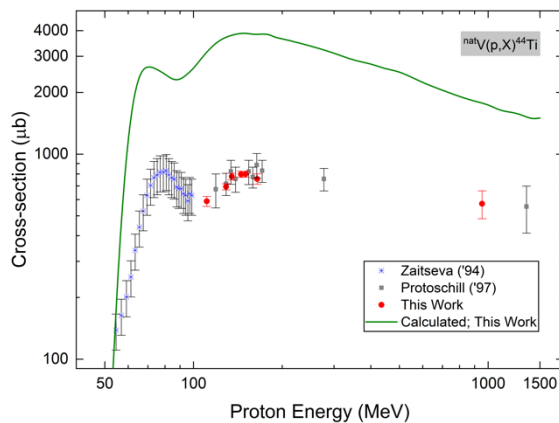


FIGURE 1: Comparison of the excitation function for the ^{44}Ti production, with additional data in the low-energy range [8] as well as theoretical calculations.

Most importantly, it seems that the shape resembles well the trend given by the experimental data, which confirms – in a nutshell – that the mechanisms responsible for the production seem to be well implemented in these model calculations. The presented data supports previous experimental results in the energy range of 111-1350 MeV while improving the precision of measured values, employing gamma-spectroscopy with both a LEGe and an HPGe detector. Combined with data from earlier measurements, a consistent data set is presented (Fig. 2). However, as the importance of ^{44}Ti as a source of the ^{44g}Sc from vanadium is addressed, on the one hand, a lower-energy range for the production of ^{44}Ti is generally preferable since it could be typically produced using, e.g., low-energy cyclotrons. Therefore, its production via $^{nat}\text{V}(p,X)$ can be realized also in the region < 80 MeV, as no significant increase in the

cross-section can be found, compared to higher energy regions.

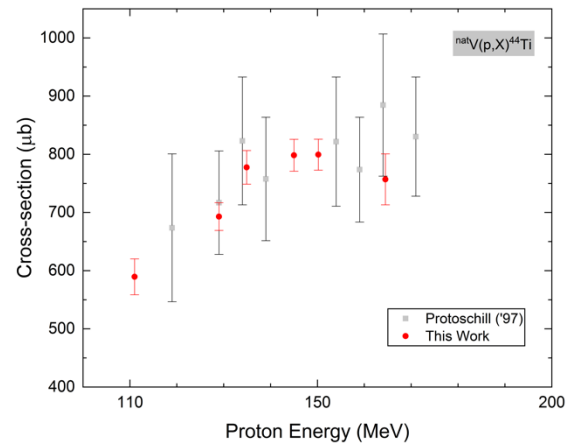


FIGURE 2: Experimental excitation function for the ^{44}Ti production from proton-induced reactions, as a comparison between two data-sets.

On the other hand, in regard to e.g., dedicated irradiation programs, ^{44}Ti can be produced as a by-product, allowing its further separation from irradiated material. Here, also higher proton energies are typically used. Finally, the advantage of such a presented indirect production route of ^{44g}Sc , lies in the application as a radionuclide generator, which could conveniently provide carrier-free ^{44g}Sc , and potentially allowing its daily routine application.

Acknowledgement

This project is funded by the Swiss National Science Foundation (SNSF) as part of SINERGIA No.177229. This project has received funding from the European Union's Horizon 2020 research and innovation program under the Marie Skłodowska-Curie grant agreement No. 701647. Moreover, funding from Swiss nuclear is appreciated. Besides, the authors thank Jan Protoschill, Prof. Rolf Michel (IRS Hanover) and Prof. Horst-Michael Prasser (ETHZ).

References

- [1] R. A. Sharp et al., *Phys. Rev.*, **2** (1954), p. 358
- [2] J. Chen et al., *Nucl. Data Sheets*, **112** (2011), pp. 2357-2495
- [3] V. Margerin, *Doctoral Dissertation, Edinburg University* (2016)
- [4] F. Roesch, *Curr. Radiopharm.*, **3** (2012), pp. 1636-1641
- [5] V. Radchenko et al., *Nucl. Med. Biol.*, **50** (2017), pp. 25-32
- [6] G. Severin et al., *Appl. Radiat. Isot.*, **8** (2012), pp. 1526-1530
- [7] J. Protoschill, *Diploma Thesis, Leibniz University Hannover* (1997)
- [8] N. Zaitseva et al., *Radiochim. Acta*, **3** (1994), pp. 157-160

Separation of long-lived, non-carrier-added calcium, titanium, and aluminum isotopes from high - energy proton irradiated vanadium

J. Wilson (Univ. Bern & PSI), I. Mihalcea (PSI), M. Veicht (EPFL & PSI), D. Cvjetinovic (Univ. Belgrade), D. Schumann (PSI)

Introduction

High-energy proton irradiation of vanadium disks creates a large number of isotopes including ^{41}Ca , ^{44}Ti , and ^{26}Al . ^{41}Ca and ^{26}Al are rare cosmogenic radionuclides, whereas ^{44}Ti is created via nucleosynthesis in supernovae. All three have astrophysics applications, studying supernovae [1], the solar system [2], and meteorites [3]. Medically, ^{41}Ca is used for long-term bone adsorption studies [4] and ^{44}Ti is of high interest as a $^{44}\text{Ti}/^{44}\text{Sc}$ generator [5]. ^{26}Al is used as a short-lived geological dating isotope [6]. For each of these applications, sufficient amounts of radionuclidically pure samples are required for both research and development work as well as scientific and technical use. We report here on the successful isolation of all three isotopes adapting and combining different ion exchanges techniques.

Materials and Methods

Pump-assisted liquid column chromatography was used as preferred separation method. Loading and washing solutions were collected separately from the elute, each containing different targeted ions. Separations were first optimized using model experiments with non-irradiated vanadium disks and standard solutions of the corresponding elements, employing inductively coupled plasma optical emission spectroscopy (ICP-OES) as analysis tool. γ -spectroscopy was used to trace ^{44}Ti , ^{26}Al and contaminants during treatment of the irradiated vanadium disks.

Previous sample treatments

After a two-year irradiation, the disks cooled for eight years before the sample processing started. After the disks' dissolution, ^{32}Si was initially separated using an approach described in [7]. The remaining solution, 50 ml of 3M HNO_3 per disk, containing the bulk matrix including the mentioned radionuclides, was used here for the described radiochemical separations.

Calcium Separation

Bulk Separation

According to [8], DGA (Eichrom®) extraction resin separates calcium from the vanadium solution by absorbing the calcium, which then can be eluted from the resin with 20 ml H_2O . An intermediate rinse step, consisting in 20 ml 3M HNO_3 solution, was implemented for purging impurities off the column. The

loading and rinsing fractions, summing 70 ml solution in a 3M HNO_3 matrix, were used for the next step, the titanium separation.

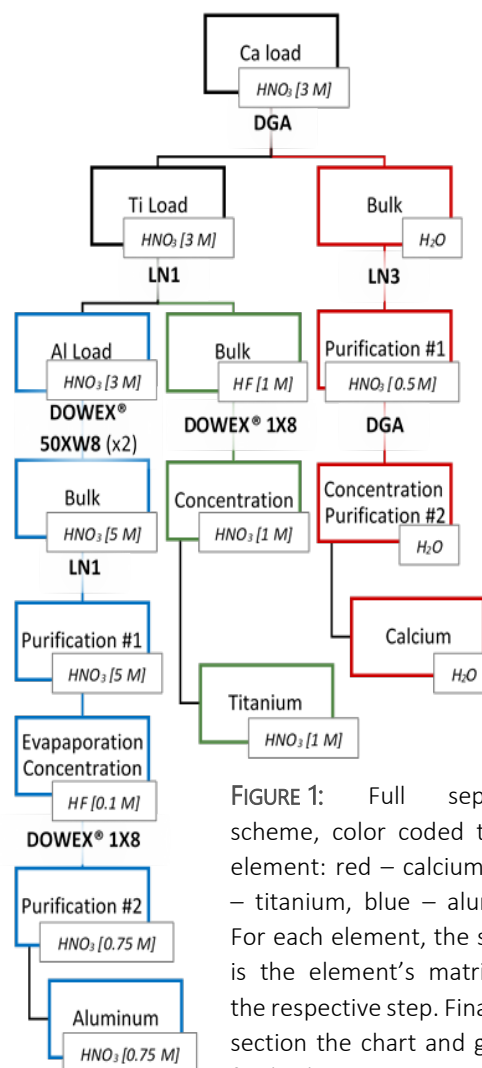


FIGURE 1: Full separation scheme, color coded to each element: red – calcium, green – titanium, blue – aluminum. For each element, the sub-box is the element's matrix after the respective step. Final boxes section the chart and give the final solution matrix.

Purification of the Ca fraction

The following radionuclides were found after removal of vanadium: ^{22}Na , $^{44}\text{Ti}/^{44}\text{Sc}$, ^{60}Co , ^{94}Nb , $^{152,154}\text{Eu}$, $^{173,174}\text{Lu}$ and $^{172}\text{Hf}/^{172}\text{Lu}$. LN3 extraction resin (TrisKem SAS, Bruz, France) was chosen to remove ^{44}Ti , ^{94}Nb , and $^{172}\text{Hf}/^{172}\text{Lu}$ as described in [9]. The calcium fraction was acidified to 0.5M HNO_3 , loaded onto the resin and washed with HNO_3 solution of the same concentration. The loading and washing fractions, containing the calcium, were combined. $^{44}\text{Ti}/^{44}\text{Sc}$ and $^{172}\text{Hf}/^{172}\text{Lu}$ could be fully and ^{94}Nb partially removed. Remaining contaminants were ^{22}Na ,

^{60}Co , ^{94}Nb traces, $^{152,154}\text{Eu}$, and $^{173,174}\text{Lu}$. Further purification could be achieved by repeating the separation on DGA resin, this time acidifying the calcium fraction to 1M HNO_3 .

Titanium Separation

Bulk Separation

Once calcium was extracted, LN1 resin (TrisKem SAS, Bruz, France) was used to separate titanium from the bulk vanadium with no matrix modifications. Under the acidic conditions of the loading solution, titanium is retained. The column was rinsed with 20 ml 3M HNO_3 and Ti was eluted with 1M HF [10]. The loading and washing solutions, 90 mL in 3M HNO_3 , were collected for aluminum separation. The γ -spectra of the ^{44}Ti solutions showed no contamination.

Concentration

A previously established method [11] was followed to concentrate titanium on the anion exchange resin, Dowex® 1X8, in 1M HF matrix, and elute it with 1M HNO_3 solution. Unfortunately, due to the HNO_3 content of the solution, ^{44}Ti was only partly retained on the resin. Consequently, the collected loading and washing fractions displayed large quantities of desorbed ^{44}Ti , as HNO_3 competes with Ti's adsorption on the anion exchanger [12]. However, the performance can be improved by lowering the HNO_3 concentration to 0.1M in 1M HF [13].

Aluminum Separation

Bulk Separation

Aluminum bulk separation was optimized as a dual Dowex® 50XW8 cation exchange separation. For the first step, the load solution was diluted with H_2O to reach HNO_3 concentrations of 1.5M, and 1.25M, respectively, for the second separation. For both steps, the ^{26}Al elution from the column was performed using 5M HNO_3 solution. The Al-fraction's γ -spectra showed $^{44}\text{Ti}/^{44}\text{Sc}$, ^{54}Mn , and ^{60}Co as contaminations.

Purification #1

Since the separated ^{26}Al solutions were in 5M HNO_3 , titanium impurities show an enhanced affinity toward LN resin under this condition. The ^{26}Al solution was passed through the LN resin and washed with 5M HNO_3 . Loading and washing fractions containing ^{26}Al , were combined into a single solution while $^{44}\text{Ti}/^{44}\text{Sc}$ remains on the column. Their removal from the main solution was confirmed by γ -spectroscopy.

Evaporation and Concentration

For the second purification, a matrix change from HNO_3 to HF was required. For this, the aluminum solution was evaporated to dryness and the residue

dissolved in 1M HF. The resulting solution was diluted with H_2O to reach a concentration of 0.1 M HF. Aluminum solutions, each corresponding to three irradiated vanadium targets, were concentrated on the evaporation dish before dissolving in HF.

Purification #2

Model experiments confirmed that aluminum shows high affinity towards Dowex® 1X8 in a 0.1M HF matrix, while ^{60}Co and ^{54}Mn contaminants remain as cations, thus are not retained. This purification step reached a decontamination factor of 1.2. Employing γ -spectrometry about 10^{10} atoms ^{54}Mn , 10^{12} atoms ^{60}Co , and 10^{15} atoms ^{26}Al per sample were identified.

Conclusion

Long-lived calcium, titanium, and aluminum isotopes were separated from the bulk target material vanadium after high-energy proton irradiation. Each element solution underwent several purification and concentration procedures. Next steps include the quantification of ^{41}Ca using liquid scintillation counting or mass spectrometric methods. Part of the ^{44}Ti is purified and ready for use, but the remaining ^{44}Ti in the loading and washing solutions should be further purified and concentrated. Finally, small amounts of ^{54}Mn and ^{60}Co still contaminate the ^{26}Al solution, making additional purification necessary.

Acknowledgement

The project is partially funded by the Swiss National Science Foundation (SNSF) (SINERGIA No. 1777229) and by the European Union's Horizon 2020 research and innovation program under the Marie Skłodowska-Curie grant agreement No. 701647.

References

- [1] A. F. Lyudin et al., *Nature*, **396** (1998), pp. 142-144
- [2] N. Bateman et al., *Astrophys. J.*, **472** (1996), pp. 119-122
- [3] S. Amari et al., *Astrophys. J.*, **470** (1996), pp. 101-104
- [4] J. A. Suarez et al., *Appl. Radiat. and Isot.*, **52** (2000), 407-413
- [5] S. M. Qaim, I. Spahn, *J. Labelled Compd. Radiopharm.*, **61** (2018), pp. 126-140
- [6] G. Balco, D. L. Shuster, *Earth Planet. Sci. Lett.*, **286** (2009), pp. 570-575
- [7] I. Mihalcea et al., *LRC Annual Report 2019* (2020) pp. 28-29
- [8] A. Pourmand et al., *Talanta*, **81** (2010), pp. 741-753
- [9] D. R. McAlister, E. P. Horwitz, E. P., *Solvent Extr. Ion Exch.*, **25** (2007), pp. 757-769
- [10] D. Schumann et al., *LRC Annual Report 2006* (2007), p. 41
- [11] J. P. Faris, R. F. Buchanna, *Anal. Chem.*, **36** (1964), pp. 1157-1158
- [12] L. Danielsson, *Acta Chem. Scand.*, **19** (1965), pp. 1859-1874

Towards implementing ^{32}Si for environmental research (SINCHRON): Final purification and master solution preparation

I. Mihalcea (PSI), M. Veicht, A. Pautz (EPFL & PSI), D. Cvjetinovic (Univ. Belgrade), D. Schumann (PSI)

Introduction

Preceding the main goal of the SINCHRON project, which is the half-life ($T_{1/2}$) redetermination of the ^{32}Si isotope, a major challenge is the final purification and preparation of the “master solution”. The master solution is the ^{32}Si sample to which all the physical measurements required for the $T_{1/2}$ redetermination are traceable too. The requirements for such a solution are to have sufficient activity for all the subsequent experiments, to be radionuclidically pure and the eventual sulfur trace impurities present to be in natural isotopic ratio. Bulk separation from the proton irradiated vanadium targets and some of the purification steps have been previously described [1]. In this work, the development of fine purification steps, the implementation of the full separation scheme and the ultimate preparation of the master solution are presented.

Experimental

Implementing the previously described bulk separation method [1], the ^{32}Si content of each individual proton irradiated vanadium disc is separated from the initial matrix and is present under the $\text{Si}(\text{OH})_4$ chemical form. Since this initial step removes the major part of the γ -emitting nuclides, γ -spectroscopy shows the presence of the trace radiochemical impurities. The spectroscopic analyses were conducted on a high-purity germanium γ -spectrometer (IGC 18 Princeton Gamma-Tech). The inventory of impurities was classified and consecutive purification methods were applied in order to remove each class (Figure 1).

First step is a solvent extraction column chromatography using LN resin (TrisKem SAS, Bruz, France). For this, an in-house tailor-made PMMA chromatography column with the inner diameter of 10 mm was loaded with 35 mm LN resin bed and connected to a pressurized peristaltic pumping system set to $1.5 \text{ mL} \times \text{min}^{-1}$ speed. The resin was preconditioned with 20 ml 0.1M HCl, followed by the load of the 120 ml of ^{32}Si solution. A subsequent washing fraction of 5 ml H_2O is collected together with the ^{32}Si load fraction, leaving the column ready for the next purification. Each batch of resin is used for six independent purification procedures before being discarded and replaced with a fresh one. The second purification step is similar to the first but this time using Monophos resin (TrisKem SAS, Bruz, France). The pumping system and chemical steps are identical to the ones

of LN purification. The PMMA column was exchanged with a smaller, 9 mm diameter one (ISOLUTE® 3 mL, Biotage Sweden AB, Sweden), while the resin bed was reduced to 30 mm.

The resulting 130 ml silicon solution is further evaporated to dryness using 25 ml capacity PTFE evaporating dishes on hot plates with the temperature set in $170^\circ - 180^\circ\text{C}$ range. The process is lengthily to avoid activity losses, each batch taking roughly 60 min. The obtained solid residue is further suspended in 25 ml ultrapure water ($18 \text{ M}\Omega\text{-cm}$) and reevaporated. This procedure is repeated five consecutive times. For ^{32}Si recovery, the evaporation dish is washed twice with 1 ml 1 M HF solution and the collected fraction is further diluted with H_2O to a final volume of 20 ml.

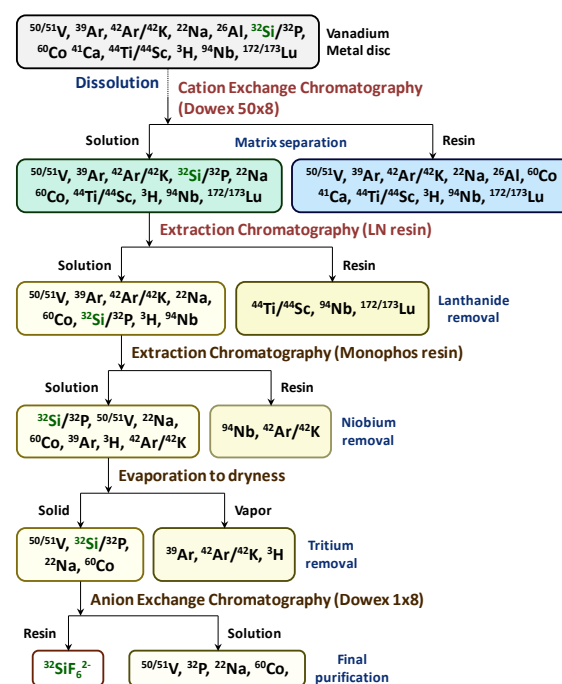


FIGURE 1: Stepwise separation and purification scheme for ^{32}Si .

The last purification step is an anion exchange column chromatography employing Dowex® 1x8 200-400 anion exchange resin and a similar setup used in previously described chromatography techniques. The 30 mm (9 mm diameter column) height resin bed was preconditioned to the F⁻ form with 50 ml 0.1M HF, process followed by the load of ^{32}Si solution. Succeeding the load procedure, three rinsing steps were implemented with the purpose of further sample purification and of shifting the traces of sulfur impurities toward a natural isotopic composition.

This procedure makes the topic of a current edition standalone report and is further detailed there [2]. The elution consists of 20 ml 0.5M HCl and is designed to completely remove silicon from resin. This ^{32}Si pure fraction is collected and stored for further use.

Results and Discussion

Once the major γ -emitters: $^{44}\text{Ti}/^{44}\text{Sc}$, ^{22}Na and ^{60}Co were bulk separated, γ spectroscopy conducted on ^{32}Si fractions showed trace of new impurities: $^{42}\text{Ar}/^{42}\text{K}$, ^{94}Nb , and rarely $^{172}/^{173}\text{Lu}$.

Although specially designed for lanthanide separation [3], the LN resin found applications, among others, also in radium separation [4]. For our purpose, under the chemical conditions of the ^{32}Si solution, LN resin manifested high affinity toward Ti, Sc, Lu and mild retention of Nb while showing no retention of $\text{Si}(\text{OH})_4$. The results of this step can be observed by, γ -spectroscopy (Figure 2).

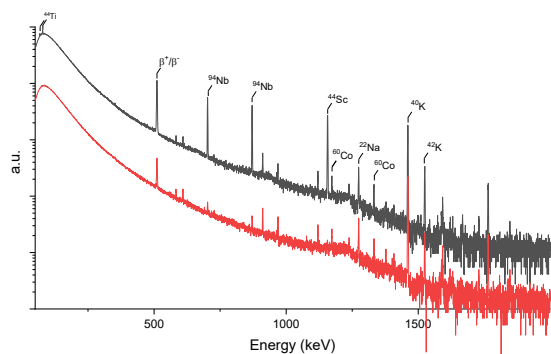


FIGURE 2: γ spectra of ^{32}Si solution before (black) and after (red) the LN purification step.

The Monophos resin, employed in the second purification step, is commercially designed for the actinide and polyvalent cations separation [5]. In our case it proved high affinity toward Nb while, similar to LN, exhibiting no Si retention (Figure 3).

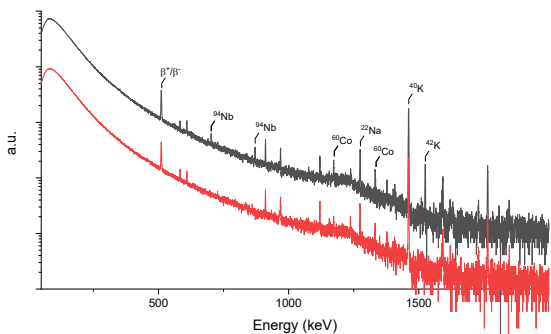
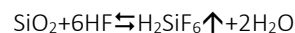


Figure 3: γ spectra of ^{32}Si solution before (black) and after (red) the Monophos purification step.

For full removal of volatile radionuclides such as ^3H and $^{39}/^{42}\text{Ar}$, an intermediate evaporation to dryness step was implemented. This step, together with HF dissolution of obtained solid residue, completely changes the silicon's chemical shape to SiF_6^{2-} while the solution matrix becomes 0.1 M HF.



Under current conditions, the anionic silicon species, including the hydrolyzed ones HSiO_3^- , manifest high affinity toward strong anion exchange resins and are retained while all other neutral and cationic species are passing through freely. This step removes the remaining traces of V, ^{60}Co and ^{22}Na . Depending on the required activity for final solution, this last purification step, can be also a concentration step. Under the described conditions, the chromatography column was capable of retaining silicon amounts corresponding to ten proton irradiated vanadium discs without significant silicon loss.

The purification steps were developed and optimized using standard inactive solutions employing inductively coupled plasma – optical emission spectrometry as quantification method. The master solution was prepared by concentrating the ^{32}Si solutions from six proton irradiated vanadium discs, resulting in a 20 ml solution, 0.5M HCl composition; with an activity concentration of 109(3) kBq/g. A subsequent long-term γ spectrum of the solution confirms the absence of any radiochemical impurity.

Conclusion and Outlook

Following the bulk separation of ^{32}Si from the proton irradiated vanadium targets, a series of subsequent purification steps were designed and implemented for obtaining a radionuclidically pure solution. Ultimately, by concentrating the ^{32}Si content of six vanadium targets, the master solution was created, achieving the radiochemical goal of the SINCHRON project. Further experiments will be focused on sample preparation for the numerous physical measurements, to which the solution will be subjected.

Acknowledgement

This project is funded by the Swiss National Science Foundation as part of SINERGIA (No. 177229) and has received funding from the European Union's Horizon 2020 program under the Marie Skłodowska-Curie grant agreement No. 701647.

References

- [1] I. Mihalcea et al., *LRC Annual Report 2019* (2020), p. 28
- [2] M. Veicht et al., *LRC Annual Report 2020* (2021)
- [3] C. Pin et al., *Anal. Chim. Acta*, **339** (1996), pp. 79-89.
- [4] W. Burnett et al., *Radioact. Radiochem.*, **6** (1995), pp. 36-44.
- [5] R. Chiarizia et al., *Sep. Sci. Technol.*, **32** (1997), pp. 1-35

Towards implementing ^{32}Si for environmental research (SINCHRON): Sample preparation and stabilization for scintillation measurements

I. Mihalcea (PSI), M. Veicht, A. Pautz (EPFL & PSI), K. Kossert, O. Nähle (PTB), C. Bailat, Y. Nedjadi (IRA), D. Schumann (PSI)

Introduction

The final aim of the SINCHRON project is a precise half-life ($T_{1/2}$) determination for the ^{32}Si isotope as the current accepted value suffers from a high degree of uncertainty [1]. Following a complex process of separation and purification from the original matrix [2], sample preparation is the one last step before the physical measurements leading to $T_{1/2}$ determination.

The $T_{1/2}$ of a specific radioactive isotope can be experimentally determined through two methods. First is a measurement of instrument readings R as a function of time. In this case, $T_{1/2}$ is obtained from fitting procedures using exponential decays. This method, however, requires excellent long-term stability of source and detector characteristics and/or known detection efficiencies. The second method requires both the measurement of number of atoms of the specific nuclide (N) and the activity (A) for the same sample. Using the two experimental values in the activity equation $A=\lambda N$, the decay constant and implicitly the $T_{1/2}$ are determined.

For the specific case of ^{32}Si , decaying with no gamma emission, the most accurate methods of activity measurement are liquid and plastic scintillation counting (LSC and PSC). The sample preparation and sample stability for the two techniques are the focus of this work.

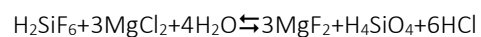
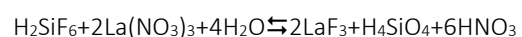
Experimental

The activity determination of a ^{32}Si master solution will be realized at IRA and PTB by means of LSC using well-established activity standardization techniques: The triple-to-double coincidence ratio (TDCR) with dedicated LSC systems with 3 photomultiplier tubes and the CIEMAT/NIST efficiency tracing technique. Both methods have never been applied to ^{32}Si before. The beta spectrum shapes of this nuclide and its daughter are key ingredients in the physical model for computing the detection efficiency. Stable LSC samples are on the other hand essential for obtaining reliable counting rates. First test measurements were carried out to obtain suitable LSC samples. To this end, various LSC cocktails, types of vials and organic-to-aqueous ratios were tested. For the time being, the preliminary results agree to better than 1%, but possibilities to improve the long-term stability are desirable.

At IRA, an additional independent method was successfully tested. In this case, ^{32}Si is measured in a $4\pi\beta\text{-}\gamma$ coincidence setup using an efficiency tracing method with ^{60}Co as a tracer. The advantage of this method is that it does not require computed beta spectra as input information.

For a potential determination or validation of the half-life by means of long-term measurements, liquid Cherenkov samples and one solid Cherenkov sample were prepared. While the liquid samples reveal an unsatisfactory long-term stability, it is anticipated that the solid sample measured in a TDCR counter may provide valuable information. However, a significant loss of volatile ^{32}Si during a first sample preparation is hindering a sound measurement and further tests need to be performed. For the liquid scintillation experiments, the organic cocktail to aqueous solution ratio was chosen to be 15:1 [3] while the aqueous matrix in three distinct experiments was selected to be H_2O , 0.5M HCl and 0.5M HCl / 0.01M HF, respectively. The scintillating cocktail used was Ultima GoldTM. In both cases, the chemical form of ^{32}Si is SiF_6^{2-} with partial hydrolysis to H_4SiO_4 . The activity used for each sample was around 720 Bq. The six samples, including a blank for each of them, were regularly measured for over six months with a TRI-CARB[®] 2250CA Liquid Scintillation Analyzer. The results are shown in Figure 1.

In the preparation of the plastic scintillation samples, ethylene-vinyl alcohol (EVOH) evaporation dishes, with a diameter of 3 cm and 0.7 cm height, were used for drying the ^{32}Si solutions. The radioactive source was a freshly separated ^{32}Si solution in a 0.5M HCl matrix, with the silicon in SiF_6^{2-} chemical shape. To prevent or limit silicon volatility, three stabilizing agents were chosen for this experiment. NaOH was selected first due to its ability to change the chemical form of silicon while $\text{La}(\text{NO}_3)_3$ and MgCl_2 were selected for the specific metal's properties of forming insoluble fluoride salts, acting as scavengers.



The stabilizing agents are commercially available and were used without further purification. Their corresponding solutions were prepared by dissolution in purified 18 M Ω ·cm water. Experimentally, specific amounts of stabilizing agent solution and the active silicon solution were placed in the center of the

evaporation dishes and left at room temperature overnight, at the end of which complete dryness is achieved. The specific quantities used are presented in Table 1.

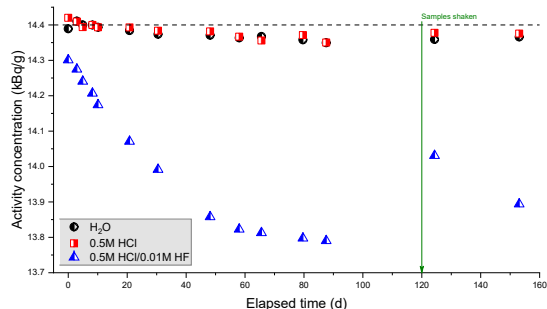


FIGURE 1: Sample stability for the HCl and HF cocktail matrices.

After complete evaporation, the flexible dishes are carefully folded and completely inserted into polyethylene (HDPE) scintillation vials. Further, 15 ml Ultima Gold™ scintillation cocktail and 1 ml, 0.5M HCl are added before capping the vial.

TABLE 1: Experimentally used specific quantities.

Label	Stab. Agent Conc.	Stab. Agent (μL)	³² Si (μL)
A1	H ₂ O	100	100
A2	NaOH 0.51 M	100	100
A3	NaOH 0.43 M	100	100
A4	La(NO ₃) ₃ 50 mM	100	100
A5	La(NO ₃) ₃ 3 mM	100	100
A6	MgCl ₂ 50 mM	100	100
A7	MgCl ₂ 4.4 mM	100	100

All samples were vortex agitated and allowed to stabilize for 20 minutes before analysis. The measurement time was set to 60 minutes.

To calculate accurately the ³²Si recovery rate following the evaporation process, reference samples were created and measured. These samples have the same composition and preparation method as the actual ones, but do not undergo a drying process. This ensures that the measurement specific parameters are similar, while volatility losses in the reference samples are zero.

Results and Discussion

Vials, made from glass or plastics, are suitable for the LSC measurement. In Figure 2, a photo of the used plastic vials is shown.

LSC samples containing H₂O or 0.5M HCl as aqueous phase are stable and the activity can be accurately determined for periods up to two weeks following sample preparation. After this period, increasing loss in activity is observed suggesting phase segregation due to micro micellar instability. This is evidenced by

the recovery of the activity concentration after shaking the vials, which restores the initial sample's homogeneity.



FIGURE 2: Plastic scintillator vials illuminated by UV light to stimulate emission of scintillation light.

This behavior is better highlighted in a parallel experiment performed at IRA on a TriCarb 2700TR Liquid Scintillation Analyzer (Figure 3).

The stability decline is even more pronounced if the aqueous phase is 0.1M HF, suggesting destructive chemical interactions between the hydrofluoric acid and scintillation cocktail components.

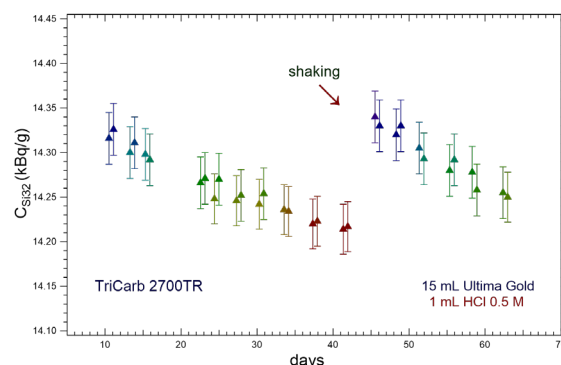


FIGURE 3: Activity concentration recovery once the sample homogeneity is restored.

In the silicon stabilization experiments, the A1 sample contained no stabilizing agent. This was to measure the hydrolysis degree of silicon in the initial solution and implicitly to establish a baseline of its volatility. The results showed an activity recovery and implicitly a hydrolysis degree for SiF₆²⁻ species of 14.1%. When NaOH was used, the 0.51 M and 0.43 M concentrations were selected to be slightly above and below the neutralization point of the 0.5M HCl matrix. The recovery rates for the two experiments were 95.5% and 94.8%, respectively. These values prove that NaOH can prevent SiF₆²⁻ volatility to an acceptable degree even when employed in concentrations below neutralization point. For the experiments A5 and A4, where La(III) was employed, the stabilizing agent concentration was selected to

match the La-F system stoichiometry (3mM) and respectively to be roughly one order of magnitude in excess (50mM). The recovery rates for these experiments were of 17.2% and 22.3%, respectively. Neither of the values is satisfactory for a PSC sample preparation.

On the same principle as in the case of La(III) experiments, the A7 and A6 samples contained Mg(II) solutions of 4.4mM and 50mM concentrations, respectively. The recovery rates for the two were of 18.8% and 46.3%. These values are slightly higher than the ones of La(III) but still unsatisfactory for the selected purpose. Inability of La(III) and Mg(II) to scavenge F⁻ can be attributed to the low pH of the initial ³²Si matrix, value at which the LaF₃ and MgF₂ solubility are high.

Conclusion and Outlook

The work of this paper tested the long-term stability of two LSC chemical systems and the stabilization upon drying of three PSC systems.

Based on the results of the stability study, LSC is an adequate technique for precise ³²Si activity determination, as long as the measurement takes place soon after sample preparation. On the contrary, it is clearly unsuitable for long-term decay measurements. For such experiments, better techniques are PSC and Cherenkov counting.

In the preparation of PSC samples, three stabilizing agents were tested, from which only NaOH showed promising results. The low recovery rates obtained using La(III) and Mg(II) are attributed to the low pH value of the system but show an ascending trend with the increase of stabilizing agent concentration. Further experiments employing higher La(III) and Mg(II) concentrations of up to 0.5M should yield satisfactory recovery rates.

Acknowledgement

This project is funded by the Swiss National Science Foundation as part of SINERGIA (No. 177229). This project has received funding from the European Union's Horizon 2020 research and innovation program under the Marie Skłodowska-Curie grant agreement No. 701647.

References

- [1] L. K. Fifield et al., *Quat. Geochronol.*, **4** (2009), pp. 400-405
- [2] I. Mihalcea et al., *LRCAnnual Report 2019*, (2019), pp. 28-29
- [3] Y. Nedjadi et al., *Appl. Radiat. Isot.*, **118** (2016), pp. 25-31

Towards implementing ^{32}Si for environmental research (SINCHRON): Elimination of isobaric interferences in ICP-MS: ^{32}Si and ^{32}S

M. Veicht (EPFL & PSI), P. Sprung (AHL/PSI), I. Mihalcea (PSI), A. Pautz (EPFL & PSI), D. Schumann (PSI)

Introduction

Inductively coupled plasma mass spectrometry (ICP-MS) is one of the versatile tools for the number of atoms' determination [1], applied in the frame of the SINCHRON project. However, for an accurate determination of the isotope composition and radionuclide inventory of interest in the presence of isobaric interferences, the isotopic composition of the interfering element(s) has to be well-known.

S 32 94.99	S 33 0.75	S 34 4.25	S 35 87.37 d	S 36 0.01
P 31 100	P 32 14.268 d β 1.71066 no γ	P 33 25.25 d	P 34 12.43 s	P 35 47.3 s
Si 30 3.092	Si 31 157.36 m	Si 32 153 a β 0.2 no γ $\sigma < 0.5$	Si 33 6.11 s	Si 34 2.77 s
Al 29 6.56 m	Al 30 3.62 s	Al 31 644 ms	Al 32 33 ms	Al 33 41.7 ms
Mg 28 20.915 h	Mg 29 1.30 s	Mg 30 335 ms	Mg 31 236 ms	Mg 32 86 ms

FIGURE 1: Part of the "Karlsruhe Nuclide Chart" (modified after 10th Edition), in which the isobar ($A = \text{const.} = 32u$) is highlighted.

^{32}Si was produced through spallation using high-purity vanadium discs as targets. As the discs were exposed to high-energy protons (HIPA, PSI) over two years, a non-natural isotopic composition is expected. As a result, the presence of by-products from the irradiation, or associated decay, might hamper the accurate amount determination of ^{32}Si , particularly if significant amounts of sulfur – including ^{32}S – were present in the vanadium discs during irradiation. Therefore, it is highly important to remove S efficiently during the radiochemical separation procedure to facilitate a mathematical correction for isobaric interference according to:

$$V^{32}\text{Si}_{\text{corrected}} = V^{32}\text{Total} - V^x\text{S} \cdot \frac{^{32}\text{S}}{^x\text{S}_{\text{nat}}} \cdot f$$

Here, V refers to the measured signals of individual ion beams, x to a stable isotope of S other than ^{32}S , and f to a factor accounting for the instrumental mass discrimination of the mass spectrometer.

Experimental Description

Previous measurements for the re-determination of the ^{60}Fe half-life highlighted the importance of the removal of isobaric interferences (here: ^{60}Ni), using multicollector (MC-) ICP-MS [1]. Thus, concerning $V^{32}\text{Si}$, the efficient S removal is vital for reliable measurements. We realized the removal while gathering the required activity of ^{32}Si on an anion-exchange resin (Dowex1X8, 200-400 mesh, Cl⁻ form, Merck KGaA, Germany), which allows in a single-step procedure highly reproducible results.

First, the column (ISOLUTE® 3 mL (9 mm diameter), Biotage Sweden AB, Sweden) was filled with 3 cm of resin bed. For each experiment, the resin was pre-conditioned with 50 mL 0.1M HF. A peristaltic pump (REGLO Digital MS-2/8, Thermo Fisher Scientific Inc., U.S.A.) was used for purging the solutions with a constant speed of 1.5 mL x min⁻¹. The chemicals used were of p.a. quality. Silicon (H_2SiF_6), vanadium (VO_2^+), and sulfate (Na_2SO_4) were added from ICP-OES standard solutions (1000 ppm, Merck KGaA, Germany). Additionally, a 10000 ppm standard solution (SPEX CertiPrep, U.S.A.) as a source for sulfur ($(\text{NH}_4)_2\text{SO}_4$) was used. For all stock solutions, ultra-pure water (18.2 M Ω x cm, Veolia Environmental S.A.) was used. All reported results are based on ICP-OES (Agilent 5110, Agilent Technologies) measurements.

Determination of ideal conditions

Since the sulfur removal takes place while gathering the hexafluorosilicate anion on the exchange resin, ideal conditions had to be found, allowing the quantitative elution of sulfur while retaining $^{32}\text{SiF}_6^{2-}$. In each of the experiments, sulfur was added to the load solution in order to investigate the behavior under HCl-free conditions. However, for the final application, the sulfur solutions were added separately and not to the load.

For small-scale experiments, a typical "Si-Load-Solution" (100 mL 0.1M HF; 400 μg Si; 200 μg V) was prepared, resembling the averaged amount of five Si-fractions obtained from the separation procedure, described in [2]. In addition, 10 mg of sulfur was added, equal to 200 ppm per load. Here, a varying HCl-concentration was used to determine the threshold value above which sulfur starts to elute. To ensure the retention of Si, HF was added to each HCl-fraction to reach $c(\text{HF}) = 0.1\text{M}$. For up-scale experiments, the amount of ten processed Si-fractions was used (200 mL 0.1M HF; 800 μg Si; 400 μg V), but with

higher sulfur amounts of 30 mg, equal to 600 ppm per load. This value exceeds the expected quantity of silicon-32 ($N(^{32}\text{Si}) = 10^{15}$ atoms) by five orders of magnitude. These experiments were employed to prove the robustness and feasibility of the experimental design but also to determine the final parameters.

Results and Discussion

Retention of silicon, vanadium, and sulfur

The results of the varying HCl-conditions (Fig. 2) highlight that both sulfur and vanadium can be quantitatively eluted, while Si is retained. The Si recovery in the 0.5M HCl-fraction is $95\% \pm 5\%$.

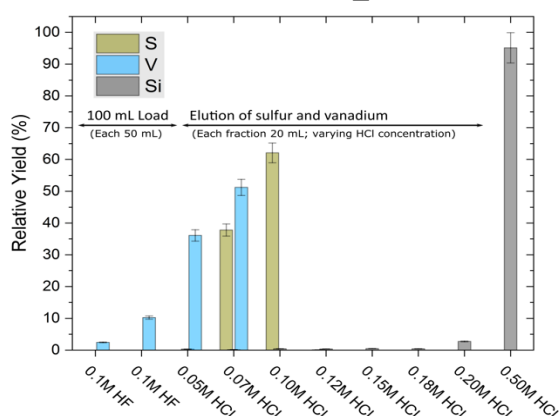


FIGURE 2: Exemplary “small-scale experiment” to study the elution behaviour of S, V, and Si, respectively, under varying HCl-concentrations.

Similar to silicon, sulfur is sufficiently retained under HCl-free conditions (= 0.1M HF matrix), while only low vanadium content can be detected. However, vanadium was not always detected in the load fraction, indicating remnant HCl contamination, likely related to previous experiments, given that the same column was used repeatedly.

As seen in Fig. 2, with increasing HCl concentration, both sulfur and vanadium are quite rapidly eluted from the column when exceeding concentrations of 0.10M HF/0.05 M HCl, which is thus considered as a threshold value. As a result, using 0.10M HF/0.10 M HCl, the highest sulfur amount was detected, indicating very low S-retention under these conditions. Therefore, utilizing higher HCl-concentrations, the quantitative removal of sulfur is achieved. Concerning Si, elution commences from 0.10M HF/0.18 M HCl onwards, which limits the HCl-concentration, to avoid Si losses during the sulfur addition.

Behaviour under ideal conditions

We learned from the previous experiments that both sulfur and silicon are retained during the load in 0.1M HF matrix. After the initial 200 mL load with $^{32}\text{SiF}_6^{2-}$, sulfur was subsequently added in the 0.10M HF/0.10M HCl matrix, as it runs over the column but

is not retained (S-Wash #1). When gradually increasing the HCl concentration (S-Wash #2), sulfur was quantitatively removed from the system. To avoid any remnant S in the Si-Fraction (0.5M HCl), 25 mL of 0.10M HF/0.16M HCl (S-Wash #3) was used. Eventually, a measurement of the undiluted Si-Fraction showed no S-presence, as the intensities were the same compared to 0.5M HCl blank samples.

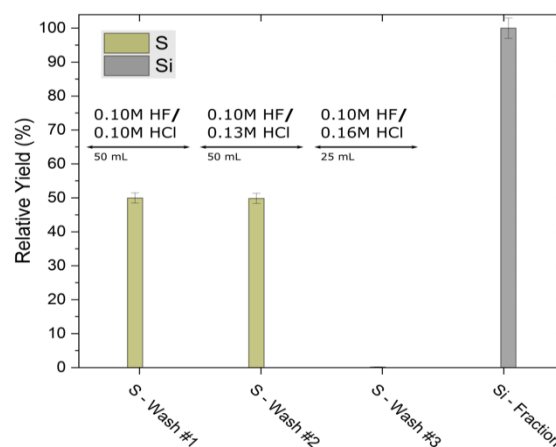


FIGURE 3: Exemplary “up-scale experiment” to highlight the quantitative removal of S. Silicon was in none of the sulfur samples detected, and the quantitative recovery ($98-100\% \pm 3\%$) of Si was repeatedly confirmed.

Conclusively, it could be demonstrated that under the chosen conditions, sulfur, along with vanadium impurities, were quantitatively removed from the system. This should allow the mathematical correction for isobaric interference, allowing the detection of the number of ^{32}Si atoms. The describe procedure was also applied to prepare a first ^{32}Si master solution, which will be measured throughout 2021 by the various methods (LSC, ICP-MS, and Accelerator Mass Spectrometry). Finally, we await the results from the ICP-MS operator to see if the solution is pure enough for an accurate measurement, since the detection limit of the ICP-OES significantly exceeds those of ICP-MS.

Acknowledgement

This project is funded by the Swiss National Science Foundation (SNSF) as part of SINERGIA No.177229 and from the European Union's Horizon 2020 research and innovation program under the Marie Skłodowska-Curie grant agreement No. 701647.

References

- [1] N. Kivel et al., *Anal. Bioanal. Chem.*, **9** (2013), pp. 2965-2972
- [2] I. Mihalcea et al., *LRC Annual Report 2020* (2021), pp. 35-36.

Towards implementing ^{32}Si for environmental research (SINCHRON): AMS measurements of ^{32}Si

M. Schlomberg, C. Vockenhuber, H.-A. Synal (ETHZ), D. Schumann, I. Mihalcea (PSI), M. Veicht (PSI & EPFL), A. Wallner (ANU Canberra)

Introduction

Within the SINCHRON collaboration, the Laboratory of Ion Beam Physics (LIP) at ETH Zurich will perform the measurements of the number of ^{32}Si atoms for the redetermination of its half-life using accelerator mass spectrometry (AMS). Therefore, an absolute and stable AMS measurement of the concentration of ^{32}Si in enriched ^{32}Si sample material produced by the PSI must be performed.

One of the main challenges is the clear identification of ^{32}Si in the presence of its intense isobar ^{32}S .

Isobar Separation for ^{32}Si

The separation of ^{32}Si from its isobar ^{32}S can be performed by utilizing the difference in stopping powers of Si and S. There are three possible approaches: 1. The current is diminished such that ^{32}Si and ^{32}S can be measured in a gas ionization chamber (GIC), where the identification of Si is achieved in the detector (direct detection). 2. A passive absorber is placed in front of a gas ionization detector (GID) that stops all ^{32}S ions and allows detection of the transmitting ^{32}Si ions. 3. A gas-filled magnet (GFM) causes different mean trajectories due to the different mean charge states and energy loss of the isobars. Therefore, most ^{32}S ions are spatially separated and can be blocked, while ^{32}Si can be measured in a GIC.

The Direct detection

The direct detection method can be used only if the intensities of ^{32}Si and ^{32}S are not too different. Since S is abundant and ^{32}S the most abundant isotope, one of the other methods must be used.

The passive absorber

The passive absorber method is based on the range difference of Si and S in the absorber (Fig. 1). First, we tried to separate the two ions using a silicon nitride (SiN) foil stack, but due to the impracticability to adjust the absorber thickness, we switched to CO_2 as absorber gas. At 15 MeV, we were able to separate the peaks of Si and S, but since stopping is a statistical process, the tail of the high current ^{32}S peak made the separation of the isobars impossible. Better separation is achieved at 30 MeV, however light recoils from the absorber materials (H, N, C, O), knocked out by the high ^{32}S intensity, produce a

background. Using Ar as absorber gas, we could reduce this recoil background and managed to achieve a preliminary identification of ^{32}Si .

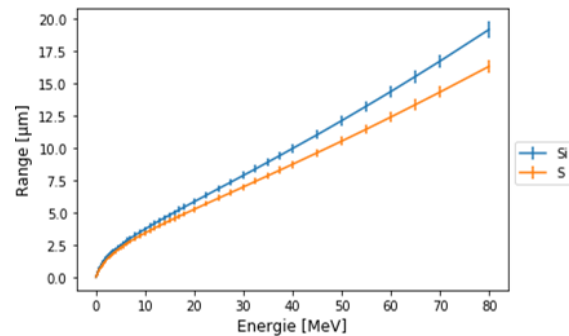


FIGURE 1: Range vs. energy of Si and S in SiN foils

The gas-filled magnet

We used the GFM method to measure the $^{32}\text{Si}/\text{Si}$ ratios of ^{32}Si samples produced and diluted to expected ratios between 10^{-9} and 10^{-12} at the PSI. At 44 MeV, we achieved a clear separation of the ^{32}Si and ^{32}S (Fig. 2). Of the stable isotopes, only the ^{30}Si current could be measured due to our beamline's geometry. Assuming natural abundance and estimating the efficiency of our GFM (between 0.1 and 0.7), we could confirm the correct isotopic ratio for the highest sample D2. Blank material showed no ^{32}Si counts corresponding to a ratio of $<10^{-13}$. However, the other samples showed ratios of 10^{-10} , indicating that the dilution material was contaminated. A new dilution series is currently prepared at PSI.

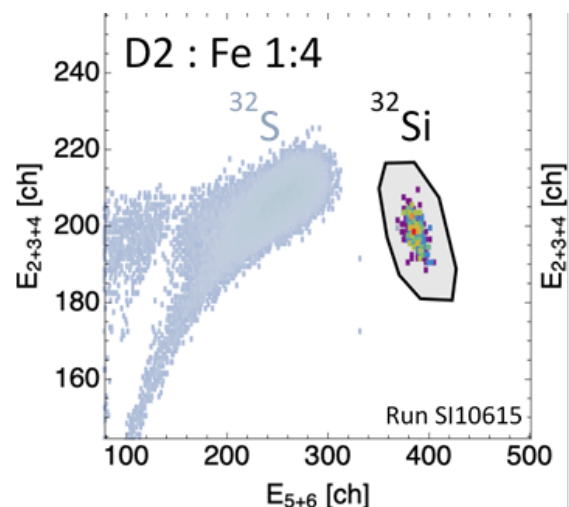


FIGURE 2: 2-dim. energy-spectrum of ^{32}Si sample after the GFM.

Report on the production of a ^{205}Tl target for a neutron capture experiment at the n_TOF facility (CERN)

A. Casanovas (UPC), E. A. Maugeri (PSI), A. Tarifeño-Saldivia, F. Calivño (UPC), S. Heinitz (PSI & SCK-CEN), D. Schumann, R. Dressler (PSI), P. Sprung (AHL/PSI), C. Guerrero (Univ. Sevilla)

Introduction

Neutron capture cross sections are one of the fundamental nuclear data for studying the *s*- (slow) process of nucleosynthesis. More interestingly, the competition between the capture and the decay rates in some unstable nuclei determines the local isotopic abundance pattern. Since decay rates are often sensible to temperature and electron density, the study of the nuclear properties of these nuclei can provide valuable constraints to the physical magnitudes of the nucleosynthesis stellar environment.

^{205}Tl is an interesting branching point, because in some stellar scenarios, it becomes unstable by bound state beta decay, intensely decaying to ^{205}Pb . Thus, the $^{205}\text{Tl}(n, \gamma)$ rate, by competing with the decay process, is key in determining the final abundance of both isotopes. ^{205}Pb , being radioactive, has potential use as an *s*-process cosmo-chronometer. Finally, an improved knowledge of the $^{205}\text{Tl}(n, \gamma)$ rate is necessary for a comprehensive understanding of the ^{204}Tl branching point. In this context, the $^{205}\text{Tl}(n, \gamma)$ measurement, performed at the n_TOF facility (CERN) in 2018 [1], came to complete the series of capture experiments of the thallium isotopes, which included ^{203}Tl and ^{204}Tl [2], both performed at n_TOF in 2015. In all three cases, the collaboration with PSI was essential for the preparation and the success of the experiments.

Materials and Methods

For the 2015 campaign, two pellets of ^{203}Tl , enriched >99.5% in ^{203}Tl for a total of 230 mg of ^{203}Tl , were produced at PSI by powder pressing. One of them was enriched up to 4% in ^{204}Tl by neutron irradiation during 55 days at the high flux reactor of the Institut Laue-Langevin (ILL). The sample was then transported back to PSI, for the final conditioning before the experiment at n_TOF.

Similarly, the ^{205}Tl samples used in 2018 were produced at PSI. Also in this case, the production process consisted in machine pressing of Tl_2O_3 powder into cylindrical samples. Prior to the production of the enriched samples, the method was tested using natural thallium powder (Sigma Aldrich). For the final samples, 5 g of highly enriched ^{205}Tl (>99.5%, Campro Scientific) were used. From this material, two samples were produced, one thick and one thinner, in order to investigate possible thickness-re-

lated effects in the capture cross-section measurement. Due to the very high toxicity of thallium, the samples were encapsulated and sealed in PEEK cylindrical containers (external diameter 21.50 ± 0.05 mm, internal diameter 19.45 ± 0.05 mm high 7.05 ± 0.05 mm), in order to prevent any loss of material, and to ensure the stability of the sample throughout the experiment.

Both samples had a diameter of about 19 mm. The “thicker” sample was 2.3 mm thick, with a ^{205}Tl mass of 3.71 g. It was important to avoid excessive thickness, which could result in large backgrounds, and excessive gamma ray self-absorption. The thinner sample was 1.0 mm thick, with a ^{205}Tl content of 1.25 g.

At the n_TOF facility, neutrons are produced by spallation of 20 GeV/c proton beams, accelerated by the CERN Proton Synchrotron, into a massive lead target. 300 neutrons per protons are produced, making n_TOF the most luminous facility of its kind. The energy of the neutrons is determined by the time-of-flight technique at the experimental area. Thanks to the long flight path of 184 m, a very high resolution in neutron energy is attained, in a wide energy range.

Capture reactions are counted by detecting the gamma rays emitted in the ensuing compound nucleus de-excitation process. For the purpose, C6D6 liquid scintillation detectors are employed, see Figure 1, which have been optimized specially for a very low neutron sensitivity.

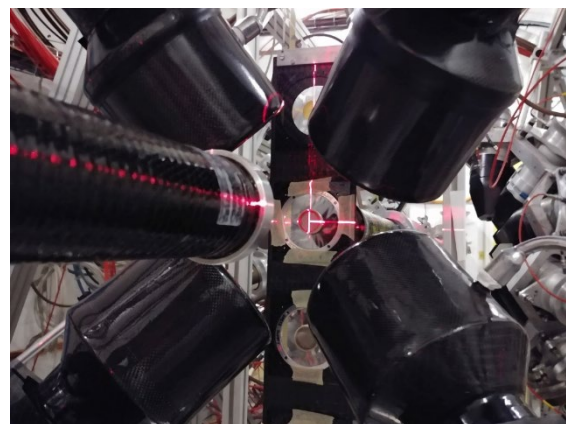


FIGURE 1: The experimental setup for the $^{205}\text{Tl}(n, \gamma)$ capture measurement, with the ^{nat}Tl sample (enclosed in the PEEK capsule) in the beam position.

Results and Conclusions

The $^{205}\text{Tl}(n, \gamma)$ campaign started at the beginning of July 2018. It was clear, since the first few hours of experiment, that both samples were heavily contaminated with bromine, identified by the observation in the preliminary data of neutron resonances of both its natural isotopes, ^{79}Br and ^{81}Br , respectively. The quantity and the cross section of these resonances were very high, making the $^{205}\text{Tl}(n, \gamma)$ measurement not feasible. The samples were sent back to PSI, where the contamination was quickly confirmed by ICP-MS and neutron activation analysis. It was verified that the “bromine contamination” was not due to the sample production process, nor from the capsule composition. The high level of contamination was rather ascribed to the chemical processes for the thallium purification followed by the producer and not reported in the material description.

In those circumstances, it was decided to produce a third sample at PSI, with natural thallium, containing 70.5% of ^{205}Tl . The new sample was ready for the experiment at n_TOF in a few days. The new sample had a natural thallium content of 3.71 g, of which 2.61 g were ^{205}Tl . Apart from the inevitable ^{203}Tl content (29.5%, 1.10 g), the material turned to be free from any other relevant contamination. ^{203}Tl has a high-resonance spacing, comparable to that of ^{205}Tl , and thus the chance of resonance overlapping is relatively low. Additionally, thanks to the measurement in 2015, the $^{203}\text{Tl}(n, \gamma)$ cross section of the strongest resonances, up to ~ 30 keV, is known accurately, thus resonance discrimination is straightforward, see Figure 2.

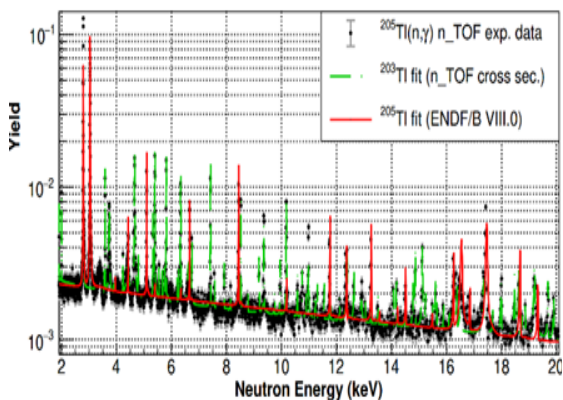


FIGURE 2: ^{203}Tl vs ^{205}Tl capture spectra in the natural thallium sample.

The data analysis from the $^{205}\text{Tl}(n, \gamma)$ measurement is currently on going. Preliminary analysis shows that ^{205}Tl capture resonances identification is possible up to, at least, 100 keV [1], see Figure 3. This should allow to calculate the ^{205}Tl Maxwellian averaged cross section (the cross section averaged by the neutron spectrum at stellar temperatures) at 30 keV, which

is the highest kT temperature at which the nucleosynthesis of the heaviest elements takes place.

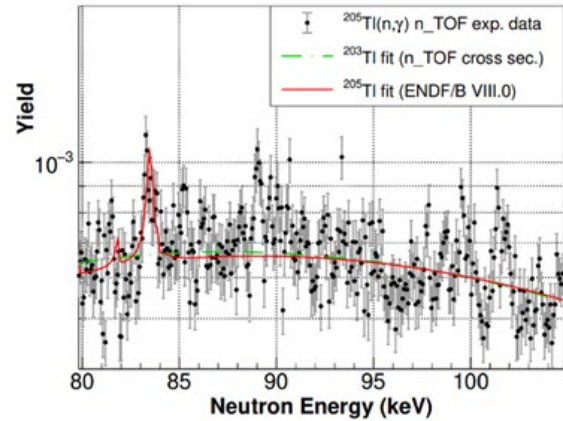


FIGURE 3: $^{205}\text{Tl}(n, \gamma)$ spectra up to 100 keV, with clearly visible resonances.

References

- [1] A. Casanovas et al., *EPJ Web of Conf.*, **178** (2018), pp. 03004
- [2] A Casanovas et al., *J. Phys.: Conf. Ser.*, **1668** (2020), pp. 012005

Sulphur-Bearing Macrocyclic Chelators for ^{64}Cu Radiopharmaceuticals: Radiolabeling and *In Vitro* Stability Evaluation

M. Tosato (Univ. of Padova), C. Favaretto (ETHZ & CRS/PSI), Z. Talip (CRS/PSI), N. P. van der Meulen (PSI)

Introduction

Among the large plethora of medically interesting metallic radionuclides, copper has attracted great interest because it possesses several radioisotopes with half-life and emission properties suitable for diagnostic and therapeutic applications [1]. Copper-64 (^{64}Cu , $T_{1/2} = 12.7$ h) is the most versatile of those since its unique decay profile, which combine β^+ ($E_{\beta^+ \text{ max}} 655$ keV, I_{β^+} 17%), β^- ($E_{\beta^- \text{ max}} 573$ keV, I_{β^-} 39%) and electron capture emissions (I_{EC} 43%), makes it suitable for both positron emission tomography (PET) imaging and cancer therapy [1].

The key to deliver ^{64}Cu to tumour cells securely is through stable complexation with a bifunctional chelator, covalently appended to a targeting biomolecule [2]. One of the main challenges for the *in vivo* successful application of Cu^{2+} complexes is their susceptibility to demetallation after the bio-induced reduction to Cu^+ [3].

In attempt to stabilize both copper oxidation states, we have recently developed two octadentate macrocyclic chelators bearing thioether sidearms, named L1 and L2, which demonstrated very promising coordination ability with $^{\text{nat}}\text{Cu}^{2+}$ and $^{\text{nat}}\text{Cu}^+$. [4] In this study, we aimed to explore their radiolabelling efficacy and *in vitro* stability with ^{64}Cu to assess their potential as ^{64}Cu ligands for radiopharmaceutical applications.

Results and Discussion

^{64}Cu was produced irradiating a ^{64}Ni enriched target with protons degraded to approximately 11 MeV at the 72 MeV PSI's Injector 2 research cyclotron. [5] ^{64}Cu was separated from the ^{64}Ni target material and radiocobalt coproduced impurities using cation exchange chromatography, according to a previously published protocol. [5]

The radiolabelling performance of L1 and L2 ligands were investigated and compared directly to the results obtained using the current "gold standard" for ^{64}Cu chelation NODAGA-RDG. Concentration-dependent labelling were performed by decreasing the ligand concentration while holding the ^{64}Cu activity constant to determine the highest molar activity that yields quantitative labelling. Different temperature (25°C and 95°C) and pH (4, 7) were tested.

At pH 4.5, the highest molar activity of ^{64}Cu -L2 obtained was 50 MBq/nmol, unlike ^{64}Cu -L1 and ^{64}Cu -NODAGA-RDG, which yielded molar activity as high as 25 MBq/nmol, after 10 min at 95°C. The

achievable maximum molar activity decreased to 10 MBq/nmol at room temperature in all systems.

At pH 7, no temperature dependence of the labelling capacity was found: L2 was able to quantitatively label ^{64}Cu at molar activity as high as 50 MBq/nmol whilst L1 and NODAGA-RDG at 10 MBq/nmol.

To gain insight into the stability of the ^{64}Cu -L1 and ^{64}Cu -L2 complexes, an *in vitro* serum stability assay was performed in the presence of an excess of human serum at 37°C for 24 hours. As control experiment, ^{64}Cu -DOTA was analyzed in parallel.

^{64}Cu -L1 and ^{64}Cu -L2 were exceptionally stable with $\geq 99\%$ of ^{64}Cu remaining chelate bound after 24 h. Contrarily, ^{64}Cu -DOTA complex showed an initial $\sim 21\%$ drop in stability after 6 h and subsequently stabilized to remain $\sim 90\%$ intact.

Conclusion

In this work, two Sulphur-bearing macrocyclic ligands, L1 and L2, were investigated for their capability to coordinate ^{64}Cu . Both ligands demonstrated comparable and often a superior labelling performance compared to the "gold standard" NODAGA-RDG. Human serum stability assays revealed ^{64}Cu -L1 and ^{64}Cu -L2 to be exceptionally inert complexes remaining 99% intact after 24 h, an improvement compared to the ^{64}Cu -DOTA complex. Further *in vivo* evaluations are necessary to fully assess the potential of these chelators for ^{64}Cu -based radiopharmaceuticals.

References

- [1] T. J. Wadas et al., *Curr. Pharm. Des.*, **13** (2207), pp. 3-16
- [2] M. Tosato et al., *Inorg. Chem.*, **59** (2020), pp. 10907-10919
- [3] E. Boros et al., *J. Label. Compd. Radiopharm.*, **61** (2019), pp. 652-671
- [4] M. Tosato et al., *manuscript in preparation*
- [5] N. P. van der Meulen et al., *J. Label. Compd. Radiopharm.*, **62** (2019), pp. 460-470

Determination of the gamma-emission probabilities of ^{169}Er

Z. Talip (CRS/PSI), F. Juget (IRA), J. Ulrich (PSI), Y. Nedjadi, T. Buchillier, M. T. Durán, F. Bochud, C. Bailat (IRA), N. P. van der Meulen (PSI)

Introduction

Erbium-169 has been used in colloidal citrate form for the treatment of chronic rheumatoid arthritis [1]. Thanks to its promising decay properties ($T_{1/2} = 9.38$ days), low β^- -energy ($\beta^-_{\text{av}} = 100$ keV) and very low gamma emission probabilities ($<10^{-4}$) (Figure 1), it has recently been considered as a radionuclide of interest in targeted radionuclide therapy of metastasized cancer diseases [2, 3].

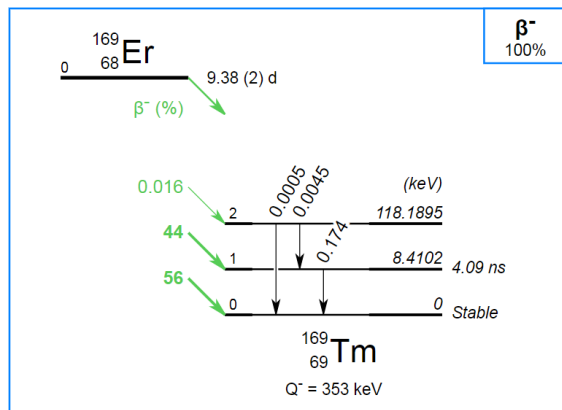


FIGURE 1: Erbium-169 decay scheme (Nucléide-LARA, 2018).

To the best of our knowledge, to date, only a few measurements were reported for the emission probabilities of ^{169}Er , with large discrepancies for the two γ -lines at 109.8 and 118.2 keV [4, 5]. In addition, different emission probability data were reported in different databases for ^{169}Er such as the Decay Data Evaluation Project (DDEP), the Evaluated Nuclear Structure Data File (ENSDF) and the Joint Evaluated Fission and Fusion (JEFF). As these values are quite discrepant and present high uncertainties ($>20\%$, Table 1), there is an urgent need to improve emission probability measurements.

TABLE 1: ^{169}Er decay data given in JEFF, ENSDF and DDEP databases with their relative standard uncertainties (u_{rel}) (DDEP, 2017, ENSDF, 2020, JEFF, 2020).

Energy (keV)	JEFF	u_{rel}	ENSDF	u_{rel}	DDEP	u_{rel}
109.78	1.3E-5	23%	1.3E-4	23%	4.5E-4	20%
118.19	1.4E-6	21%	1.4E-6	21%	5.0E-6	

In this study, the γ -emission probabilities of ^{169}Er were determined using radionuclidically pure ^{169}Er .

Independent measurements were performed using three different γ -spectrometry set-ups: one at the Institute of Radiation Physics (IRA), Lausanne, Switzerland and two at the Paul Scherrer Institute (PSI), Villigen-PSI, Switzerland. The efficiencies were computed using MCNP and validated using several experimental measurements.

Carrier-added ^{169}Er (37 MBq), was supplied as a colloidal suspension of ^{169}Er citrate from Curium (Swiss distributor b.e. imaging GmbH). After acidification of the Erbium-169 citrate solution with 7.0M HNO_3 (Suprapur Merck, Germany), ion-exchange chromatography was used to effectively separate ^{169}Er from radionuclidic impurities such as ^{169}Yb , ^{175}Yb , ^{170}Tm , ^{172}Tm , ^{172}Lu , and ^{177}Lu to obtain radionuclidically pure ^{169}Er solution [3].

After chemical separation, the stock solution (Er1) was divided into two parts (Er2 and Er5) (Figure 2). The first fraction (Er2) was diluted with 0.1M HCl and sent to IRA for standardization using the Triple to Double Coincidence Ratio (TDCR) technique (Er3) [6]. An aliquot from the standardized solution (Er3) was used to fill a 20 mL Zinsser plastic vial, which was completed with Er carrier (ErCl_3 25 $\mu\text{g/g}$ in 0.1M HCl) (Er4) to be used for γ -spectrometry measurement at IRA. The second fraction (Er5) taken from the stock solution, was used to prepare an ^{169}Er point-like source by evaporating multiple droplets on a circular polyethylene support for the γ -spectrometry measurement at PSI.

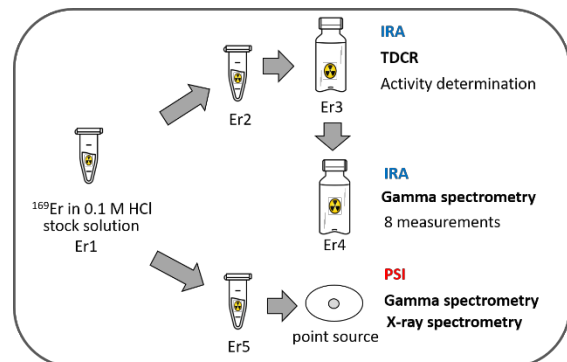


FIGURE 2: Scheme of the sources used for the TDCR, gamma and X-ray spectrometry measurements.

The ^{169}Er point-like source was measured for 15 days; no radionuclidic impurities were observed in the spectrum. The background spectrum was taken

shortly after the measurement to check for potential interference (Figure 3).

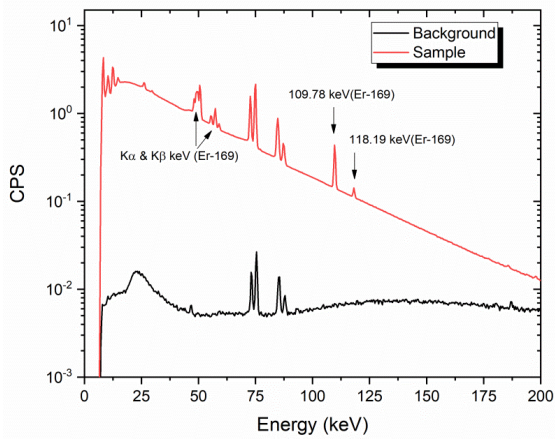


FIGURE 3: γ -spectrum of the ^{169}Er point-like source measured over 15 days at 15 cm (red line) distance from the detector, along with the background measurement performed for 43 h (black line). The spectrum was normalized to the counting time.

The emission probability P_γ was calculated according to:

$$P_\gamma = \frac{N}{t \cdot A \cdot \varepsilon_\gamma} \cdot C_{dec} \cdot C_{meas} \cdot C_{sum}$$

where N is the net number of counts in the peak area, t is the measurement live-time, A is the source activity and ε_γ is the FEP efficiency. C_{dec} is the correction factor for the source decay between the start of the measurement and the reference date, C_{meas} is the correction for the decay during the measurement. C_{sum} accounts for the coincidence summing correction.

The final values were calculated by combination of the three measurements. These were compared with the literature values (Figure 4). Gamma-emission probabilities of the two lines at 109 keV (a) and 118 keV present a large uncertainty reduction compared to previous evaluations. The emission probabilities per decay of ^{169}Er are reported as $1.4035(409) \cdot 10^{-5}$ for the 109.8 keV line and $1.5155(195) \cdot 10^{-6}$ for the 118.2 keV line. The uncertainties were dramatically reduced from 20% to 1.29% and 2.91%, respectively ($k=1$).

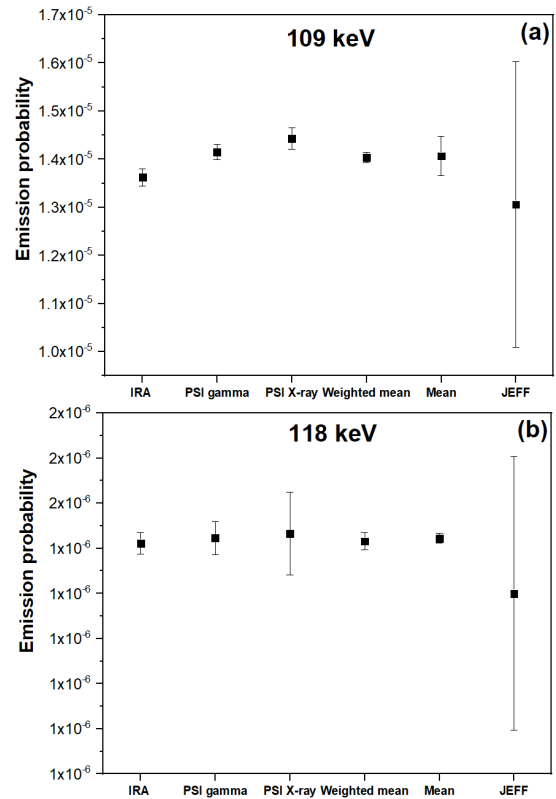


FIGURE 4: Comparison of the results of this study with JEFF data for the γ -emission probabilities of the two γ -lines at 109 keV (a) and 118 keV (b), respectively.

References

- [1] J. Farahati et al., *Clin. Case Reports*, **5** (2017), pp. 1048–1050
- [2] Formento et al., *Nucl. Instruments Methods Phys. Res. Sect. B Beam Interact. with Mater. Atoms*, **463** (2019) pp. 1–4
- [3] Talip et al., *Frontiers*, submitted 2021
- [4] A. Bisi et al., *Niova Cim.*, **4** (1956) pp. 758-763
- [5] R. P. Sharma et al., *Nucl. Phys. A*, **152**, (1970), pp. 225
- [6] Y. Nedjadi et al., *Appl. Radiat. Isot.* **97** (2015), pp. 113-117

Development of direct Ga-68 production by cyclotron irradiation of Zn-68 solid targets: preliminary results

P. V. Grundler (CRS/PSI), A. Varbella (PSI & EPFL), N. P. van der Meulen (PSI)

Introduction

Ga-68 is a positron emitter with a half-life of 68 minutes and therefore suited for PET imaging [1]. Its short half-life ideally requires on-site generation. Two options are available: i) the use of a generator loaded with Ge-68 or ii) the production with a cyclotron from a suitable target material.

Generators are commercially available, but there are limitations to the amount of Ga-68 they can deliver and their supply is limited as well. Therefore, it is worthwhile developing a method to produce Ga-68 directly. For this purpose, Zn-68 is a suitable target material since its cross section maximum for the reaction $^{68}\text{Zn}(p,n)^{68}\text{Ga}$ lies within the energy range of medical cyclotrons [2]. Furthermore, the cross section is high, ensuring the production of high activities from small targets. With a natural abundance of 18.8% for Zn-68, enriched material is still available at a relatively affordable price.

As legacy from the research on Cu-67 production about 20 years ago [3], solutions containing Zn-68 are still in storage. However, they are contaminated with Co-60. Recovering the Zn-68 and concentrating the Co-60 will provide the material needed for this project and help reduce old radioactive waste.

Furthermore, knowledge about efficient recycling of Zn-68 will also provide a plus value for the production of Ga-68, since a given stock of target material can then be recycled many times.

Results

A cation exchange resin that, under the given conditions, strongly retains Co but only weakly binds Zn was selected for the decontamination of the Zn-68 from Co-60. Since the exact composition of the starting material was unknown, Zn was precipitated with NaOH (Co-60 is co-precipitated), decanted and then re-dissolved in the eluent for the chromatographic separation.

Initially, traces of Zn-65 were present in the starting material but, finally, it was not enough to follow the elution of Zn by γ -spectrometry. Seeking an alternative for assessing the presence of Zn in the eluate fractions, the decision was taken to use UV-vis spectrophotometry with 1-(2-pyridylazo)-2-naphthol (PAN) as colorimetric reagent for Zn [4].

The Zn bearing Co-60 free fractions were combined and the solvent evaporated using a rotatory evaporator.

Since metallic Zn is a stable form of this element, it was decided to make the solid target out of this material. Metallic Zn was recovered by electrodeposition [5] from the product of the chromatographic separation. The thin dendrites formed during the electrodeposition proved to be very easy to press into solid discs of 6 mm diameter (Figure 1).

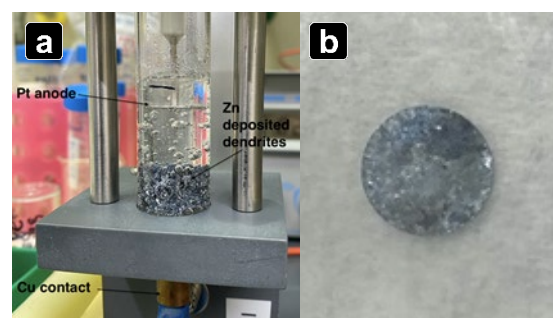


FIGURE 1: a) electrodeposition of Zn. b) Zn dendrite pressed into a 6 mm disc.

Such a disc was used for a test irradiation at the isotope production (IP2) irradiation station of the High Intensity Proton Accelerator (HIPA) facility at PSI. The 72 MeV proton beam was degraded to ~ 10.3 MeV using a 3.4 mm-thick Nb degrader and the target, encapsulated in Al, irradiated for 10 minutes.

After irradiation, the disc was processed to isolate the Ga-68 from the target material. For this purpose, a panel assembled mainly from medical infusion supplies (tap banks, tubing with Luer lock connectors etc.) [6] was used in a shielded cell. After dissolution of the disc in HCl, the solution was passed through a resin that selectively retained the Ga-68, whereas Zn-68 and the other impurities passed through and were collected for Zn-68 recycling. The Ga-68 was eluted and loaded onto an extraction resin column to finally recover it in saline solution suitable for further experimentation (*in vitro*, eventually *in vivo*).

From the 41 mg target an activity of ~ 140 MBq was obtained at the end of separation, which was about 1 h 50 min after the end of irradiation. The activity of the recovered product was checked at later time points and a slower decrease in activity than expected from the Ga-68 half-life (68 min) indicated

the presence of another radionuclide, most likely Ga-67 (half-life 78.3 h).

Conclusion and outlook

Methods for recovering Zn-68 from old samples and separating Ga-68 from an irradiated Zn-68 target have been developed and successfully demonstrated the feasibility of the whole process. However, optimization is required at several steps, in particular, to reduce the time between end of irradiation and end of separation. Procedures for the extensive quality control of the final product with respect to chemical, radiochemical and radionuclidic purity also needs to be implemented.

References

- [1] I. Velikyan, *Theranostics*, **4** (2014), pp. 47-80
- [2] M. Sadeghi et al., *Pramana*, **72** (2009), pp. 335-341
- [3] R. Schwarzbach et al., *J. Labelled Compd. Radiopharm.*, **44** (2001), pp. S809-S811
- [4] K. L. Cheng et al., *Anal. Chem.*, **27** (1955), pp. 782-785
- [5] S. Flisch, Master thesis, University of Bern, 2017
- [6] N. P. van der Meulen et al., *Molecules*, **25** (2020), pp. 4706

Production and radiochemical purification of ^{155}Tb for SPECT imaging purposes

C. Favaretto (ETHZ & PSI), Z. Talip (CRS/PSI), F. Borgna, P. Grundler (CRS/PSI), R. Schibli (ETHZ & PSI), C. Müller (CRS/PSI), N. P. van der Meulen (PSI)

Introduction

^{155}Tb is an interesting radionuclide for nuclear medicine. In particular, its γ -emissions (87, 105 and 180 keV, $T_{1/2} = 5.32$ d [1]) make it particularly promising with respect to tumor imaging and diagnosis by means of Single Photon Emission Computed Tomography (SPECT) [2]. Moreover, ^{155}Tb can form part of the dosimetry determination towards radionuclide therapy with ^{161}Tb – a novel radionuclide produced at Paul Scherrer Institute (PSI) [3]. Together with ^{161}Tb , it can play an important role towards the radiotheragnostics concept, as ^{155}Tb forms the diagnostic part of the “matched pair” principle - with ^{161}Tb used for β^- -therapy [4].

Methods

^{155}Tb was produced by proton irradiation via both $^{155}\text{Gd}(p,n)^{155}\text{Tb}$ and $^{156}\text{Gd}(p,2n)^{155}\text{Tb}$ nuclear reactions. Enriched gadolinium oxide targets ($^{155}\text{Gd}_2\text{O}_3$ and $^{156}\text{Gd}_2\text{O}_3$, respectively) were irradiated at the PSI’s IP2 irradiation station using the 72 MeV proton beam from the Injector 2 separated sector cyclotron. The energy of the beam was degraded to the desired windows using Nb degraders of specific thickness. After irradiation of the target material, ^{155}Tb was separated from the enriched Gd and other impurities using cation exchange and extraction chromatic resins, respectively, using a separation system designed for this purpose (Figure 1). The final product’s ($^{155}\text{TbCl}_3$) pH, radionuclidic purity and radiolabeling yield with DOTATOC were determined. Several *in vitro* and *in vivo* imaging studies were performed with the product obtained.



FIGURE 1: ^{155}Tb radiochemical separation panel.

Results and Discussion

Several $^{155}\text{Gd}_2\text{O}_3$ and $^{156}\text{Gd}_2\text{O}_3$ targets were successfully irradiated at PSI’s IP2 irradiation station and resulted in yields of up to 1.7 GBq ^{155}Tb . The developed purification method demonstrated an efficient separation of ^{155}Tb from the target material. The final product ($^{155}\text{TbCl}_3$) was eluted in 1 mL 0.05M HCl (pH 1-2) at an activity concentration of 0.03-1.3 MBq/ μL . The radionuclidic purity measurements showed the presence of the short-lived impurities ^{154}Tb (7-12%), ^{154m}Tb (35-70%) and $^{154m2}\text{Tb}$ (~1%), together with the long-lived radioisotope ^{156}Tb (6-8%), in ratios that depend on the nuclear reaction induced. Radiolabeling of DOTATOC with ^{155}Tb was reproducible at a molar activity of 50 MBq/nmol, with >99% radiochemical yield. Depending on the activity concentration of the ^{155}Tb solution, it was also possible to label DOTATOC, with a radiolabeling yield >99%, at higher molar activities of up to 100 MBq/nmol. The characteristics of the product were suitable to perform pre-clinical studies. In particular, promising cell uptake and internalization studies were performed with four compounds. With the same compounds, SPECT/CT imaging studies were successfully performed and revealed excellent tumor visualization up to 24 h post injection.

References

- [1] NuDat 2.8, Decay radiation search. Available online: <https://www.nndc.bnl.gov/nudat2/> (accessed January 2021)
- [2] C. Müller et al., *Nuclear Medicine and Biology*, **41** (2014), pp. 58-65
- [3] N. Gracheva et al., *EJNMMI Radiopharmacy and Chemistry*, **4** (2019), pp. 1-16
- [4] C. Müller et al., *Journal of Nuclear Medicine*, **53** (2012), pp. 1951-1959

Determination of the gamma and X-ray emission probabilities of ^{161}Tb

F. Juget (IRA), Z. Talip (PSI), T. Buchillier, M. T. Durán, Y. Nedjadi, F. Bochud (IRA), J. R. Zeevaart (NESCA), P. Grundler (CRS/PSI), N. P. van der Meulen (PSI), C. Bailat (IRA)

Introduction

The beta-emitting ^{161}Tb ($E\beta_{\text{av}}^- = 154$ keV (100%), $T_{1/2} = 6.9$ d) is an attractive radionuclide for targeted radionuclide therapy. Recent preclinical *in vivo* and *in vitro* studies performed using ^{161}Tb -PSMA-617 have shown very promising results compared to ^{177}Lu -PSMA-617 [1].

At this stage, the precision of the ^{161}Tb decay data has crucial importance to help shorten the transition period of this radionuclide to the clinics. Therefore, this study aimed to determine the γ - and X-ray emission probabilities of ^{161}Tb using a high-purity germanium (Ge) spectrometer.

^{161}Tb was produced by irradiating highly enriched (98.2%) $^{160}\text{Gd}_2\text{O}_3$ targets in SAFARI-1 (Necsa, South Africa, 2.10^{14} n.cm $^{-2}$.s $^{-1}$) nuclear research reactor. After irradiation, separation of ^{161}Tb was performed at PSI using a method developed previously [2]. A sample of $^{161}\text{TbCl}_3$ solution (400 MBq/mL) was transported to IRA. The solution was prepared to consist of 0.1M HCl solvent with a Tb $^{3+}$ -ion concentration of 25 $\mu\text{g.g}^{-1}$ (stock solution). The stock solution was diluted by a factor of 15 to prepare the master solution. Two 3-g aliquots of the master solution were dispensed into 5 mL glass ampoules for activity measurements in the reference ionization chamber CIR (Figure 1)[3].

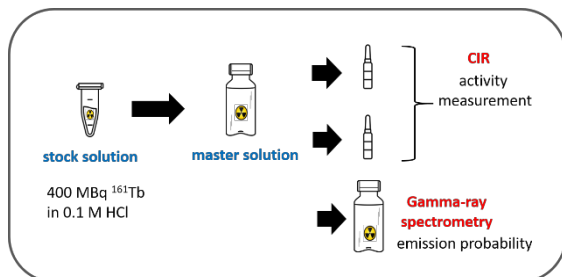


FIGURE 1: Scheme of the samples used for the CIR activity and γ -spectrometry measurements.

An aliquot (45.8024 mg) of the master solution was diluted to 20 mL in a Zinsser plastic vial prefilled with terbium carrier, so that the total mass was 20.02627(11) g. The total activity in the vial was 1116.84(890) kBq at the reference date. This vial was used for the γ -spectrometry measurements to determine γ - and X-ray emission probabilities of ^{161}Tb .

A total of 28 γ -rays and 4 X-rays were measured and compared with previous measurements. A large reduction of uncertainties was obtained, thanks to the

high radionuclidic purity of the source ($^{160}\text{Tb} \leq 0.007\%$), a precise activity measurement of the source [3], a precise ^{161}Tb half-life measurement [4], and a precise Monte Carlo calculation for the coincidence-summing correction.

TABLE 1: Comparison of the measured γ -emission probabilities for ^{161}Tb with different databases and data from Vylov, 1984 [5] (only the data with large discrepancies are presented).

Energy (keV)	This work	JEFF	ENSDF	LARA	Vylov et al. 1984
59.243	2.00E-03	2.10E-06	2.22E-04	2.22E-04	2.04E-04
84.73	2.13E-05	4.00E-06	4.20E-06	4.00E-06	4.00E-06
100.5	1.80E-05	3.00E-08	1.02E-06	1.00E-06	1.00E-06
131.8	1.25E-05	1.10E-06	1.02E-06	1.02E-06	<4.64E-5
315.1	5.54E-05	5.00E-06	6.00E-06	6.00E-06	4.00E-06

Most of the lines are in agreement, while large discrepancies were observed for five γ -energy lines (Table 1). The uncertainties from this determination are dramatically decreased in comparison to the previous measurements made.

References

- [1] C. Muller et al., *Eur. J. Nucl. Med. Mol. Imaging*, **46** (2019), pp. 1919-1930
- [2] N. Gracheva et al., *Eur. J. Nucl. Med. Mol. Imaging*, **4** (2019), pp. 1-16
- [3] Y. Nedjadi et al., *App. Radiat. and Isot.*, **166** (2020), pp. 109411
- [4] T. Duran et al., *App. Radiat. and Isot.*, **159** (2020) pp. 109085-109093.
- [5] Vylov et al., *Bull. Acad. Sci. USSR Phys. Res.*, **48** (1984)

Efficient production of high specific activity ^{167}Tm at PSI and CERN-MEDICIS

Z. Talip (CRS/PSI), R. Heinke (CERN/KU Leuven), E. Chevally, K. Chrysalidis (CERN), T. E. Cocolios (KU Leuven), C. Duchemin (CERN/KU Leuven), V. Fedosseev, L. Lambert, B. Marsh, T. Stora (CERN), M. Tosato (PSI), S. Wilkins (CERN), N. P. van der Meulen, H. Zhang (PSI)

Introduction

Auger electrons can be highly radiotoxic when they decay in the vicinity of DNA in the cell nucleus [1], which makes them attractive for radiotherapy. However, the radiobiological effects of Auger electrons are still not well understood. Further and systematic investigations using different Auger electron-emitting radionuclides to understand their therapeutic effects are urgently needed.

^{167}Tm is a potential radionuclide for both conversion/Auger electron therapy and imaging using single-photon emission computed tomography (SPECT) (γ -line at 207 keV). Previously, ^{167}Tm -citrate was used for tumor imaging [2], and dosimetry calculations showed that ^{167}Tm has a high ratio of absorbed dose rate in the tumor to the normal tissue [3].

The availability of radionuclidically and chemically pure ^{167}Tm is only possible with the combination of mass and chemical separation processes. We report here on the production of radionuclidically pure ^{167}Tm from proton-irradiated natural Er_2O_3 samples using mass separation at the CERN-MEDICIS facility [4], with a particular focus on the mass separation efficiency.

To assess the efficiency of the mass separation process, initial test experiments were performed using non-irradiated ^{169}Tm and $\text{Er}_2\text{O}_3/^{169}\text{Tm}$ samples. Resonance laser ionization was used to enhance the thulium fraction in the final product, yielding higher specific activity. Samples were gradually heated up over three days until exhaustion, resembling the actual collection process. A thulium resonance ionization scheme suitable to the MEDICIS Ti: sapphire laser system [5], initially developed for radioactive ion beam production at TRIUMF, was employed [6]. The temperature dependence of both element's release was investigated systematically, showing the favorable release of thulium at lower temperatures, and the influence of separator and laser parameters was determined.

The obtained data were applied for optimal mass separation of the irradiated Er_2O_3 targets. The 6 mm $^{nat}\text{Er}_2\text{O}_3$ targets were irradiated at PSI IP2 irradiation

station, using the 72 MeV proton beam from Injector II. A 3.4 mm Nb disc was used as a degrader to decrease the proton energy to 22.8 MeV. The beam current was set to 50 μA and several test irradiations were performed using 30 mg $^{nat}\text{Er}_2\text{O}_3$ targets for 8 hours.

TABLE 1: Comparison of the separation efficiencies.

Target activity (MBq)	Foil	Implanted activity on foil (MBq)	Target activity at time of spectrometry (MBq)	Sep. eff. for each foil (%)	Sep. eff. total (%)
105.4	1A	8.6	65.7	13.1	13
	1B	0.2	65.5	0.2	
97.8	2A	7.0	62.1	11.3	24
	2B	7.7	62.0	12.4	
	2C	0.6	62.1	1.0	
154	3A	13.5	98.0	13.8	16
	3B	2.5	98.0	2.6	
	3C	2.3	97.8	2.4	

Three targets (105, 98 and 154 MBq ^{167}Tm) were shipped then to the CERN MEDICIS facility. After mass separation, mass 167 implanted foils (zinc-coated gold foils) were shipped back to PSI for gamma-ray spectrometry and ICP-MS measurements. Gamma-ray spectrometry measurements performed before and after mass separation showed that collection efficiencies in the order of 20% were achieved (Table 1). Up to date, it presents the highest achieved values at the CERN MEDICIS facility. ICP-MS measurements of the samples (natural Er_2O_3 , proton-irradiated Er_2O_3 and mass separated ^{167}Tm samples) are currently ongoing.

References

- [1] A. Ku et al. *EJNMMI Radiopharma Chem.*, **4** (2019) pp. 1-36
- [2] A. Ando et al. *Eur. J. Nucl. Med.*, **8** (1983) pp.440-446
- [3] H. Uusijarvi et al., *J. Nucl. Med.*, **47** (2006) pp. 807-815
- [4] C. Duchemin et al., *Proc. IPAC2020*, pp. 75-79
- [5] Gadelshin et al., *Nucl. Instrum. And Methods Phys. Res. B* **463** (2020) pp. 460-463
- [6] M. Mostamand, PhD thesis, The University of Manitoba, 2020

LIST OF PUBLICATIONS

Aerts A, Gonzalez Prieto B, Neuhausen J

Behavior of spallation, activation and fission products in LBE

Konings RJM, Stoller RE, eds. Comprehensive nuclear materials. sine loco: Elsevier; 2020:735-765.

<https://doi.org/10.1016/B978-0-12-803581-8.11612-1>

Alcayne V, Mendoza E, Cano-Ott D, Kimura A, Aberle O, Amaducci S et al.

Measurement of the ^{244}Cm capture cross sections at both CERN n_{TOF} experimental areas

Ge Z, Shu N, Chen Y, Wang W, Zhang H, eds. ND 2019: international conference on nuclear data for science and technology. Vol. 239. EPJ web of conferences. Sine loco: EDP Science; 2020:01034 (5 pp.).

<https://doi.org/10.1051/epjconf/202023901034>

Antognini A, Berger N, Cocolios TE, Dressler R, Eichler R, Eggenberger A et al.

Measurement of the quadrupole moment of ^{185}Re and ^{187}Re from the hyperfine structure of muonic X rays. Physical Review

C: Nuclear Physics. 2020; 101(5): 054313 (14 pp.). <https://doi.org/10.1103/PhysRevC.101.054313>

Babiano-Suarez V, Aberle O, Alcayne V, Amaducci S, Andrzejewski J, Audouin L et al.

$^{80}\text{Se}(n,\gamma)$ cross-section measurement at CERN n_{TOF}

Nuclear physics in astrophysics IX (NPA-IX), 15-20 September 2019, Frankfurt, Germany. Vol. 1668. Journal of physics: conference series. Bristol, United Kingdom: IOP Publishing; 2020:012001 (8 pp.). <https://doi.org/10.1088/1742-6596/1668/1/012001>

Bacak M, Aïche M, Bélier G, Berthoumieux E, Diakaki M, Dupont E et al.

A compact fission detector for fission-tagging neutron capture experiments with radioactive fissile isotopes Nuclear Instruments and Methods

Physics Research, Section A: Accelerators, Spectrometers, Detectors and Associated Equipment. 2020; 969: 163981 (10 pp.). <https://doi.org/10.1016/j.nima.2020.163981>

Balibrea-Correa J, Mendoza E, Cano-Ott D, González E, Capote R, Krτίčka M et al.

Measurement of the α ratio and (n, γ) cross section of ^{235}U from 0.2 to 200 eV at n_{TOF}

Physical Review C: Nuclear Physics. 2020; 102(4): 044615 (18 pp.). <https://doi.org/10.1103/PhysRevC.102.044615>

Breur PA, Nobelen JCPY, Baudis L, Brown A, Colijn AP, Dressler R et al.

Testing claims of the GW170817 binary neutron star inspiral affecting β -decay rates

Astroparticle Physics. 2020; 119: 102431 (3 pp.). <https://doi.org/10.1016/j.astropartphys.2020.102431>

Casanovas A, Tarifeño-Saldivia AE, Domingo-Pardo C, Calviño F, Maugeri E, Guerrero C et al.

Neutron capture measurement at the n_{TOF} facility of the ^{204}Tl and ^{205}Tl s-process branching points

Nuclear physics in astrophysics IX (NPA-IX), 15-20 September 2019, Frankfurt, Germany. Vol. 1668. Journal of physics: conference series. Bristol, United Kingdom: IOP Publishing; 2020:012005 (9 pp.). <https://doi.org/10.1088/1742-6596/1668/1/012005>

Chiera NM, Talip Z, Fankhauser A, Schumann D

Separation and recovery of exotic radiolanthanides from irradiated tantalum targets for half-life measurements

PLoS One. 2020; 15(7): e0235711 (19 pp.). <https://doi.org/10.1371/journal.pone.0235711>

De Gerone M, Alpert B, Becker D, Bennett D, Biasotti M, Ceriale V et al.

Probing the absolute neutrino mass scale with the ^{163}Ho : the HOLMES project

XV international conference on topics in astroparticle and underground physics 24-28 June 2017, Sudbury, ON, Canada. Vol. 1342. Journal of physics: conference series. Philadelphia: IOP Publishing; 2020:012092 (5 pp.).

<https://doi.org/10.1088/1742-6596/1342/1/012092>

Domingo-Pardo C, Babiano-Suarez V, Balibrea-Correa J, Caballero L, Ladarescu I, Leredegui-Marco et al.

Review and new concepts for neutron-capture measurements of astrophysical interest

Nuclear physics in astrophysics IX (NPA-IX), 15-20 September 2019, Frankfurt, Germany. Vol. 1668. Journal of physics: conference series. sine loco: IOP Publishing; 2020:012013 (13 pp.). <https://doi.org/10.1088/1742-6596/1668/1/012013>

- Duchemin C, Ramos JP, Stora T, Aubert E, Audouin N, Barbero E et al.
on behalf of the CERN-MEDICIS collaboration *CERN-MEDICIS: A unique facility for the production of non-conventional radionuclides for medical research*
Proc. IPAC20, JACoW Publishing, Geneva (2020). ISBN: 978-3-95450-213-4. DOI: 10.18429/JACoW-IPAC2020-THVIR13
- Durán MT, Juget F, Nedjadi Y, Bochud F, Grundler PV, Gracheva N et al.
Determination of ^{161}Tb half-life by three measurement methods
Applied Radiation and Isotopes. 2020; 159: 109085 (9 pp.). <https://doi.org/10.1016/j.apradiso.2020.109085>
- Eleme Z, Patronis N, Stamatopoulos A, Tsinganis A, Kokkoris M, Michalopoulou V et al.
First results of the $^{241}\text{Am}(n,f)$ cross section measurement at the experimental area 2 of the n_TOF facility at CERN
Ge Z, Shu N, Chen Y, Wang W, Zhang H, eds. ND 2019: international conference on nuclear data for science and technology. Vol. 239. EPJ web of conferences. Sine loco: EDP Science; 2020:05014 (5 pp.).
<https://doi.org/10.1051/epjconf/202023905014>
- Faverzani M, Alpert B, Balata M, Backer D, Bennet D, Bevilacqua A et al.
Status of the HOLMES experiment
Journal of Low Temperature Physics. 2020; 199: 1098-1106. <https://doi.org/10.1007/s10909-020-02385-7>
- Figuera P, Maugeri EA, Buompane R, Cosentino L, Di Leva A, Di Pietro A et al.
Development of an intense ^{10}Be radioactive beam in 'off-line mode' at the Catania Tandem accelerator
Nuclear Instruments and Methods in Physics Research, Section A: Accelerators, Spectrometers, Detectors and Associated Equipment. 2020; 972: 164120 (5 pp.). <https://doi.org/10.1016/j.nima.2020.164120>
- Forstner O, Bemmerer D, Cowan TE, Dressler R, Junghans AR, Schumann D et al.
Opportunities for measurements of astrophysical-relevant alpha-capture reaction rates at CRYRING@ESR
X-Ray Spectrometry. 2020; 49(1): 129-132. <https://doi.org/10.1002/xrs.3071>
- Gallucci G, Alpert B, Balata M, Becker DT, Bennett DA, Bevilacqua A et al.
Status of the HOLMES experiment to directly measure the electron neutrino mass with a calorimetric approach
The 21st international workshop on neutrinos from accelerators. Vol. 369. Proceedings of science. Trieste, Italy: Sissa Medialab srl; 2020:106 (6 pp.). <https://doi.org/10.22323/1.369.0106>
- Gracheva N, Carzaniga TS, Schibli R, Braccini S, van der Meulen NP
 ^{165}Er : A new candidate for Auger electron therapy and its possible cyclotron production from natural holmium targets
Applied Radiation and Isotopes. 2020; 159: 109079 (8 pp.). <https://doi.org/10.1016/j.apradiso.2020.109079>
- Grundler PV, Eichler R, Talip Z, Schubiger PA, Schibli R, van der Meulen NP
The metamorphosis of radionuclide production and development at Paul Scherrer Institute
Chimia. 2020; 74(12): 968-975. <https://doi.org/10.2533/CHIMIA.2020.968>
- Guerrero C, Lerendegui-Marco J, Paul M, Tessler M, Heinitz S, Domingo Pardo C et al.
Neutron capture on the s-process branching point ^{171}Tm via time-of-flight and activation
Physical Review Letters. 2020; 125(14): 142701 (8 pp.). <https://doi.org/10.1103/PhysRevLett.125.142701>
- Karlsson E, Neuhausen J, Eichler R, Vögele A, Türlér A
Adsorption properties of iodine on fused silica surfaces when evaporated from tellurium in various atmospheres
Journal of Radioanalytical and Nuclear Chemistry. 2020; 326: 711-718. <https://doi.org/10.1007/s10967-020-07326-y>
- Karlsson E, Neuhausen J, Eichler R, Aerts A, Danilov II, Vögele A et al.
Thermochromatographic behavior of iodine in fused silica columns when evaporated from lead-bismuth eutectic
Journal of Radioanalytical and Nuclear Chemistry. 2020; 326: 1249-1258. <https://doi.org/10.1007/s10967-020-07420-1>
- Karlsson E, Neuhausen J, Aerts A, Danilov II, Eichler R, Türlér A et al.
Polonium behavior following a vacuum window rupture in a lead-bismuth eutectic based accelerator driven system
Applied Radiation and Isotopes. 2021; 168: 109551 (7 pp.). <https://doi.org/10.1016/j.apradiso.2020.109551>

- Khuyagbaatar J, Yakushev A, Düllmann CE, Ackermann D, Andersson LL, Asai M et al.
Search for elements 119 and 120
 Physical Review C: Nuclear Physics. 2020; 102(6): 064602 (9 pp.). <https://doi.org/10.1103/PhysRevC.102.064602>
- Kraus B, Steinegger P, Aksenov NV, Dressler R, Eichler R, Griesmayer E, Herrmann D, Türler A, Weiss C
Charger carrier properties of single-crystal CVD diamond up to 473 K
 Nuclear Inst. and Methods in Physics Research, A, 989 (2021), DOI: 10.1016/j.nima.2020.164947
- Kraus B, Steinegger P, Aksenov NV, Dressler R, Eichler R, Griesmayer E et al.
Charge carrier properties of single-crystal CVD diamond up to 473 K
 Nuclear Instruments and Methods in Physics Research, Section A: Accelerators, Spectrometers, Detectors and Associated Equipment. 2021; 989: 164947 (6 pp.). <https://doi.org/10.1016/j.nima.2020.164947>
- Leya I, David J-C, Faestermann T, Froehlich M, Kivel N, Koll D et al.
 ^{53}Mn and ^{60}Fe in iron meteorites -new data, model calculations
 Meteoritics and Planetary Science. 2020; 55(4): 818-831. <https://doi.org/10.1111/maps.13466>
- Lima TVM, Gnesin S, Nitzsche E, Ortega PG, Müller C, van der Meulen NP
First phantom-based quantitative assessment of scandium-44 using a commercial PET device
 Frontiers in Physics. 2020; 8: 241 (10 pp.). <https://doi.org/10.3389/fphy.2020.00241>
- Lin M, Kajan I, Schumann D, Türler A, Fankhauser A
Selective Cs-removal from highly acidic spent nuclear fuel solutions
 Radiochimica Acta. 2020; 108(8): 615-626. <https://doi.org/10.1515/ract-2019-3187>
- Manna A, Aberle O, Alcayne V, Amaducci S, Andrzejewski J, Audouin L et al.
Setup for the measurement of the $^{235}\text{U}(n,f)$ cross section relative to n-p scattering up to 1 GeV.
 Ge Z, Shu N, Chen Y, Wang W, Zhang H, eds. ND 2019: international conference on nuclear data for science and technology. Vol. 239. EPJ web of conferences. Sine loco: EDP Science; 2020:01008 (5 pp.).
<https://doi.org/10.1051/epjconf/202023901008>
- Mărginean N, Little D, Tsunoda Y, Leoni S, Janssens RVF, Fornal B et al.
Shape coexistence at zero spin in ^{64}Ni driven by the monopole tensor interaction
 Physical Review Letters. 2020; 125(10): 102502 (7 pp.). <https://doi.org/10.1103/PhysRevLett.125.102502>
- Marin I, Rydèn T, Van Essen M, Svensson J, Gracheva N, Köster U et al.
Establishment of a clinical SPECT/CT protocol for imaging of ^{161}Tb
 EJNMMI Physics. 2020; 7(1): 45 (16 pp.). <https://doi.org/10.1186/s40658-020-00314-x>
- Mastromarco MM, Mazzone A, Massimi C, Cristallo S, Colonna N, Aberle O et al.
The ^{154}Gd neutron capture cross section measured at the n_TOF facility and its astrophysical implications
 Ge Z, Shu N, Chen Y, Wang W, Zhang H, eds. ND 2019: international conference on nuclear data for science and technology. Vol. 239. EPJ web of conferences. Sine loco: EDP Science; 2020:07003 (5 pp.).
<https://doi.org/10.1051/epjconf/202023907003>
- Mazzone A, Cristallo S, Aberle O, Alaerts G, Alcayne V, Amaducci S et al.
Measurement of the $^{154}\text{Gd}(n,\gamma)$ cross section and its astrophysical implications
 Physics Letters, Section B: Nuclear, Elementary Particle and High-Energy Physics. 2020; 804: 135405 (6 pp.).
<https://doi.org/10.1016/j.physletb.2020.135405>
- Mengoni A, Damone LA, Barbagallo M, Aberle O, Alcayne V, Amaducci S et al.
New reaction rates for the destruction of ^7Be during big bang nucleosynthesis measured at CERN/n_TOF and their implications on the cosmological lithium problem
 Ge Z, Shu N, Chen Y, Wang W, Zhang H, eds. ND 2019: international conference on nuclear data for science and technology. Vol. 239. EPJ web of conferences. Sine loco: EDP Science; 2020:07001 (4 pp.).
<https://doi.org/10.1051/epjconf/202023907001>

- Michalopoulou V, Stamatopoulos A, Vlastou R, Kokkoris M, Tsinganis A, Diakaki M et al.
First results of the $^{230}\text{Th}(n,f)$ cross section measurements at the CERN n_TOF facility
Ge Z, Shu N, Chen Y, Wang W, Zhang H, eds. ND 2019: international conference on nuclear data for science and technology. Vol. 239. EPJ web of conferences. Sine loco: EDP Science; 2020:05004 (6 pp.).
<https://doi.org/10.1051/epjconf/202023905004>
- Müller C, Béhé M, Geistlich S, van der Meulen NP, Schibli R
Targeted radiotherapeutics from 'bench-to bedside'
Chimia. 2020; 74(12): 939-945. <https://doi.org/10.2533/CHIMIA.2020.939>
- Nedjadi Y, Juget F, Desorgher L, Durán MT, Bochud F, Müller C et al.
Activity standardisation of ^{161}Tb
Applied Radiation and Isotopes. 2020; 166: 109411 (13 pp.). <https://doi.org/10.1016/j.apradiso.2020.109411>
- Neuhausen J
Radionuclide chemistry in nuclear facilities based on heavy liquid metal coolants: past, present and future
Chimia. 2020; 74(12): 976-983. <https://doi.org/10.2533/chimia.2020.976>
- Nizou G, Favaretto C, Borgna F, Grundler PV, Saffon-Merceron N, PlatasIglesias C et al.
Expanding the scope of pyclen-picolinate lanthanide chelates to potential theranostic applications
Inorganic Chemistry. 2020; 59(16): 11736-11748. <https://doi.org/10.1021/acs.inorgchem.0c01664>
- Oprea A, Günsing F, Schillebeeckx P, Aberle O, Bacak M, Berthoumieux E et al.
Neutron capture cross section measurements of ^{241}Am at the n_TOF facility
Ge Z, Shu N, Chen Y, Wang W, Zhang H, eds. ND 2019: international conference on nuclear data for science and technology. Vol. 239. EPJ web of conferences. Les Ulis Cedex A: EDP Sciences; 2020:01009 (5 pp.).
<https://doi.org/10.1051/epjconf/202023901009>
- Schiffer M, Stolz A, López DA, Spanier R, Herb S, Müller-Gatermann C et al.
Method developments for accelerator mass spectrometry at CologneAMS, $^{53}\text{Mn}/^3\text{He}$ burial dating and ultra-small $^{14}\text{CO}_2$ samples
Global and Planetary Change. 2020; 184: 103053 (7 pp.). <https://doi.org/10.1016/j.gloplacha.2019.103053>
- Schumann D, Maugeri E, Dressler R
Exotic radionuclides - What are they good for?
Chimia. 2020; 74(12): 932-938. <https://doi.org/10.2533/CHIMIA.2020.932>
- Schumann D, Heule M
Radioanalytics - an indispensable tool for radiological and nuclear safety
Chimia. 2020; 74(12): 995-999. <https://doi.org/10.2533/CHIMIA.2020.995>
- Stamatopoulos A, Tsinganis A, Colonna N, Kokkoris M, Vlastou R, Diakaki M et al.
Investigation of the $^{240}\text{Pu}(n, f)$ reaction at the n_TOF/EAR2 facility in the 9 meV-6 MeV range
Physical Review C: Nuclear Physics. 2020; 102(1): 014616 (23 pp.). <https://doi.org/10.1103/PhysRevC.102.014616>
- Steinegger P, Eichler R
Radiochemical research with transactinide elements in Switzerland
Chimia. 2020; 74(12): 924-931. <https://doi.org/10.2533/chimia.2020.924>
- Steyn GF, van der Walt TN, Szelecsényi F, Perrang C, Brümmer JW, Vermeulen C et al.
Large-scale production of ^{88}Y and $^{88}\text{Zr}/^{88}\text{Y}$ generators: a proof of concept study for a 70 MeV H- cyclotron
Applied Radiation and Isotopes. 2021; 168: 109469 (11 pp.). <https://doi.org/10.1016/j.apradiso.2020.109469>
- Studer D, Ulrich J, Braccini S, Carzaniga TS, Dressler R, Eberhardt K et al.
High-resolution laser resonance ionization spectroscopy of $^{143-147}\text{Pm}$
European Physical Journal A: Hadrons and Nuclei. 2020; 56(2): 69 (13 pp.). <https://doi.org/10.1140/epja/s10050-020-00061-8>

- Taddio MF, Castro Jaramillo CA, Runge P, Blanc A, Keller C, Talip Z et al.
In vivo imaging of local inflammation: monitoring LPS-induced CD80/CD86 upregulation by PET
Molecular Imaging and Biology. 2020. <https://doi.org/10.1007/s11307-020-01543-3>
- Talip Z, Favaretto C, Geistlich S, van der Meulen NP
A step-by-step guide for the novel radiometal production for medical applications: case studies with ^{68}Ga , ^{44}Sc , ^{177}Lu and ^{161}Tb
Molecules. 2020; 25(4): 966 (29 pp.). <https://doi.org/10.3390/molecules25040966>
- Terranova N, Aberle O, Alcayne V, Amaducci S, Andrzejewski J, Audouin L et al.
Monte Carlo simulations and n-p differential scattering data measured with Proton Recoil Telescopes
Ge Z, Shu N, Chen Y, Wang W, Zhang H, eds. ND 2019: international conference on nuclear data for science and technology. Vol. 239. EPJ web of conferences. Les Ulis Cedex A: EDP Sciences; 2020:01024 (5 pp.).
<https://doi.org/10.1051/epjconf/202023901024>
- Ulrich J, Ayranov M, Kaestner A, Schumann D, Sprung P, Türler A et al.
Neutron capture cross section of ^{53}Mn from irradiation with cold and reactor neutrons
Physical Review C: Nuclear Physics. 2020; 102(2): 024613 (9 pp.).<https://doi.org/10.1103/PhysRevC.102.024613>
- van der Meulen NP, Hasler R, Talip Z, Grundler PV, Favaretto C, Umbricht CA et al.
Developments toward the implementation of ^{44}Sc production at a medical cyclotron
Molecules. 2020; 25(20): 4706 (16 pp.). <https://doi.org/10.3390/molecules25204706>
- van der Meulen NP, Eichler R, Grundler PV, Hasler R, Hirzel W, Joray S et al.
The use of PSI's IP2 beam line towards exotic radionuclide development and its application towards proof-of-preclinical and clinical studies
Conradie L, Garrett De Villiers J, Schaa VRW, eds. CYC2019. 22nd international conference on cyclotrons and their applications. Vol. 22. International conference on cyclotrons and their applications. Geneva: JACoW Publishing; 2020:132-135. <https://doi.org/10.18429/JACoW-Cyclotrons2019-TUA03>
- van der Meulen NP, Hasler R, Talip Z, Grundler PV, Favaretto C, Umbricht CA, Müller C, Dellepiane G, Carzaniga TS, Braccini S
The Development of ^{44}Sc Towards Implementation at a Medical Cyclotron
Molecules (2020), 25(20), 4706. <https://doi.org/10.3390/molecules25204706>.
- van Heerden MR, Cole K, van der Meulen NP, Franzidis J-P, Buffler A
Extending the life of SnO_2 $^{68}\text{Ge}/^{68}\text{Ga}$ generators used in the radiolabelling of ion exchange resins
Applied Radiation and Isotopes. 2020; 158: 109044 (6 pp.). <https://doi.org/10.1016/j.apradiso.2020.109044>
- Volkmandt M, Eberhardt K, Endres A, Erbacher P, Fix M, Göbel K et al.
Neutron capture cross section for ^{10}Be
Nuclear physics in astrophysics IX (NPA-IX), 15-20 September 2019, Frankfurt, Germany. Vol. 1668. Journal of physics: conference series. IOP Publishing Ltd; 2020:012048 (7 pp.). <https://doi.org/10.1088/1742-6596/1668/1/012048>
- Zhang H, Eichler R, Grillenberger J, Hirzel W, Joray S, Kiselev D.C et al.
BDSIM simulation of the complete radionuclide production beam line from beam splitter to target station at the PSI cyclotron facility
Conradie L, Garrett De Villiers J, Schaa VRW, eds. CYC2019. 22nd international conference on cyclotrons and their applications. Vol. 22. International conference on cyclotrons and their applications. Geneva: JACoW Publishing; 2020:275-278. <https://doi.org/10.18429/JACoWCyclotrons2019-WEB04>

INTERNAL REPORTS

N.P. van der Meulen

TATTOOS meeting (as part of the PSI Roadmap), "TATTOOS – Targeted Alpha Therapy using Terbium and Other Oncological Solutions" presented to PSI Division Heads, 22 January 2020

Z. Talip

CERN-MEDICIS 5th Board Meeting, "Project updates to the MEDICIS collaboration board"
CERN, Geneva, 20 February 2020

R. Eichler

TATTOOS @ HIPA PSI Presentation to PSI personell, 29 October 2020

CONTRIBUTIONS TO CONFERENCES, WORKSHOPS AND SEMINARS

N.M. Chiera

Chemical investigation of exotic radionuclides

Seminar für Kern- und Radiochemie, Johannes-Gutenberg-Universität Mainz, Germany, 06 January 2020

N.M. Chiera

Chemistry with exotic radionuclides

Seminar of the Laboratory of Radiochemistry, Paul Scherrer Institute, Villigen PSI, Switzerland, 04 December 2020 (online)

C. Favaretto

The introduction of ^{161}Tb to the clinic through the Good Manufacturing Practice compliant production of ^{161}Tb -DOTATOC
CRS Seminar Day, Paul Scherrer Institute, Villigen PSI, Switzerland, 12 August 2020

P. Ionescu

Trace Gas Effects on the Chromatographic Yield of Hg and At - Development of Fast On-Line Detector (FOLD)

Seminar of the Laboratory of Radiochemistry, Paul Scherrer Institute, Villigen PSI, Switzerland, 04 December 2020

I. Kajan

Challenges in half-life determinations by gamma spectroscopy

Seminar of the Laboratory of Radiochemistry, Paul Scherrer Institute, Villigen PSI, Switzerland, 23 October 2020

I. Kajan, M. Lin, D. Schumann

Waste treatment and Isotope Reclamation

Meeting on SwissNuclear research projects, 28 October 2020

E. Karlsson

The adsorption behavior of volatile radionuclides present in a lead-bismuth eutectic reactor system

PhD Defense, University of Bern, Bern, Switzerland, 24 July 2020

B. Kraus

Optimization of Vacuum Adsorption Chromatography for Superheavy Element Experiments

PhD Defense, University of Bern, Bern, Switzerland, 17 January 2020

M. Lin

Disposal of highly acidic spent nuclear fuel solutions at PSI: Cs removal process

PhD Defense, University of Bern, Bern, Switzerland, 21 October 2020

J. Neuhausen

WP12- Chemistry control experiments and modelling

PATRICIA Virtual Kick-off meeting, 28 October 2020 (online)

J. Neuhausen

WP12- Chemistry control experiments and modelling

PATRICIA Virtual WP12 Meeting, Task 12.2, 01 December 2020 (online)

J. Neuhausen, A. Folgado de Lucena, A. Aerts

Task 3.1 – Fission product release from HLM and deposition from the gas phase

PASCAL Virtual WP3 meeting, 20 November 2020 (online)

J. Neuhausen, A. Folgado de Lucena, A. Aerts

Task 3.1 – Fission product release from HLM and deposition from the gas phase

PASCAL Kick-off meeting, 27 November 2020 (online)

D. Schumann

WP3: Target Preparation for Improvement of Nuclear Data Measurements

SANDA WP leader meeting, 10 September 2020 (online)

D. Schumann

Samples and Targets: Peanuts or Core Components?

n_TOF annual meeting, Geneva, Switzerland, 23 September 2020

P. Steinegger

How to chemically characterize superheavy elements – from production to separation

CRS Seminar Day, Paul Scherrer Institute, Villigen PSI, Switzerland, 12 August 2020

P. Steinegger

Radiochemistry at PSI and the Chemistry of Transactinide Elements

Swiss Chemical Society Fall Meeting 2020, Switzerland, 25 August 2020 (online)

Z. Talip

Scientific career across Europe

Ege University Career Days, Izmir, Turkey, 12 June 2020 (online)

Z. Talip

Expanding the Nuclear Medicine Periodic Table

Tenure track talk, Paul Scherrer Institute, Villigen PSI, Switzerland, 18 June 2020

J. Ulrich

High precision nuclear data of Mn-53 for astrophysics and geosciences

Award talk of the Young Scientist Prize, General Assembly of the Swiss Neutron Science Society (SNSS)

Paul Scherrer Institute, Villigen, Switzerland, 29 October 2020

M. Veicht

Re-determination of the ³²Si Half-Life

Annual Report No. 1 (formal meeting for EPFL), Paul Scherrer Institute, Villigen PSI, Switzerland, 02 June 2020

M. Veicht

Re-determination of the ³²Si Half-Life: Volatility of H₂SiF₆

Internal Presentation, Institute de Radiophysique (IRA), Lausanne, Switzerland, 20 October 2020

M. Veicht

Nanoscale mechanisms of UO₂ formation through uranium reduction by magnetite (Pan et al., 2020)

Applications and Spin-Offs in Inorganic Chemistry, École polytechnique fédérale de Lausanne (EPFL), Lausanne, Switzerland, 09 November 2020

M. Veicht

Re-determination of the ³²Si Half-Life

Annual Report No. 2 (informal meeting with supervisors), Paul Scherrer Institute, Villigen PSI, Switzerland, 11 November 2020

M. Veicht

Determination of the Excitation Function for the Production of Ti-44 in Proton-Irradiated Vanadium Discs

Seminar of the Laboratory of Radiochemistry, Paul Scherrer Institute, Villigen PSI, Switzerland, 20 November 2020

M. Veicht

Implementing new isotopes for environmental research: Redetermination of the ³²Si half-life

Bi-annual Meeting (SINCHRON Project), Laboratory of Radiochemistry, Paul Scherrer Institute, Villigen PSI, Switzerland, 25 November 2020

Y. Wittwer

Optimization of Formation and Transport Yields for Metal Carbonyl Complexes under Single-Atom Chemistry Conditions
PhD Defense, University of Bern, Bern, Switzerland, 29 May 2020

N.P. van der Meulen

The development and use of exotic radionuclides towards the radiotheragnostic principle
Swiss Radiopharmacy Day, Bern, Switzerland, 04 March 2020

N.P. van der Meulen

Pursuing the theragnostic principle at Paul Scherrer Institute
PSI Physics Colloquium, Villigen PSI, Switzerland, 29 October 2020

POSTER PRESENTATIONS

N.M. Chiera

Towards high precision half-life measurements of exotic radiolanthanides
Swiss Chemical Society Fall Meeting 2020, 25 August 2020 (online)

C. Favaretto, Z. Talip, P. Grundler, S. Geistlich, R. Schibli, R. Eichler, N.P. van der Meulen

Production and radiochemical purification of terbium isotopes towards radiotheragnostic applications
Director's Visit, Paul Scherrer Institute, Villigen PSI, Switzerland, 02 July 2020

C. Favaretto, Z. Talip, P.V. Grundler, S. Geistlich, S. Landolt, J. R. Zeevaart, U. Köster, R. Schibli, C. Müller, N.P. van der Meulen

The introduction of ^{161}Tb to the clinic through the Good Manufacturing Practice compliant production of ^{161}Tb -DOTATOC_{Swiss}

Swiss Chemical Society Fall meeting 2020, 25 August 2020 (online)

P.V. Grundler, R. Hasler, C. Favaretto, Z. Talip, G. Dellepiane, T.S. Carzaniga, S. Braccini, U. Köster, C. Müller, N.P. van der Meulen

Development of the matched pair Sc-44/Sc-47 for diagnosis and therapy
Swiss Chemical Society Fall meeting 2020, 25 August 2020 (online)

P. Ionescu, N.M. Chiera, R. Dressler, R. Eichler, D. Herrmann, D. Piguet, P. Steinegger, A. Vögele

The Chemistry of Superheavy Elements

Director's Visit, Paul Scherrer Institute, Villigen PSI, Switzerland, 02 July 2020

P. Ionescu

Residual Gas Effects on the Gas Chromatographic Yield of Mercury and Astatine, and Their Impact on the Study of Transactinides Copernicium and Flerovium

Swiss Chemical Society Fall Meeting 2020, Switzerland, 25 August 2020 (online)

M. Veicht

Implementing new isotopes for environmental research: Redetermination of the ^{32}Si half-life

Director's Visit, Paul Scherrer Institute, Villigen PSI, Switzerland, 02 July 2020

M. Veicht

Dating the Recent Past. Chronometric Potential of Si-32: Part 1 / Chemical Separation and Preparation in a Pure State

Swiss Chemical Society Fall Meeting 2020, Switzerland, 25 August 2020 (online)

MEMBERS OF SCIENTIFIC COMMITTEES AND EXTERNAL ACTIVITIES

Dr. Robert Eichler

- Associate Editor of the International Journal of Modern Physics E (IJMPE) World Scientific Publishing
- Labor für Ionenstrahlphysik, Kuratorial Board on behalf of PSI
- Radiochimica Acta, Scientific Advisory Board

Prof. Dr. Patrick Steinegger

- Nuklearforum Schweiz, member

Dr. Dorothea Schumann

- Nuklearforum Schweiz, member
- Schweizerische Gesellschaft der Kernfachleute, member

Dr. Nicholas van der Meulen

- United States Department of Energy (DOE Isotope R&D FOA), Panel Reviewer
- Accelerator for Research in Radiochemistry and Oncology at Nantes Atlantique (ARRONAX), International Scientific Committee, member
- PSI internal research commission (FoKo), member
- International Advisory Committee for the Workshop on Targetry and Target Chemistry
- Academic Editor for Public Library Of Science (PLOS)
- Reviewer Board member: Instruments (MDPI)

PUBLIC RELATION AND OUTREACH ACTIVITIES

M. Veicht

Sonntagsdienst psiFORUM – PSI's outreach to the public

LECTURES AND COURSES

R. Eichler

Physikalische Chemie IV Grundlagen Radiochemie
University of Bern, Spring Semester 2020

R. Eichler

Master course Physikalische Chemie Radiochemie The Chemistry and Physics of Heaviest Elements
University of Bern, Autumn Semester 2020

M. Veicht

Practical lab course: "Introduction to Chemical Engineering"
École Polytechnique Fédérale de Lausanne (EPFL), ChE-203, Spring Semester 2019/2020

M. Veicht

Practical lab course: "Chemistry Analytic Laboratory I"
University de Lausanne (UNIL), UNIL-103, Autumn Semester 2019/2020

M. Veicht

Supervision: "General and Analytical Chemistry I (BIO+PHARM)"
University de Lausanne (UNIL), UNIL-101, Autumn Semester 2019/2020

N.P. van der Meulen, Z. Talip, P. Grundler. C. Favaretto

Production of novel radionuclides
ETHZ CAS Chemistry/Radiopharmacy Practical, 6 sessions, 04-06 February 2020

SEMESTER WORK

Maxime Jotterand

Performance of a SiC-based detector
Prof. Dr. Andreas Pautz (EPFL/PSI)
Prof. Dr. Patrick Steinegger (PSI)
December 2020

DOCTORAL THESES

Benjamin Kraus

Optimization of Vacuum Adsorption Chromatography for Superheavy Element Experiments

Dr. Robert Eichler (PSI)

Prof. Dr. Andreas Türler (Uni Bern)

January 2020

Jiri Ulrich

High precision nuclear data of Mn-53 for astrophysics and geosciences

Robert?

Dr. Rugard Dressler (PSI)

Prof. Dr. Andreas Türler (Uni Bern)

March 2020

Yves Wittwer

Optimization of Formation and Transport Yields for Metal Carbonyl Complexes under Single-Atom Conditions

Dr. Robert Eichler (PSI)

Prof. Dr. Andreas Türler (Uni Bern)

May 2020

Erik Karlsson

The adsorption behavior of volatile radionuclides present in a lead-bismuth eutectic reactor system

Dr. Jörg Neuhausen (PSI)

Prof. Dr. Andreas Türler (Uni Bern)

July 2020

Mu Lin

Disposal of highly acidic spent nuclear fuel solutions at PSI: Cs removal process

Dr. Dorothea Schumann (PSI)

Prof. Dr. Andreas Türler (Uni Bern)

October 2020

AWARDS

Mario Veicht

Teaching Excellence Award - Assistants

Section de Chimie et Génie Chimique (SGCS): Ten best PhD Students of 2020

École Polytechnique Fédérale de Lausanne (EPFL), Switzerland

August 2020

Dr. Jiri Ulrich

High precision nuclear data of Mn-53 for astrophysics and geosciences

Young Scientist Prize of the Swiss Neutron Science Society (SNSS)

for his thesis work

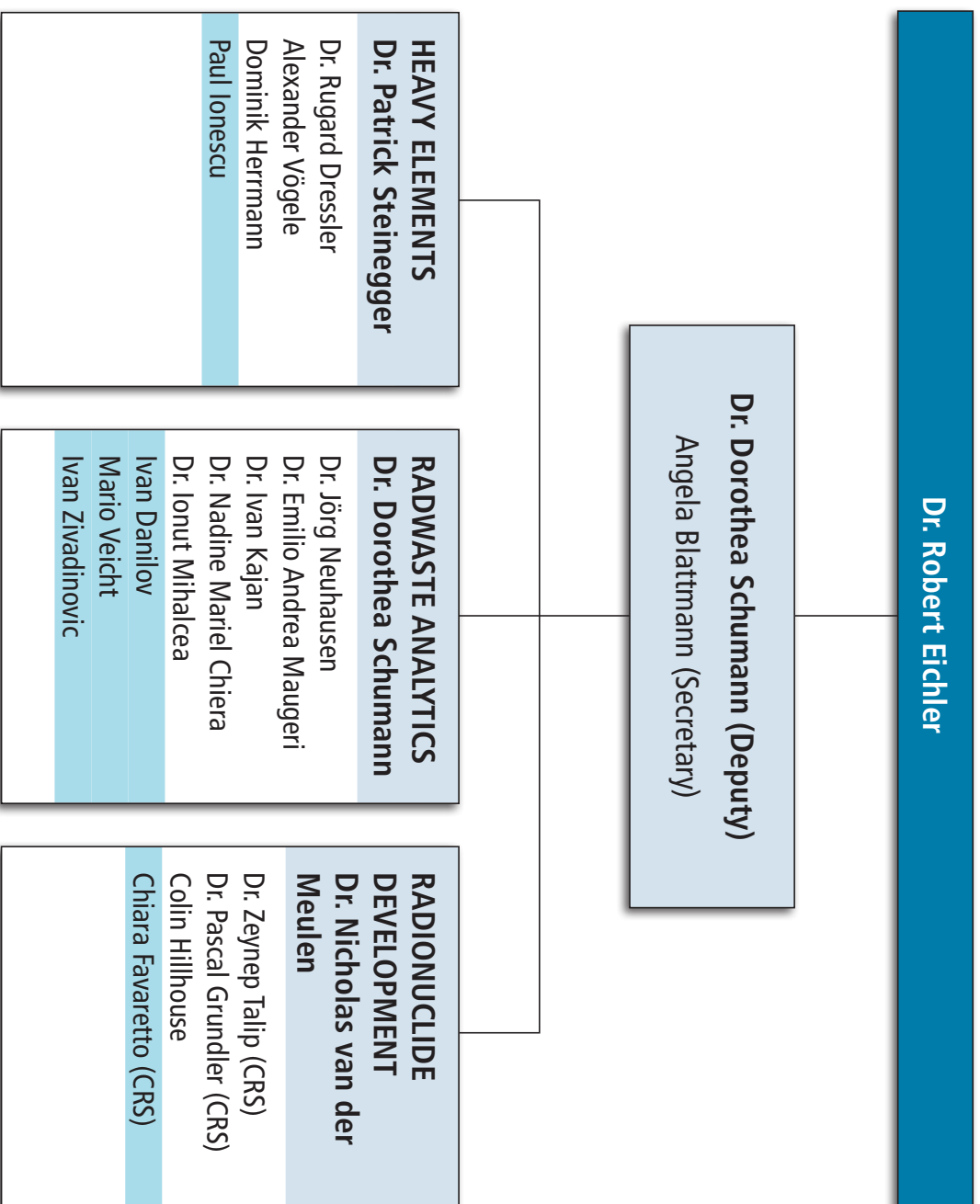
October 2020

Nicholas P. van der Meulen, Roger Hasler, Zeynep Talip, Pascal V. Grundler, Chiara Favaretto, Christoph A. Umbricht, Cristina Müller, Gaia Dellepiane, Tommaso S. Carzaniga, Saverio Braccini.

The Development of ^{44}Sc Towards Implementation at a Medical Cyclotron

IBA Award 2020 for best paper

LABOR FÜR RADIOCHEMIE DES PAUL SCHERRER INSTITUTS
31.12.2020



AUTHOR INDEX

- Bailat, C., 37, 46, 51
- Baudis, L., 29
- Bochud, F., 46, 51
- Borgna, F., 50
- Breur, P.A., 29
- Brown, A., 29
- Buchillier, T., 46, 51
- Calivno, F., 43
- Carulla, M., 9
- Casanovas, A., 43
- Cassette, P., 21
- Chen, S., 31
- Chevallay, E., 52
- Chiera, N.M., 23, 25
- Chrysalidis, K., 52
- Cocolios, T.E., 52
- Colijn, A.P., 29
- Cvjetinovic, D., 33, 35
- David, J.C., 31
- De Bodin de Galembert, G., 27
- Dressler, R., 9, 21, 23, 29, 43
- Duchemin, C., 52
- Duran, M.T., 46, 51
- Eichler, B., 13
- Eichler, R., 3, 5, 11, 13
- Favaretto, C., 45, 50
- Fedosseev, V., 52
- Gäggeler, H., 13
- Garg, R., 17
- Grundler, P.V., 48, 50, 51
- Guerrero, C., 43
- Heinitz, S., 43
- Heinke, R., 52
- Ionecu, P., 3, 5
- Jost, D.T., 13
- Jotterand, M., 9
- Juget, F., 46, 51
- Kajan, I., 17, 19, 31
- Kneip, N., 21
- Kossert, K., 21, 37
- Kovrizhnykh, N., 11
- Lambert, L., 52
- Lang, R.F., 29
- Lederer-Woods, C., 17
- Mash, B., 52
- Massafferri, A., 29
- Maugeri, E.A., 27, 43
- Mihalcea, I., 31, 33, 35, 37, 42
- Mougeot, X., 21
- Müller, C., 50
- Nähle, O., 37
- Nedjadi, Y., 37, 46, 51
- Neuhausen, J., 15
- Nobelen, J.C.Y., 29
- Pautz, A., 35, 37
- Perci, R., 29
- Pumar, C., 29
- Reuter, C., 29
- Sato, T.K., 5
- Schibli, R., 50
- Schomberg, M., 42
- Schumann, D., 17, 19, 21, 23, 25, 29, 31, 33, 35, 37, 42, 43
- Schumann, M., 29
- Smagghe, A., 7
- Solovjov, D., 11
- Sprung, P., 21, 23, 43
- Steinegger, P., 3, 5, 7, 9, 11
- Stora, T., 52
- Strub, E., 31
- Studer, D., 21
- Synal, H.-A., 42
- Talip, Z., 23, 45, 46, 50, 51, 52
- Tarifeno-Saldivia, A., 43
- Tiebel, G., 5
- Tosato, M., 45, 52

Towers, S., 29

Türler, A., 3

Ulrich, J., 21, 46

Van der Meulen, N.P., 45, 46,
48, 50, 51, 52

Varbella, A., 48

Veicht, M., 19, 31, 33, 35, 37, 42

Vockenhuber, C., 42

Wallner, A., 42

Wendt, K., 21

Wilkins, S., 52

Wilson, J., 33

Zeevaart, J.R., 51

Zhang, H., 52

AFFILIATION INDEX

AHL	Hot Laboratory, Division of the Nuclear Energy and Safety Department (NES), Paul Scherrer Institut, 5232 Villigen PSI, Switzerland
ANU	The Australian National University, Canberra ACT 0200, Australia
CBPF	Centro Brasileiro de Pesquisas Físicas - COHEP, R. Dr. Xavier Sigaud, 150 - Urca, Rio de Janeiro, Brazil
CEA	Commissariat à l'énergie atomique, D36, 91190 Saclay, France
CRS	Center for Radiopharmaceutical Sciences, Paul Scherrer Institut, 5232 Villigen PSI, Switzerland
EPFL	École polytechnique fédérale de Lausanne, Route Cantonale, 1015 Lausanne, Switzerland
ETHZ	Eidgen. Technische Hochschule Zürich, 8092 Zürich, Switzerland
FLNR	Flerov Laboratory of Nuclear Reactions, Joliot-Curie, 6, Dubna, Moscow region 141980, Russia
IRA	Institute de radiophysique, Rue du Grand-Pré 1, 1007 Lausanne, Switzerland
JAEA	Japan Atomic Energy Agency, Tokai, Ibaraki 319-1195, Japan
JGU Mainz	Johannes Gutenberg-Universität Mainz, 55099 Mainz, Germany
LMN	Laboratory for Micro and Nanotechnology, Division of the Nuclear Energy and Safety Department (NES) Paul Scherrer Institut, 5232 Villigen PSI, Switzerland
LNE/LNHB	Laboratoire National de métrologie et d'Essais / Laboratoire National Henri Becquerel, C.E.A. Saclay, 91191 Gif-sur-Yvette Cedex, France
Nikhef	Nikhef and the University of Amsterdam, Science Park, Amsterdam 1098 XG, the Netherlands
Nikhef Utrecht	Institute for Subatomic Physics, Utrecht University, Netherlands
NESCA	South African Nuclear Energy Corporation, Pelindaba, 0240, South Africa
PSI	Paul Scherrer Institut, Forschungsstrasse 111, 5232 Villigen PSI, Switzerland
PTB	Physikalisch-Technische Bundesanstalt, Bundesallee 100, 38116 Braunschweig, Germany
Purdue U	Department of Physics and Astronomy, Purdue University, West Lafayette, IN 47907, USA
SCK-CEN	Studiecentrum voor Kernenergie Boeretang 200, 2400 Mol, Belgium
SFU	Simon Fraser University, 8888 University Dr, Burnaby, BC V5A 1S6, Canada
U Freiburg	Physikalisches Institut, Universität Freiburg, Freiburg 79104, Germany
Univ. Belgrade	University of Belgrade, 1 Studentski trg, 11000 Belgrade, Serbia
Univ. Bern	Departement für Chemie und Biochemie, Universität Bern, Freiestr. 3, 3012 Bern, Switzerland
Univ. of Edinburgh	University of Edinburgh, Old College, South Bridge, Edinburgh EH8 9YL, United Kingdom
Univ. of Cologne	Universität zu Köln, Albertus-Magnus-Platz, 50923 Köln, Germany
Univ. Padova	Università degli Studi di Padova, Via VIII Febbraio, 2, 35122 Padova PD, Italia
Univ Sevilla	University of Seville, 4 San Fernando Str. Sevilla 41004, Spain
UPC	Universitat Politècnica de Catalunya, BarcelonaTech (UPC) C/ Jordi Girona 1-3, 08034 Barcelona, Spain
UZH	Universität Zürich, Rämistrasse 71, 8006 Zürich, Switzerland

